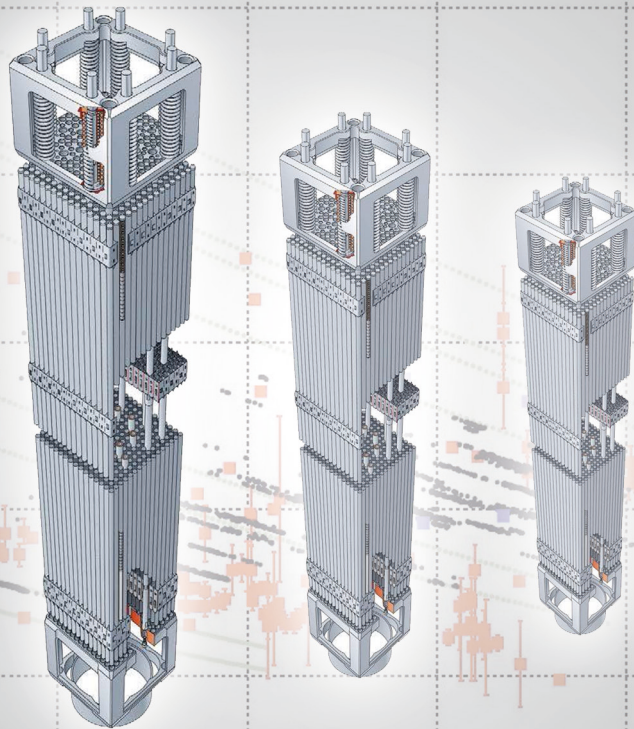


Realistic Bandwidth Estimation in the Theoretically Predicted Radionuclide Inventory of PWR-UO₂ Spent Fuel Derived from Reactor Design and Operating Data

Ivan Fast



Energie & Umwelt /
Energy & Environment
Band / Volume 358
ISBN 978-3-95806-206-1

Forschungszentrum Jülich GmbH
Institut für Energie- und Klimaforschung
Nukleare Entsorgung und Reaktorsicherheit (IEK-6)

Realistic Bandwidth Estimation in the Theoretically Predicted Radionuclide Inventory of PWR-UO₂ Spent Fuel Derived from Reactor Design and Operating Data

Ivan Fast

Schriften des Forschungszentrums Jülich
Reihe Energie & Umwelt / Energy & Environment

Band / Volume 358

ISSN 1866-1793

ISBN 978-3-95806-206-1

Bibliographic information published by the Deutsche Nationalbibliothek.
The Deutsche Nationalbibliothek lists this publication in the Deutsche
Nationalbibliografie; detailed bibliographic data are available in the
Internet at <http://dnb.d-nb.de>.

Publisher and
Distributor: Forschungszentrum Jülich GmbH
Zentralbibliothek
52425 Jülich
Tel: +49 2461 61-5368
Fax: +49 2461 61-6103
Email: zb-publikation@fz-juelich.de
www.fz-juelich.de/zb

Cover Design: Grafische Medien, Forschungszentrum Jülich GmbH

Printer: Grafische Medien, Forschungszentrum Jülich GmbH

Copyright: Forschungszentrum Jülich 2017

Schriften des Forschungszentrums Jülich
Reihe Energie & Umwelt / Energy & Environment, Band / Volume 358

D 82 (Diss. RWTH Aachen University, 2017)

ISSN 1866-1793
ISBN 978-3-95806-206-1

The complete volume is freely available on the Internet on the Jülicher Open Access Server (JuSER)
at www.fz-juelich.de/zb/openaccess.



This is an Open Access publication distributed under the terms of the [Creative Commons Attribution License 4.0](https://creativecommons.org/licenses/by/4.0/),
which permits unrestricted use, distribution, and reproduction in any medium, provided the original work is properly cited.

To Natalia and Alice

Abstract

Nuclear energy for power generation produces heat-generating high- and intermediate level radioactive waste (HLW and ILW) for which a safe solution for the handling and disposal has to be found. Currently, many European countries consider the final disposal of HLW and ILW in deep geological formations as the most preferable option. In Germany the main stream of HLW and ILW include spent fuel assemblies from nuclear power plants (NPPs), the vitrified waste and compacted metallic waste of the fuel assembly structural parts originate from reprocessing plants. An important task that occurs within the framework of the Product Quality Control (PQC) of nuclear waste is the assessment of the compliance of any reprocessed waste product inventory with the prescribed limits for each relevant radionuclide (RN). The PQC task is to verify the required quality and safety of nuclear waste prior to transportation to a German repository and to avert the disposal of non-conform waste packages. The verification is usually based on comparing the declared radionuclide inventory of the waste with the presumed or expected composition, which is estimated, based on the known history of the waste and its processing. The difficulty of such estimations for radioactive components from nuclear fuel assemblies is that reactor design parameters and operating histories can have a significant influence on the nuclide inventory of any individual fuel assembly. Thus, knowledge of these parameters is a key issue to determine the realistic concentration ranges, or bandwidths, of the radionuclide inventory.

As soon as a governmental decision on the construction of a high-level waste repository will be made, comprehensive radionuclide inventories of the wastes assigned for the deposition will be required. The list of final repository relevant radionuclide is based on the safety assessment for this particular repository, thus it is likely to comprise more-or-less the same radionuclides that need to be declared for compacted metallic waste residual from the reprocessing of spent fuel assemblies. In Germany, the radionuclide declaration list for the disposal of used fuel assemblies is not yet specified. Although information of radionuclide composition of used nuclear fuel assemblies assigned to a specific repository would be provided by the nuclear industry. An estimation of the average radionuclide composition of the burnt-up fuel including the realistic inventory bandwidths for each of relevant radionuclides would be highly desirable beforehand. This information is needed for the development of proof tools for the product quality control or safeguards, but also for the evaluation of various safety scenarios regarding the radionuclide mobility or contamination.

This work is focused on the development of a method for the determination of realistic radionuclide bandwidths in cases when no information of reactor design and operating data is available. Reactor parameters are classes as Primary Reactor Parameters of burn-up (BU) and cooling time (CT) that are considered to be known, and so-called Secondary Reactor Parameters (SRPs) that include nine parameters that are analysed: initial enrichment (IE), fuel density (FD), fuel temperature (FT), specific power (SP), downtime (DT), irradiation time (IT), moderator density (MD), moderator temperature (MT) and boric acid concentration (BA) used in the water for reactor control. All the SRP values are fuel assembly and whole irradiation time averaged values and varied independently in burn-up calculation models. The realistic range limits of each such SRP are obtained from 339 international PWR-UO₂ spent fuel assemblies with well-known fuel design and reactor operating data. The methodology is systematically tested ensuring transparency, traceability and repeatability of the individual

steps.

For the SRP analysis and determination of RN bandwidths uniform distribution of assemblies with burn-up up to 71 GWd/t_{HM} are assumed. In the future work dependent on application the effective RN inventory concentration bandwidths could be determined using realistic or relevant FA distribution.

The modelling of radionuclide inventories is carried out with the burn-up code SCALE 6.1 using the nuclear data library ENDF/B-VII.0. The input data include geometry of the fuel assembly and a set of the associated SRP values.

The theoretical (calculated) bandwidths of each radionuclide show different behaviour in the response to different SRPs. The magnitude of the bandwidth significantly varies for different radionuclides and depends strongly on the primary parameters of burn-up and cooling time.

The theoretical bandwidths are validated with experimental data. For this purpose the destructive radiochemical assay (RCA) data are taken from the Spent Fuel Isotopic Composition Database (SFCOMPO), which is maintained by the OECD Nuclear Energy Agency. The PWR data of this database comprise measurements for more than 300 fuel samples with an associated burn-up range between 3 and 75 GWd/t_{HM}.

For most final disposal relevant radionuclides the realistic bandwidths can be determined accurately with only information of burn-up and cooling time. For some radionuclides (¹⁴C, ¹²⁶Sn, ^{108m}Ag etc.) additional parameters characterizing fuel impurities, burnable absorber exposure etc. are required.

There is, however, presently insufficient experimental data to validate the bandwidths for all radionuclides of interest to waste management. It is however possible to perform a comprehensive verification by comparing the bandwidths obtained with other reference inventory calculations used by several countries for long-term safety assessment, spent fuel transportation and storage, or other applications. In this work, predicted theoretical isotope bandwidths are compared with:

- calculated inventories of approximately 2000 US PWR-UO₂ spent fuel assemblies with a burn-up range between 7 and 53 GWd/t_{HM};
- calculated inventories of fuel assembly families that represent average data for approximately 3300 Swiss PWR-UO₂ SNF;
- calculated average inventory of the Swedish PWR-UO₂ SNF;
- calculated average inventory of German PWR-UO₂ SNF.

The present work highlights the importance, for the estimation of radionuclide inventories of spent nuclear fuel, of considering available experimental and international reference data to address uncertainties in spent fuel compositions when information on fuel impurities, initial composition, design and operating data are insufficiently known.

This work provides realistic radionuclide bandwidths that support methods for a long-term safety analysis of final repositories as well as for the development of efficient and validated tools for the PQC of HLW disposal and for safeguard applications.

Kurzzusammenfassung

Die Kernenergie erzeugt bei der Stromproduktion Wärme erzeugende hoch- und mittel-radioaktive Abfälle (HAW und MAW), für die eine sichere Lösung für die Handhabung und Entsorgung gefunden werden muss. Derzeit halten die europäischen Länder die Endlagerung von HAW und MAW in tiefen geologischen Formationen für die bevorzugte Option. Einen großen Anteil am HAW und MAW in Deutschland haben abgebrannte Brennelemente aus Kernkraftwerken (KKW), aber auch verglaste und kompaktierte metallische Abfälle aus der Wiederaufarbeitung von abgebrannten Kernbrennelementen. Eine wichtige und zu erfüllende Aufgabe, die im Rahmen der Produktkontrollstelle (PKS) von nuklearen Abfällen auftritt, ist die Beurteilung der wiederaufbereiteten Abfallprodukt Inventare hinsichtlich der vorgeschriebenen Grenzwerte für jedes Endlager-relevante Radionuklid (RN). Das Gleiche gilt auch für direkt endzulagernde abgebrannte Kernbrennstäbe. Die PKS Aufgabe ist es, die erforderliche Qualität und Sicherheit von nuklearen Abfällen vor dem Transport in ein deutsches Endlager zu verifizieren und die Entsorgung nicht-konformer Abfallgebilde zu verhindern. Diese Verifikation basiert üblicherweise auf dem Vergleich der vermutlichen oder erwarteten Zusammensetzung des angegebenen Radionuklidinventars des betreffenden Abfalls, basierend auf der normalerweise hinreichend bekannten Vorgeschichte der Abfälle und ihrer endlagerechten Konditionierung. Die Schwierigkeit solcher Schätzungen für radioaktive Komponenten der abgebrannten Brennelemente ist, dass Reaktordesign und Betriebsgeschichten Parameter einen signifikanten Einfluss auf das Nuklidinventar eines jeden einzelnen Brennelements haben. Somit ist die genaue Kenntnis dieser Parameter eine zentrale Frage bei der Abschätzung der realistischen Konzentrationsbereichen oder Bandbreiten des Radionuklidinventars.

Sobald eine Entscheidung über Art und Bau eines HAW-Endlagers getroffen wird, wird eine umfassende Bestimmung und Zertifizierung des Radionuklid-Inventars für die zur Endlagerung vorgesehenen Abfälle erforderlich sein. Die Liste der Endlager-relevanten Radionuklide basiert auf der Sicherheitsbewertung für dieses spezielle Endlager. Somit erscheint es sinnvoll, die gleichen Radionuklide zu betrachten, die für kompaktierte metallische Abfälle bestehend aus den Brennelementstrukturteilen aus den Wiederaufarbeitungsanlagen zu deklarieren. In Deutschland ist die Radionuklid-Deklarationsliste für die Entsorgung abgebrannter Brennelemente derzeit noch nicht festgelegt. Obwohl Informationen über Radionuklidzusammensetzungen der abgebrannten Brennelemente durch die Atomindustrie zur Verfügung gestellt werden, ist eine Abschätzung der durchschnittlich zu erwartenden Zusammensetzung des Radionuklidinventars einschließlich der realistischen Bandbreiten für jedes einzelne relevante Radionuklid sehr wünschenswert. Diese Informationen werden sowohl für die Entwicklung passender Proof-Tools für die Produktqualitäts-Kontrollstelle oder auch Safeguards als auch für die Bewertung der verschiedenen Sicherheitsszenarien in Bezug auf die Radionuklid-Mobilität oder Kontamination erforderlich sein.

Der Schwerpunkt dieser Arbeit ist die Bestimmung von realistischen Radionuklid Bandbreiten insbesondere für die Fälle, bei denen keine oder unzureichende Informationen über Reaktordesign- und Betriebsdaten zur Verfügung stehen. Folgende Reaktorparameter werden als Primäre Reaktor Parameter (PRP) klassifiziert: Abbrand (BU) und Kühlzeit (CT); die beide bekannt werden müssen. Dem gegenüber stehen die sogenannten Sekundären Reaktor Parameter (SRP), neun in der Anzahl, deren Einfluss auf das RN-Inventar hier umfassend untersucht und analysiert wird. Es sind dies die Parameter: Anfangsanreicherung (IE), Brenn-

stoffdichte (FD), Brennstofftemperatur (FT), spezifische Leistung (SP), Downtime (DT), Bestrahlungszeit (IT), Moderatorichte (MD), Moderatortemperatur (MT) und Borsäurekonzentration (BA) im Kühlwasser für die Verwendung bei der Reaktorsteuerung. Alle SRP-Werte sind über ein ganzes Brennelement und die ganze Bestrahlungszeit gemittelte Werte. Die realistischen Bereichsgrenzen eines jeden solchen SRP sind aus 339 internationalen DWR-UO₂ abgebrannten Brennelementen mit bekannten Reaktordesign- und Betriebsdaten bestimmt worden. Diese Methodik erlaubt Transparenz, Nachvollziehbarkeit und Reproduzierbarkeit der einzelnen Berechnungsschritte.

Die Modellierung des Radionuklid-Inventars wird mit dem Abbrand-Code SCALE 6.1 und der Kerndatenbibliothek ENDF/B-VII.0 durchgeführt. Die Eingangsdaten umfassen die Geometrie des Brennelements und einen Satz der zugehörigen SRP Werte.

Die theoretischen (berechneten) Bandbreiten eines jeden Radionuklids zeigen unterschiedliches Verhalten in Bezug auf die verschiedenen SRP. Die Größe der Bandbreite variiert signifikant für unterschiedliche Radionuklide und hängt stark von den Primären Reaktor Parametern ab: dem Abbrand und der Kühlzeit.

Die theoretischen Bandbreiten werden mit experimentellen Daten verglichen und validiert. Dazu werden die radiochemischen Messungen (experimentelle Daten) aus zerstörenden Probenahmen aus der Datenbank „Spent Fuel Isotopic Composition Database“ (SFCOMPO) genommen, die von der OECD Nuclear Energy Agency verwaltet wird. Die Daten für Druckwasserreaktoren (DWR) in dieser Datenbank umfassen Messungen für mehr als 300 Kernbrennstoffproben mit einem zugehörigen Abbrandbereich zwischen 3 und 75 GWd/t_{HM}.

Für die meisten Endlager-relevanten Radionuklide sind Informationen von Abbrand und Kühlzeit für die genaue Bestimmung der realistischen Bandbreiten ausreichend. Für einige Radionuklide (¹⁴C, ¹²⁶Sn, ^{108m}Ag usw.) sind außerdem noch zusätzliche Parameter wie Verunreinigungen im Kernbrennstoff, Einsetzten von Absorberstäben usw. erforderlich.

Es gibt jedoch derzeit nicht genügend experimentelle Daten, die für eine Validierung der theoretischen Bandbreiten aller RN nötig wären und die von Interesse für nukleares Abfallmanagement sind. Es ist jedoch möglich, eine umfassende Überprüfung durchzuführen, indem man die theoretischen Bandbreiten mit anderen berechneten Referenzinventaren vergleicht, die von mehreren Ländern für die Langzeitsicherheitsbewertung, für Transport und Lagerung abgebrannter Brennelemente oder andere Anwendungen verwendet werden. In dieser Arbeit werden die theoretischen RN Bandbreiten verglichen mit den:

- berechneten Inventaren für etwa 2000 US DWR-UO₂ abgebrannten Brennelementen mit einem Abbrandbereich zwischen 7 und 53 GWd/t_{HM};
- berechneten Inventaren von Brennelementfamilien, die durchschnittliche Daten für rund 3300 Schweizer DWR-UO₂ abgebrannte Brennelemente darstellen;
- berechnetem durchschnittlichen Inventar von schwedischen DWR-UO₂ abgebrannten Brennelementen;
- berechnetem durchschnittlichen Inventar von deutschen DWR-UO₂ abgebrannten Brennelementen.

Die Ergebnisse dieser Arbeit liefern realistische Radionuklid Bandbreiten, welche herangezogen werden müssen bei einer Langzeit-Sicherheitsanalyse von Endlagern, aber auch bei der Entwicklung von effizienten und validierten Tools für die Produktqualitätskontrolle oder bei der HAW Entsorgung und für Safeguards Anwendungen.

Contents

Abbreviations	VI
List of figures	X
List of tables	XI
1 Introduction	1
1.1 Task and objectives of the work	1
1.2 Short description of method development	3
1.3 Previous studies	4
1.4 Calculated RN inventory of international PWR-UO ₂ SNF	7
2 Theoretical background	9
2.1 Physical and mathematical basis to the build-up of radionuclide inventory	9
2.2 SCALE as a burn-up code system	13
3 Methodology to the determination of realistic bandwidths of SNF RN inventory	16
4 SRP Analysis	19
4.1 Available data of fuel assembly design and reactor operating parameters .	19
4.2 Correlations between SRPs	21
4.3 Boundaries and typical values of SRPs	23
4.4 Downtime analysis	29
5 Modelling	34
6 Realistic bandwidths of PWR-UO ₂ RN inventory	36
6.1 Theoretical bandwidths of RNs	36
6.2 Available experimental or RCA data	38
6.3 Available RN inventory of international PWR-UO ₂ SNF	40
6.4 Realistic bandwidths of RN	43
6.4.1 Realistic bandwidths of fission products and light radionuclides .	46
6.4.2 Realistic bandwidths of actinides	76
7 Conclusion	121
Bibliography	127

Abbreviations

BA	Boric Acid concentration
BONAMI	Bondarenko AMPX Interpolator
BPR	Burnable Poison Rods
BU	Burn-up
BWR	Boiling Water Reactor
CENTRM	Continuous Energy Transport Module
COUPLE	A nuclear decay and cross section data processing code
CT	Cooling time
DT	Downtime
DWR	Druckwasserreaktor
FA	Fuel Assembly
FD	Fuel Density
FI	Fuel Impurities
FT	Fuel Temperature
GKN	Gemeinschaftskernkraftwerk Neckar
GRS	Gesellschaft für Anlagen- und Reaktorsicherheit (GRS) mbH
HAW	Hoch Radioaktiver Abfall
HLW	High-Level Radioactive Waste
IC	Initial Composition
IE	Initial Enrichment
IT	Irradiation Time
KKW	Kernkraftwerk
KWO	Kernkraftwerk Obrigheim
LWR	Light Water Reactor
MAW	Mittel Radioaktiver Abfall
MD	Moderator Density
MT	Moderator Temperature
NAGRA	Nationale Genossenschaft für die Lagerung radioaktiver Abfälle
NEA	Nuclear Energy Agency
NEI	Nuclear Engineering International
NEWT	New ESC-based Weighting Transport code
NPP	Nuclear Power Plant
OECD	Organisation for Economic Co-operation and Development
ORIGEN	Oak Ridge Isotope Generation code
ORNL	Oak Ridge National Laboratory
PKS	Produktkontrollstelle
PMC	Produce Multigroup Cross sections
PQC	Product Quality Control
PRP	Primary Reactor Parameter
PWR	Pressurized Water Reactor

RCA	Destructive Radiochemical Assay
SCALE	Nuclear Modeling and Simulation Code System
SFCOMPO	Spent Fuel Isotopic Composition Database
SKB	Swedish Nuclear Fuel and Waste Management Co
SNF	Spent Nuclear Fuel
SP	Specific Power
SRP	Secondary Reactor Parameter
TD	Theoretical Density
TENDL	TALYS-based Evaluated Nuclear Data Library
TRITON	Transport Rigor Implemented with Time-dependent Operation for Neutronic depletion
UNF	Used Nuclear Fuel
WAC	Waste Acceptance Criteria
WTI	Wissenschaftlich Technische Ingenieurberatung GmbH

List of Figures

1.1	Scheme of this work's objective	2
1.2	Scheme of method development	3
2.1	Fission yields and fission cross-section	11
2.2	Flowchart of TRITON	15
3.1	Simplified scheme of the methodology to determine realistic bandwidths of the radionuclide inventory	16
3.2	Scheme of the determination method for the RN bandwidths derived from reactor design and operating data	17
4.1	BU vs. IE	25
4.2	BU vs. SP	26
4.3	DT distribution	30
4.4	DT _i distribution	30
5.1	Second optimization step of the number of models	35
6.1	Example of RN sensitivity by variation of SRPs	37
6.2	Decay of fission products	46
6.3	Theoretical bandwidth of ^{108m} Ag and effect of fuel impurities	47
6.4	Realistic bandwidth of ^{110m} Ag	48
6.5	Theoretical bandwidth of ¹⁴ C and effects of fuel impurities and of model properties	49
6.6	Realistic bandwidth of ¹⁴⁴ Ce	51
6.7	Realistic bandwidth of ¹³⁴ Cs	52
6.8	Realistic bandwidth of ¹³⁵ Cs	53
6.9	Realistic bandwidth of ¹³⁷ Cs	54
6.10	Realistic bandwidth of ¹⁵² Eu	55
6.11	Realistic bandwidth of ¹⁵⁴ Eu	56
6.12	Realistic bandwidth of ¹⁵⁵ Eu	57
6.13	Theoretical bandwidth of ³ H and effects of fuel impurities and of model properties	58
6.14	Realistic bandwidth of ¹²⁹ I	59
6.15	Realistic bandwidth of ⁸⁵ Kr	60
6.16	Theoretical bandwidth of ⁹³ Mo and effect of fuel impurities	61
6.17	Theoretical bandwidth of ⁹⁴ Nb and effect of fuel impurities	62
6.18	Realistic bandwidth of ⁹⁵ Nb	63
6.19	Realistic bandwidth of ¹⁰⁷ Pd	64
6.20	Realistic bandwidth of ¹⁴⁷ Pm	65
6.21	Realistic bandwidth of ¹⁰⁶ Ru	66
6.22	Realistic bandwidth of ¹⁰³ Ru	67

6.23	Realistic bandwidth of ^{124}Sb	68
6.24	Realistic bandwidth of ^{125}Sb	69
6.25	Realistic bandwidth of ^{79}Se	70
6.26	Realistic bandwidth of ^{151}Sm	71
6.27	Realistic bandwidth of ^{126}Sn	72
6.28	Realistic bandwidth of ^{90}Sr	73
6.29	Realistic bandwidth of ^{99}Tc	74
6.30	Realistic bandwidth of ^{93}Zr	75
6.31	Chart of actinide's mother-daughter behaviour	76
6.32	Decay chain of ^{250}Cf	77
6.33	Realistic bandwidth of ^{246}Cm	78
6.34	Realistic bandwidth of ^{242}Pu	79
6.35	Decay chain of $^{242\text{m}}\text{Am}$	80
6.36	Realistic bandwidth of $^{242\text{m}}\text{Am}$	81
6.37	Realistic bandwidth of ^{242}Cm	82
6.38	Realistic bandwidth of ^{238}Pu	83
6.39	Decay chain of ^{238}U	84
6.40	Decay chain of ^{238}U	85
6.41	Realistic bandwidth of ^{238}U	86
6.42	Effect of initial composition on ^{234}U concentration	87
6.43	Realistic bandwidth of ^{234}U	88
6.44	Realistic bandwidth of ^{230}Th	89
6.45	Realistic bandwidth of ^{226}Ra	90
6.46	Decay chain of ^{247}Cm	91
6.47	Realistic bandwidth of ^{251}Cf	92
6.48	Realistic bandwidth of ^{247}Cm	93
6.49	Realistic bandwidth of ^{243}Am	94
6.50	Realistic bandwidth of ^{243}Cm	95
6.51	Realistic bandwidth of ^{239}Pu	96
6.52	Decay chain of ^{235}U	97
6.53	Realistic bandwidth of ^{235}U	98
6.54	Realistic bandwidth of ^{231}Pa	99
6.55	Realistic bandwidth of ^{227}Ac	100
6.56	Decay chain of ^{245}Cm	101
6.57	Decay chain of ^{249}Cf	102
6.58	Realistic bandwidth of ^{249}Cf	103
6.59	Realistic bandwidth of ^{245}Cm	104
6.60	Realistic bandwidth of ^{241}Pu	105
6.61	Realistic bandwidth of ^{241}Am	106
6.62	Decay chain of ^{237}Np	107
6.63	Realistic bandwidth of ^{237}Np	108
6.64	Realistic bandwidth of ^{233}U and effect of fuel impurities in Th	109
6.65	Realistic bandwidth of ^{229}Th	111
6.66	Decay chain of ^{244}Pu	112

6.67	Realistic bandwidth of ^{248}Cm	113
6.68	Realistic bandwidth of ^{244}Pu	114
6.69	Realistic bandwidth of ^{244}Cm	115
6.70	Realistic bandwidth of ^{240}Pu	116
6.71	Realistic bandwidth of ^{236}U	117
6.72	Decay chain of ^{232}Th	118
6.73	Realistic bandwidth of ^{232}Th and effect of fuel impurities	119
6.74	Realistic bandwidth of ^{232}U	120

List of Tables

1.1	The list of repository relevant radionuclides in Germany	2
1.2	SRPs	4
1.3	Previous studies	5
1.4	Calculated RN inventory of international PWR-UO ₂ SNF	8
4.1	Secondary Reactor Parameters	19
4.2	Publicly available fuel assembly design and reactor operating data on 69 FA	20
4.3	Correlation coefficients between BU and SRPs and between different SRPs	21
4.4	Variability ranges of SRP values	24
4.5	DT _i distribution	31
4.6	Model of DT analysis	32
4.7	Multiplication DT-correction factor for averaged DT=400 days	33
5.1	Model of RN analysis	34
5.2	Optimization of the number of models	34
6.1	Available RCA data from SFCOMPO	39
6.2	Properties of calculated international RN inventory	40
6.3	Fuel impurities	42
6.4	RN classification based on the CT up to 35 years and their SRPs sensitivity	45
7.1	RNs with major impact of FI, Lib and IC	122

1 Introduction

Nuclear energy for power generation produces heat-generating high- and intermediate level radioactive waste (HLW and ILW). Yet there is not a single final HLW repository in operation, world-wide. However, many countries are currently searching for the most appropriate location for such a repository (Sweden, Germany, Switzerland, France, etc.). Recently, the construction of a final repository has commenced in Finland [Posiva, 2013]. The heat-generating HLW and ILW include both, spent fuels from nuclear power reactors and nuclear waste from reprocessing plants. In Germany, these two types of waste make up approximately 10500 [DAEF, 2015] and 6662 [Aksyutina et al., 2015] tonnes of heavy metal, respectively, as estimated for the year 2022. A large fraction of spent fuel waste in Germany is represented by used fuel assemblies from pressurized water reactors (PWR). The present work is focused on the analysis of inventories of a variety of UO_2 spent fuel assemblies from PWR.

The wide variety of spent fuel assemblies ranges over different burn-ups, cooling times, fuel design and reactor operational conditions. In Germany, there are about 35'000 fuel assemblies [Peiffer et al., 2011] from PWR, BWR and VVER, thus, a wide range of radionuclide inventory and activity must be expected and is actually observed for a certain burn-up. Throughout this work the burn-up (BU) and cooling time (CT) of a single spent fuel assembly are defined as so-called Primary Reactor Parameters, and they determine the radionuclide inventory at a given time. Thereby information of BU and CT is required for the estimate of an average radionuclide composition. However, additional information of the fuel design and reactor operational conditions, i.e. the so-called Secondary Reactor Parameters, is required for the determination of the realistic bandwidths of the radionuclide inventory.

1.1 Task and objectives of the work

An important task that occurs within the framework of radioactive waste maintenance is the assessment of the compliance of radionuclide inventories of disposable HLW radwaste packages with the prescribed limits for each relevant radionuclide and thus verifying the consistency of declared RN compositions of waste packages with the waste acceptance criteria (WAC) prior their disposal into a repository. In Germany this range of tasks is referred to as the Product Quality Control (PQC). The verification is usually based on comparing the declared composition of the waste with the presumed radionuclide inventory, which is estimated based on known history and type of the waste. The difficulty of such an estimate is that each individual waste product could consist of radioactive wastes from various nuclear fuel assemblies, whose histories cannot be traced back exactly. In such a case no information on the Primary Reactor Parameters (BU and CT) and on the Secondary Reactor Parameters (fuel design and reactor operating data) is available. Indeed, a reprocessed waste package is composed of many individual fuel assemblies, whose compositions depend on their individual maintenance record,

which is determined by the fuel design and by the reactor operating history. The lack of such information causes a significant variability of the RN inventory of a waste package, which can be quantified by determining the intervals (bandwidths) of individual RN compositions for a given burn-up and cooling time. Waste packages, whose declared inventories are consistent with the predicted bandwidths and with WAC criteria, can be characterized as conformal. A similar range of tasks would presumably appear within the frame of the final disposal of spent nuclear fuel.

In this study the theoretical bandwidths are calculated for the range of 0 – 71 GWd/t_{HM}. These bandwidths could be used for estimation of total activities of waste packages provided that the distribution of the constituent fuel assemblies on burn-up is known.

The aim of this work is to develop a method for the determination of realistic bandwidths for radionuclides that are relevant for the final disposal of heat-generating high- and intermediate-level nuclear waste. This comprises 64 radionuclides (cf. Table 1.1) contained in spent nuclear fuel (excluding activation products) which must be declared in Germany by NPP operators [Brennecke, 2011]. An independent assessment has to be made for each radionuclide of this list irrespectively of its actual amount or radiotoxicity. The set of tasks involved in this development is shown as the "Black-box" in Figure 1.1. The "Input" required for this development comprises the list of relevant RNs and the primary reactor parameters and the "Output" corresponds to the desired realistic bandwidths at the specified cooling time. The set of tasks including in the "Black-box" is explained in detail throughout this thesis. In this study the analysis is constrained by the CT=0. A recalculation to CT=t can be performed trivially using standard decay simulating software, e.g. ORIGEN.

In short, the task of the thesis is to obtain a realistic estimate for the bandwidths of any RN of a PWR-UO₂ spent fuel assembly at CT=0 using the burn-up only.

Table 1.1: The list of repository relevant radionuclides in Germany

64 radionuclides
²²⁷ Ac, ^{108m} Ag, ^{110m} Ag, ²⁴¹ Am, ^{242m} Am, ²⁴³ Am, ¹⁴ C, ¹⁴⁴ Ce, ²⁴⁹ Cf, ²⁵¹ Cf, ²⁴² Cm, ²⁴³ Cm, ²⁴⁴ Cm, ²⁴⁵ Cm, ²⁴⁶ Cm, ²⁴⁷ Cm, ²⁴⁸ Cm, ¹³⁴ Cs, ¹³⁵ Cs, ¹³⁷ Cs, ¹⁵² Eu, ¹⁵⁴ Eu, ¹⁵⁵ Eu, ³ H, ¹²⁹ I, ⁸⁵ Kr, ⁹³ Mo, ⁹⁴ Nb, ⁹⁵ Nb, ²³⁷ Np, ²³¹ Pa, ¹⁰⁷ Pd, ¹⁴⁷ Pm, ¹⁴⁴ Pr, ²³⁸ Pu, ²³⁹ Pu, ²⁴⁰ Pu, ²⁴¹ Pu, ²⁴² Pu, ²⁴³ Pu, ²⁴⁴ Pu, ²²⁶ Ra, ¹⁰⁶ Rh, ¹⁰³ Ru, ¹⁰⁶ Ru, ¹²⁴ Sb, ¹²⁵ Sb, ⁷⁹ Se, ¹⁵¹ Sm, ¹²⁶ Sn, ⁹⁰ Sr, ⁹⁹ Tc, ²²⁹ Th, ²³⁰ Th, ²³² Th, ²³² U, ²³³ U, ²³⁴ U, ²³⁵ U, ²³⁶ U, ²³⁸ U, ⁹⁰ Y, ⁹³ Zr, ⁹⁵ Zr

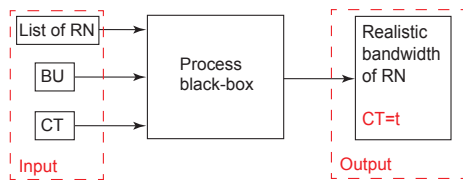


Figure 1.1: Scheme of this work's objective.

The main achievement of this study is the development of a modular and systematic methodology for predicting the radionuclide bandwidths based on propagation of variability in the reactor design and operating data. The validity of this approach is proved by comparing the theoretical bandwidths with an extensive experimental database. The developed methodology is focused on PWR-UO₂ fuel assemblies. However, it can be similarly applied to other types of spent fuel and nuclear waste products from reprocessing.

1.2 Short description of method development

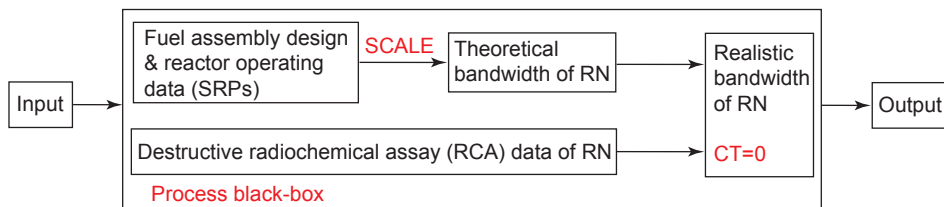


Figure 1.2: Scheme of method development for the determination of realistic RN bandwidths based on variability in fuel assembly design and reactor operating data.

The determination of realistic bandwidths requires validation of the calculated theoretical bandwidths against available experimental data (cf. Figure 1.2). The theoretical calculations are performed with SCALE software system [ORNL, 2011]. The available experimental data include radionuclide concentrations obtained from destructive radiochemical assay (RCA).

The determination of realistic bandwidths requires a realistic variability range for each SRP (cf. Table 1.2). In this work the variability for the values of these parameters is estimated on the basis of fuel design and reactor operating data on 339 PWR-UO₂ assemblies. For covering of fuel assemblies with BU up to 71 GWd/t_{HM} it is necessary to divide burn-up range in several intervals, where for each SRP individual range values (minimum, typically and maximum values) are determined. Based on this analysis a representative quantity of about 1700 models (i.e. sets of the SRP) is created. Further details on the burn-up divisions and on the choice of models is given in paragraphs 4 and 5, respectively.

The modelling of the radionuclide inventories is carried out with the burn-up code SCALE 6.1 [ORNL, 2011] using the nuclear data library ENDF/B-VII.0 [Chadwick et al., 2006]. Table 1.2 lists the nine SRPs analysed in the study.

The RCA data used for validating the theoretical bandwidths are taken from the Spent Fuel Isotopic Composition Database (SFCOMPO), which is maintained by the OECD Nuclear Energy Agency [NEA, 2015b]. The PWR data of this database comprise

Table 1.2: Secondary Reactor Parameters

Initial composition and properties of fuel	Irradiation history	Moderator properties
Initial Enrichment (IE)	Specific Power (SP)	Moderator Density (MD)
Fuel Density (FD)	Downtime (DT)	Moderator Temperature (MT)
Fuel Temperature (FT)	Irradiation Time (IT)	Boric Acid concentration (BA)

measurements for more than 300 fuel samples with an associated burn-up range between 3 and 75 GWd/ t_{HM} . However, the available information covers only 41 radionuclides that are relevant for the safety of high-level radioactive waste deposition. For the other, remaining relevant radionuclides the experimental data are missing, and for these the bandwidths could only be estimated theoretically.

1.3 Previous studies

This section gives an overview of the previous studies of the SRP impact on the radionuclide inventory of PWR spent fuel. All these studies were performed either for the analysis of burn-up credit or for the validation of software systems like SCALE and for the benchmarking with main focus of isotopic uncertainties. Thus, the radionuclides which were analysed are more relevant for the burn-up credit than for the waste management. This corresponds to about 20 disposal relevant RNs. However, the SRPs impact on some relevant radionuclides can be observed and the most important parameters can be identified. In the following the results of these studies are summarized in Table 1.3. In Table these studies are divided into those, which do not use any measurements (so-called theoretical studies) and those based on available destructive radiochemical assay data.

Previous theoretical studies

The study of [Cerne et al., 1987] investigated the effect of the initial enrichment on the reactivity and isotopic composition of PWR spent fuel up to 60 GWd/ t_{HM} . The main focus of this study was to present the reactivity loss of PWR spent fuel. However, this report included the results of atom densities for dominant absorbers in spent fuel for each of combination of initial enrichments between 3.0 and 4.25 wt % ^{235}U and burn-up between 5 and 60 GWd/ t_{HM} . Thus, the bandwidths of these RNs, that also include 20 final disposal relevant RNs, can be recalculated from these data for the associated ranges of initial enrichment and burn-up.

The characteristic parameters and physical phenomena that are important for the understanding of the burn-up credit were identified in [Parks et al., 2001]. Parks et al. discussed the effects of several SRPs, such as the fuel and moderator temperatures, the soluble boron concentration, the presence of burnable absorbers, the specific power and

Table 1.3: Overview of previous studies of the SRPs impact on the radionuclide inventory of PWR spent fuel

Studied parameter	BU [GWd/t _{HM}]	RCA data included	Objective of work (final disp. rel. RNs)	Reference
<i>Previous theoretical studies</i>				
IE: 3.0 – 4.25 wt % ²³⁵ U, CT: 2 – 20 years	5 – 60	no	burn-up credit (20 RNs)	[Cerne et al., 1987]
SP, DT, FT, MT, BA	up to 45	no	burn-up credit (14 RNs)	[Parks et al., 2001]
Effects of burnable poison rods	up to 45	no	burn-up credit (13 RNs)	[Wagner and Parks, 2002]
Control Rod Effects	30 and 45	no	burn-up credit (14 RN)	[Barreau, 2006]
<i>Previous studies based on RCA data</i>				
IE: 2.45 – 3.04 wt % ²³⁵ U, FT: 743 – 923 K, SP: 13 – 45 MW/t _{HM} etc.	16 – 46	yes, 19 samples	Validation of the SCALE System (22 RNs)	[Hermann et al., 1995]
IE: 3.0 – 4.5 wt % ²³⁵ U, SP, DT, BA: 0 – 1000 ppm, FT: 700 – 1100 K, MT: 500 – 600 (theoretically)	10 – 50 (theoretically)	yes, 19 samples	burn-up credit (13 RNs)	[DeHart, 1996]
IE, SP, FT, MD	11 – 46 (from RCA data), 10 – 60 (theoretically)	yes, 56 samples	Isotopic uncertainties in burn-up credit (14 RNs)	[Gauld, 2003]
IE: 2.45 – 4.65 wt % ²³⁵ U (from RCA data), 1.5 – 5.5 wt % ²³⁵ U (theoretically)	7.2 – 70.4 (from RCA data), up to 75 (theoretically)	yes, 118 samples	Isotopic bias and uncertainty in burn-up credit (15 RNs)	[Radulescu, 2010]
IE: 2.6 – 4.7wt % ²³⁵ U, etc.	7.8 – 78.3	yes, 51 samples	Uncertainties in predicted isotopic compositions for high BU (24 RNs)	[Gauld et al., 2011]
IE: 2.45 – 4.65 wt % ²³⁵ U, etc.	7 – 60	yes, 100 samples	Isotopic bias and bias uncertainty (14 RNs)	[Radulescu et al., 2012]

downtime on the composition of radionuclides relevant for the burn-up credit. 14 RNs out of this list are relevant for the final disposal.

The study of [Wagner and Parks, 2002] investigated the effect of burnable poison rods (BPR) for PWR burn-up credit. This effect was analysed for 13 final disposal relevant RNs for the burn-up up to 45 GWd/t_{HM}.

The effect of control rods on the spent fuel composition was studied by the Nuclear Energy Agency (NEA) Expert Group on Burn-up Credit Criticality Safety [Barreau, 2006] for the burn-up values of 30 and 45 GWd/t_{HM}. This analysis considered 14 RNs that are relevant for the final disposal.

Previous studies based on RCA data

Precise and detailed information on the operational history has been used also for the validation of several computer codes. In the study of [Hermann et al., 1995] the analyses of PWR spent fuel isotopic composition were used for the validation of the SCALE system. 19 benchmarks were made using the samples from Calvert Cliffs (Unit 1), H. B. Robinson (Unit 2) and Obrigheim PWR plants. These samples correspond to the burn-up of up to 46 GWd/t_{HM}. Moreover, the uncertainties for 22 final disposal relevant radionuclides were determined. These 19 samples with the addition of other 99 samples were also investigated by [Radulescu, 2010]. Here, the main focus was on the propagation of the isotopic bias and uncertainty to criticality safety analyses of PWR waste packages. This study included only 15 RNs relevant for final disposal. However, the [Radulescu, 2010] analysed more data within wider ranges of the parameters. The range of initial enrichment for the experimental data was between 2.45 and 4.65 wt % ²³⁵U and burn-up range was between 7.2 and 70.4 GWd/t_{HM}. Additionally, in this study included the theoretical analysis of the effect of initial enrichment in the range of 1.5 – 5.5 wt % ²³⁵U and of burn-up in the range of 0 – 75 GWd/t_{HM}. The study of [Radulescu, 2010] also comprised the data on 56 samples from the study of [Gauld, 2003], which considered the impact of isotopic uncertainties in burn-up credit.

The study of [DeHart, 1996] investigated the sensitivity and parametric evaluations of significant aspects of the burn-up credit for PWR spent fuel packages. Here, the effect of all SRPs and the modelling assumptions on the criticality of spent fuel up to 50 GWd/t_{HM} were theoretically analysed. The statistical methods for treating isotopic calculational bias were applied to same 19 samples studied by [Hermann et al., 1995]. The study of [DeHart, 1996] included the isotopic compositions for 13 final disposal relevant RNs.

Gauld et al. [Gauld et al., 2011] performed an important study of uncertainties in the predicted isotopic compositions of high burn-up PWR spent nuclear fuel. This comprehensive computational validation exercise evaluated the isotopic assay measurements from different experiments and compiled them into a single document. The isotopic data for 24 final disposal relevant RNs for 51 UO₂ fuel samples from different PWR assemblies were analysed. Selected samples were obtained from fuel rods with initial enrichments from 2.6 to 4.7 wt % ²³⁵U and the burn-up range from 7.8 to 78.3 GWd/t_{HM}.

Radulescu et al. [Radulescu et al., 2012] performed a comprehensive study for the validation of the depletion and criticality computer codes. This report described an approach for establishing a depletion code bias and bias uncertainty in terms of the reactivity difference between measured and calculated radionuclide concentrations. The measured radionuclide concentrations were investigated for 100 PWR fuel samples with initial enrichments varying from 2.453 to 4.657 wt % ²³⁵U and burn-up varying from

7 to 60 GWd/ t_{HM} . The 100 PWR fuel samples were selected from the 118 PWR fuel samples studied by [Radulescu, 2010]. The study of [Radulescu et al., 2012] focused on the RNs that are important for burn-up credit. Only 14 final disposal relevant RNs were investigated.

Conclusion on previous studies

Very often operational history data are incomplete [Hermann et al., 1998]. This is especially true for the moderator density and temperature, fuel density and temperature, boric acid concentration or for the concentration of ^{234}U and ^{236}U in the initial fuel composition data that are required as input for the depletion calculations. In these cases meaningful assumptions are necessary to estimate missing data [Radulescu et al., 2010].

The main focus of all previous studies was the applications for burn-up credit. Thus, not all final disposal relevant RNs (cf. Table 1.1) were investigated. In previous theoretical studies only few SRPs were analysed. Their spectrum of values were not investigated to a sufficient detail. The spread of the SRP values which could be obtained from previous studies based on destructive radiochemical assay (RCA) data is insufficient for the estimation of true variability ranges of these parameters. For some RNs there are only a few RCA data available.

The realistic SRP value ranges can be wider than those investigated in previous studies. As a conclusion, it is necessary to extend the radionuclide inventory analysis to all disposal relevant RNs, whereby realistic variability ranges of all relevant SRP should be covered.

1.4 Calculated RN inventory of international PWR-UO₂ SNF

The information on fuel assembly design and reactor operating data (the SRP data) is owned by nuclear facilities and usually is not publicly available. The knowledge of the SRP impact on the radionuclide inventory composition does not provide particularly valuable information for the nuclear plant personnel, while all the necessary data required for a precise prediction of the total radionuclide inventory is already available. These predictions are typically performed with numerical burn-up calculations and validated by non-destructive measurement methods. Therefore, the inventory data on real spent nuclear fuel assemblies, which could be requested from nuclear agencies, cannot be regarded as true experimental data, while only the concentrations of few RNs are accessible by the non-destructive analysis. Nevertheless, these data represent a great value for validating the presently predicted bandwidths as they are based on realistic fuel design and reactor operating history data.

Therefore, for the validation of bandwidths estimations performed in the present study a wide database of calculated RN inventory of SNF was acquired from several nuclear agencies in USA, Sweden, Switzerland and Germany. Our bandwidths calculations, in which the SRP ranges are estimated based on a limited number (339) of fuel assem-

blies, can be thus compared to the realistic inventory data on a much larger collection of spent fuel assemblies. Table 1.4 gives a short description of the calculated SNF RN inventory data obtained from these countries.

Table 1.4: Calculated RN inventory of international PWR-UO₂ SNF

BU [GWd/t _{HM}]	RCA data included	Objective of work (final disp. rel. RNs)	Reference (country)
7 – 53	no	(59 RNs)	[ORNL, 2016] (USA)
44.8	no	final disposal (44 RNs)	[SKB, 2010] (Sweden)
32.9 – 56.6	no	final disposal (64 RNs)	[NAGRA, 2014] (Switzerland)
55	no	final disposal (64 RNs)	[Peiffer et al., 2011] (Germany)

The Oak Ridge National Laboratory (ORNL) provided calculated inventories (for 59 final disposal relevant RNs) for approximately 2000 US PWR-UO₂ spent fuel assemblies with a burn-up range between 7 and 53 GWd/t_{HM} [ORNL, 2016].

The "Nationale Genossenschaft für die Lagerung radioaktiver Abfälle" (NAGRA) provided calculated inventories of fuel assembly families that represent average data for approximately 3300 Swiss PWR-UO₂ SNF [NAGRA, 2014]. These fuel assembly families correspond to the average burn-up between 32.9 and 56.6 GWd/t_{HM}. All 64 final disposal relevant RNs are included in this data set.

The Swedish inventory data were taken from the "Swedish Nuclear Fuel and Waste Management Co" (SKB) report [SKB, 2010]. This report provides calculated total radionuclide inventory from about 6000 PWR-UO₂ assemblies with an average burn-up of 44.8 GWd/t_{HM}. The calculated inventories give the total mean activity values for 44 disposal relevant radionuclides.

The German inventory data were taken from the "Gesellschaft für Anlagen- und Reaktorsicherheit mbH" (GRS) report [Peiffer et al., 2011]. This report provides calculated activities in Bq per t_{HM} for all 64 final disposal relevant radionuclides. The calculation was performed assuming the average burn-up of 55 GWd/t_{HM} and the initial enrichment of 4.4 % ²³⁵U.

2 Theoretical background

2.1 Physical and mathematical basis to the build-up of radionuclide inventory

The radionuclide composition of used nuclear fuel is largely determined by its behaviour in the reactor core. The principles of reactor physics are very well described in the literature. Here, only the main aspects are highlighted that are important for the understanding of the methodology and results of this study. The main topic is to identify and to understand the process of build-up of the radionuclide inventory of used nuclear fuel, and the phenomena and factors that influence its composition during the time of reactor operation and after shutdown. It is also important to describe the relevant mathematical models and the implementation in the simulation software.

The radionuclide inventory of nuclear fuel changes with the burn-up in the reactor core. The build-up of the radionuclide inventory is caused by the formation and disintegration of nuclides due to radioactive decay and neutron transmutation. The rates of these processes are determined by current RN concentrations, the neutron flux, cross-sections, fission product yields, (n,*)-reaction branching factors and decay constants. In general, the differential balance equation defines the difference between the production and loss terms (cf. equation (2.1)).

$$\frac{dN_i}{dt} = \text{production} - \text{loss}, \quad \text{where } N_i \text{ corresponds to the } i^{\text{th}} \text{ RN from whole radionuclide inventory,} \quad (2.1)$$

and where the production terms include

- + production by fission of precursor RN,
- + production by (n,*)-reaction of precursor RN,
- + production by decay of precursor RN,

and where the loss terms include

- loss by (n,*)-reaction,
- loss by own decay,
- leaks and removal (for PWR can be neglected).

The differential balance equation (2.2) summarizes the physical process of build-up of radionuclide inventory in the reactor core.

$$\begin{aligned}
\frac{dN_i(E, \vec{r}, t)}{dt} = & \underbrace{+ \sum_{k=1}^m \hat{\gamma}_{ik} \int_V \int_E \phi(E, \vec{r}, t) \cdot \sigma_{fk}(E) \cdot N_k(E, \vec{r}, t) \, dE \, dV}_{\text{production by fission of precursor RN}} \\
& + \underbrace{\sum_{j=1}^m \tilde{\gamma}_{ij} \int_V \int_E \phi(E, \vec{r}, t) \cdot \sigma_j(E) \cdot N_j(E, \vec{r}, t) \, dE \, dV}_{\text{production by } (n,*)\text{-reactions of precursor RN}} \\
& + \underbrace{\sum_{q=1}^m l_{iq} \lambda_q \int_V \int_E N_q(E, \vec{r}, t) \, dE \, dV}_{\text{production by decay of precursor RN}} \\
& - \underbrace{\int_V \int_E \phi(E, \vec{r}, t) \cdot \sigma_i(E) \cdot N_i(E, \vec{r}, t) \, dE \, dV}_{\text{loss by } (n,*)\text{-reactions}} \\
& - \underbrace{\lambda_i \int_V \int_E N_i(E, \vec{r}, t) \, dE \, dV}_{\text{loss by own decay}}
\end{aligned} \tag{2.2}$$

where

$i = 1 \dots m$: i is the index of the current RN and m is the total number of all RNs

$\{k, j, q\} = 1 \dots m$: running indices, describe the considered RN

$N_i = f(E, \vec{r}, t)$ [atoms]: atom density of currently considered RN

$\phi = f(E, \vec{r}, t)$ [n/cm²]: neutron flux

$\sigma = f(E)$ [barn]: cross-section for the $(n, *)$ -reactions

$\sigma_f = f(E)$ [barn]: fission cross-section

$\lambda = \text{const}$ [s⁻¹]: decay rate constant

$\hat{\gamma}_{ik} = \text{const}$: fission product yields for the fission of a k^{th} RN into an i^{th} RN

$\tilde{\gamma}_{ij} = \text{const}$: branching fractions for the $(n, *)$ -reaction of an j^{th} RN into an i^{th} RN

$l_{iq} = \text{const}$: branching fractions for decay of a q^{th} RN into an i^{th} RN

The differential balance equation (2.2) is written for a homogeneous medium with a continuous process of nuclide build-up. Before discussing of method for solving this equation, the production and loss terms will be described in some detail.

The fission process (cf. production term by fission of precursor RN in equation (2.2)) depends on the neutron flux, fission product yields, fission cross-section and concentration of precursor radionuclides. The neutron flux is a decisive parameter and it is very complex, it plays an essential role in reactor core. Though for further aspects of the reactor neutronics and kinetics, reference is made here to the literature [Lamarsh and Baratta, 2001]. Note that neutron flux depends on the energy, space and time. The fission product yields are constant parameters of individual quantity for each fissile radionuclide (cf. Figure 2.1). The main part that contributes to the depletion process is ²³⁵U and a non-negligible part about 1/3 yielding from ²³⁹Pu. The fission cross-section

depends on the neutron energy (cf. Figure 2.1). By the fission process the dominant amount of light radionuclides, the so-called fission products, are built-up or mainly with a mass number between 90 and 140 (cf. Figure 2.1).

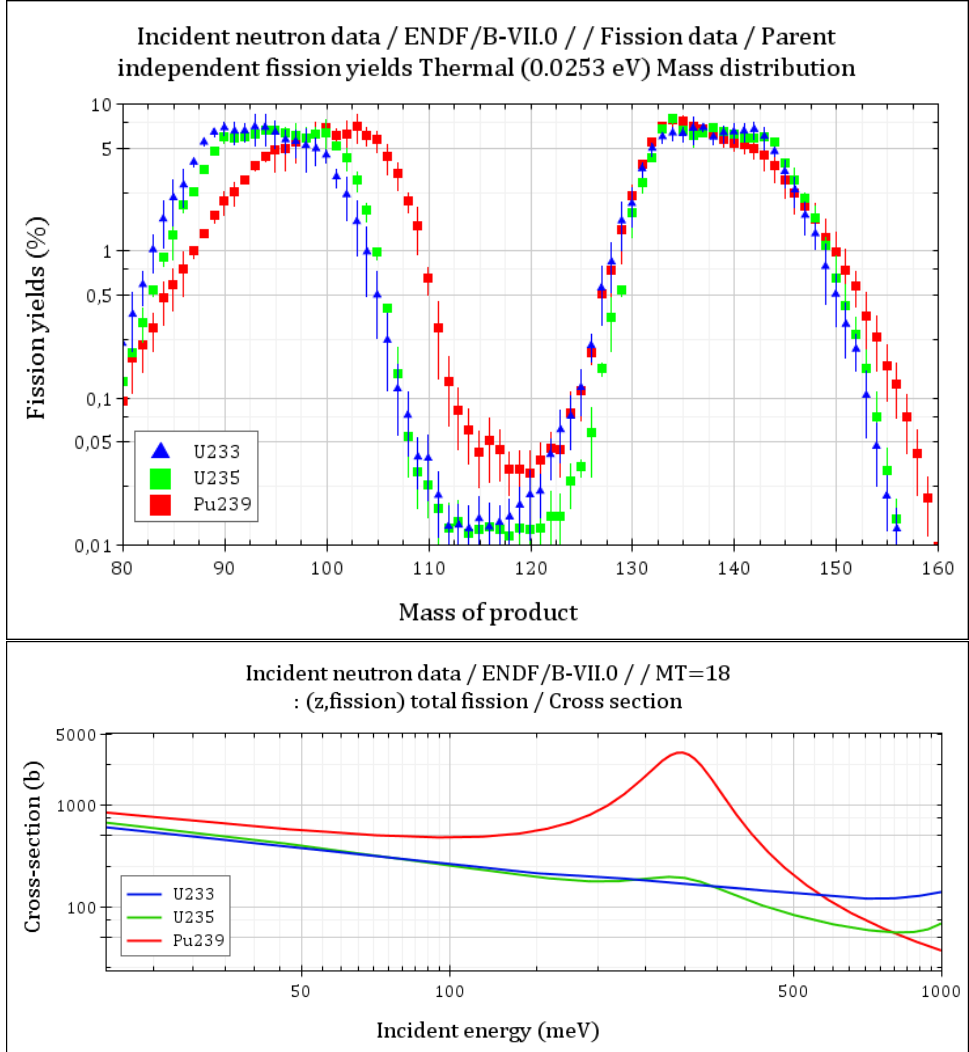


Figure 2.1: Fission product yields for the thermal (0.0253 eV) mass distribution and fission cross-section of ^{235}U , ^{239}Pu and ^{233}U [NEA, 2015a].

Some neutron capture reactions, such as (n,γ) , (n,p) etc. (cf. production and loss terms by $(n,*)$ -reactions of precursor RN in equation (2.2)) don't induced a fission process

rather lead to activation of the surrounding material (fuel, cladding etc.). Thus, in the burnt fuel minor actinides are built-up by chains of the n-capture reactions and decay processes. (n,*)-reactions also depend on the neutron flux, cross sections, branching fractions and their own or precursor RN concentrations.

The last terms of equation (2.2) describes the production by decay of the precursor RN or the loss from self-decay. The decay rate depends on the decay constant and the initial concentration of the considered RN or its precursor RN.

Thus, the solution of this integral differential equation requires the knowledge of the functions ϕ and σ . One possibility of solving equation (2.2) is using of approximations with numerical discretization methods [Dahmen and Reusken, 2006]. Here, the neutron flux is discretized into the multiple energy groups, where each of the group associated with a space- and energy- averaged value. For the sufficiently small time interval by the discretization the space- and energy-averaged neutron flux can be considered constant. Thus, the energy and time continuous neutron flux can be written in the discretized form for each energy group:

$$\phi(E, \vec{r}, t) \longrightarrow \bar{\phi} = \sum_{g=1}^n \phi_g, \quad n : \text{number of energy groups} \quad (2.3)$$

Likewise, the cross-section is discretized to the multiple energy groups and the spectrum-averaged flux-weighted cross sections can be written as:

$$\sigma(E) \longrightarrow \bar{\sigma} = \sum_{g=1}^n \phi_g \sigma_g / \sum_{g=1}^n \phi_g, \quad n : \text{number of energy groups} \quad (2.4)$$

The fission product yields and (n,*)-reaction branching fractions are summarized into common branching fractions for the neutron absorption by any nuclide, which leads to the formation of the currently considered nuclide.

$$\begin{pmatrix} \hat{\gamma}_{ik} \\ \hat{\gamma}_{ij} \end{pmatrix} \longrightarrow \gamma_{ik} \quad (2.5)$$

In equation (2.2) all variables except N_i are time independent constant quantities (assumed over a sufficiently small time interval) and, therefore, this equation can be written in discrete and implemental form (2.6).

$$\frac{dN_i(t)}{dt} = \sum_{q=1}^m l_{iq} \lambda_q N_q(t) + \bar{\phi} \sum_{k=1}^m \gamma_{ik} \bar{\sigma}_k N_k(t) - (\lambda_i + \bar{\phi} \bar{\sigma}_i) N_i(t), \quad i = 1 \dots m \quad (2.6)$$

Reshaping of the equation (2.6) in a matrix form a homogeneous linear system of coupled ordinary first-order differential equations (2.7) with the analytical solution (2.8) is obtained.

$$\dot{N}(t) = A \cdot N(t) \quad (2.7)$$

$$N(t) = e^{At} \cdot N(t_0) \quad (2.8)$$

Here, $N(t) \in \mathbb{R}^m$ is the nuclide vector of the dimension m at a given irradiation time t ; $N(t_0)$ is the initial state of the nuclide vector at a considered time t_0 (typically this corresponds to zero irradiation time of the fresh fuel); $A \in \mathbb{R}^{m \times m}$ is the system matrix containing the rate coefficients for nuclide production and destruction by decay and neutron transmutation, i.e. all constant factors of equation (2.6):

$$\left. \begin{array}{l} \bar{\phi} : \text{space and energy averaged neutron flux} \\ \bar{\sigma} : \text{averaged flux weighted cross sections} \\ \lambda : \text{decay rate constants} \\ l : \text{branching fractions for decays} \\ \gamma : \text{branching fractions for neutron absorption} \end{array} \right\} \rightarrow A \quad (2.9)$$

During the calculations the system matrix A is updated for each new time interval. Thereby, the space-energy-averaged neutron flux is calculated separately and, hence, the flux-weighted cross sections are determined for each successive time step. The values of the continuous energy cross sections and of the remaining quantities of matrix A can be obtained from data libraries, such as ENDF/B-VII.0 [Chadwick et al., 2006] or JEFF-3.2 [NEA, 2014].

Next chapter describes the software system SCALE that is used throughout this work for burn-up calculations and shows analogous steps of solving the differential equation (2.6) or (2.7).

2.2 SCALE as a burn-up code system

SCALE (Nuclear Modelling and Simulation Code System) is a software system developed by Oak Ridge National Laboratory (ORNL) in USA. This software is used in the field of nuclear reactors and transport cask technology for the burn-up credit analysis and calculations of radionuclide composition of used nuclear fuel. For this work SCALE 6.1.0 [ORNL, 2011] with the data library ENDF/B-VII.0 [Chadwick et al., 2006] was used.

The SCALE version 6.1.0 uses the nuclear decay library developed for the ORIGEN code [Bowman, 2011], which was upgraded from ENDF/B-VI.8 to -VII.0 and released in 2011. Experience with the ENDF/B-VII.0 library identified errors and performance issues affecting the evaluated decay sub-library [Gauld et al., 2014]. To address the performance issues, the decay data library in SCALE was upgraded to ENDF/B-VII.1 and released as an user update in 2013 as SCALE 6.1.3. Unfortunately, all calculations throughout this work were done before release 2013. Non-the-less, the deviations in radionuclide composition of SNF associated with this update do not exceed a few percent [Gauld et al., 2014] and, thus, make it a negligible impact to the results for the scope of this work. It was therefore decided to not to revise all the calculations made forward through the work.

SCALE is a very powerful and comprehensive tool. Its particularity is the modular configuration, i.e. that its components are managed from a control sequence called TRITON (Transport RIGor Implemented with Time-dependent Operation for Neutronic depletion) that is used for the BU analysis [ORNL, 2011, p. 4766]. The solution of equation (2.8) is obtained in several steps. In following the components of TRITON that are used in this work will be discussed (cf. Figure 2.2).

TRITON provides several options for the processing of the multigroup problem-dependent cross-section library [ORNL, 2011, p. 4782]. In this work all calculations included the sequence of BONAMI/CENTRM/PMC (cf. Figure 2.2). The BONAMI module uses the Bondarenko method to create unresolved resonance cross-sections [ORNL, 2011, p. 880]. The main scope of CENTRM/PMC calculation is to compute self-shielded and flux-weighted multigroup cross sections (cf. σ_g in equation (2.4)). The flux weighting provides problem-dependent multigroup cross sections in the resolved resonance range [ORNL, 2011, p. 4782]. In this work ENDF/B-VII.0 library with 238 energy groups is used.

In the next step the multigroup neutron flux (cf. ϕ_g in equation (2.3)) is calculated from the NEWT module (cf. Figure 2.2). NEWT is a multigroup discrete-ordinates radiation transport computer code with flexible meshing capabilities that allows two-dimensional (2-D) neutron transport calculations using complex geometric models [ORNL, 2011, p. 2785].

COUPLE collapses the multigroup cross sections using the neutron flux spectrum from a transport calculation and adds the resulting weighted cross sections to produce a binary ORIGEN library that is representative of the user-specified conditions (cf. Figure 2.2) [ORNL, 2011, p. 1256]. At this step the system matrix A of equation (2.8) is completed.

In the last step the time-dependent radionuclide isotopic concentration $N(t)$ is calculated by ORIGEN – an isotope generation and depletion code with the capability to generate accurate problem-dependent cross sections for user-specified designs and conditions. ORIGEN solves the exponential function e^{At} by a matrix exponential approximation method [ORNL, 2011, p. 1299]. The discretization steps imply for sufficiently small time intervals and depletion zones.

For depletion calculations, it is important to add trace quantities of certain nuclides to the inventories of depletion materials in order to accurately track the nuclides impact on cross-section processing and transport calculations as a function of burn-up. By default, TRITON automatically adds to all fuel materials trace quantities of a set of nuclides that have been determined to be important in the characterization of spent fuel. TRITON recognizes fuel materials as any material containing quantities of heavy metals ($Z > 89$) in the standard composition specification. TRITON provides user control of the set of nuclides added to a fuel material through the $parm = (addnux = N)$ control parameter, where N is an integer value [ORNL, 2011, p.4826]. There are four options, for $N = 2$, default setting for the TRITON depletion sequences, 94 nuclides are added (cf. Table T1.3.3. in [ORNL, 2011, p.4827]). This option is also used for all burn-up calculations of this work. Note that at any time a user may add as many trace quantity nuclides as desired, as long as those nuclides exist on the SCALE cross-section library being used in

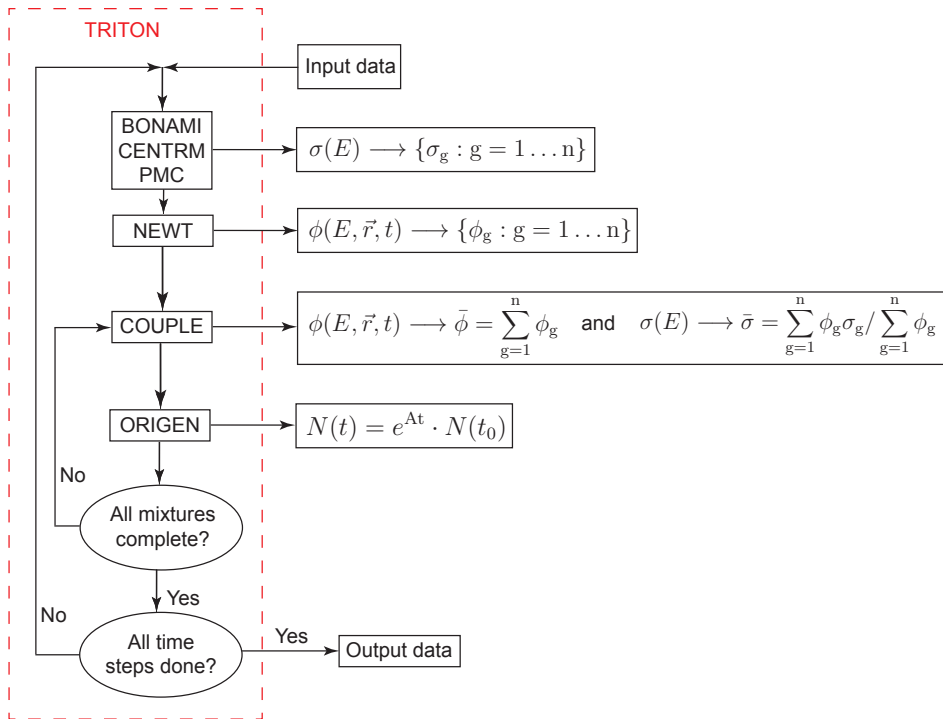


Figure 2.2: Flowchart of control sequence TRITON for the calculation of radionuclide vector [ORNL, 2011]

the calculation. So, the *addnux* option together with cross-section library can be crucial for calculated radionuclide composition, where their impact on individual radionuclides is discussed at the results of this work in the chapter 6.4.

3 Methodology to the determination of realistic bandwidths of SNF RN inventory

The chapter introduces the methods and approaches which constitute the "black-box" (cf. Figure 1.1). The main problem here consists in obtaining realistic RN inventory bandwidths of a spent nuclear fuel at the cooling time zero, i.e. at the discharge time of the assembly, using only the information on the burn-up.

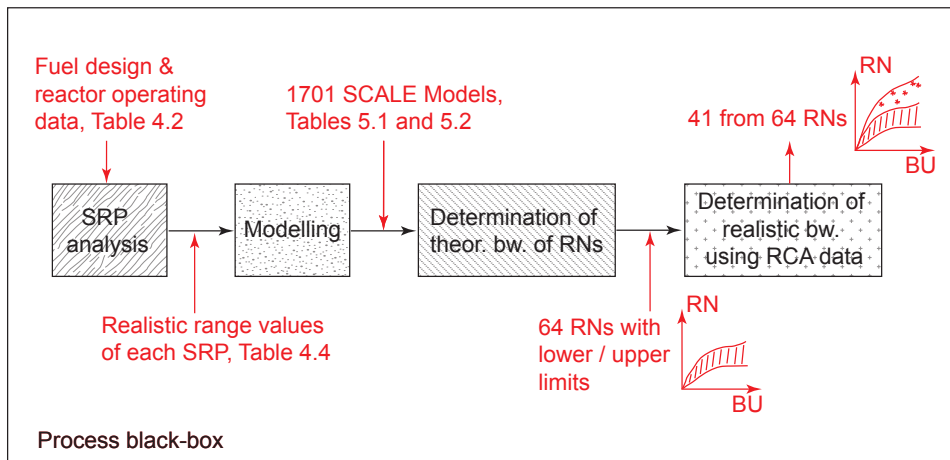


Figure 3.1: Simplified scheme of the methodology to determine realistic bandwidths of the radionuclide inventory.

The Figure 3.1 further subdivides the methodology of the black-box into the four steps (modules), where each module is linked to the specific input and output streams. These streams also define the tasks to be solved by each module. The main idea of this study is to develop the methodologies behind these modules in such a way that their functionalities could be tested and modified independently, and new modules could be added according to the needs of a specific application, e.g. a different type of fuel may require a specific set of SRP, or different accuracy requests may lead to a need of increasing the number of SCALE models, or new available RCA data set could require a change in the size of RN vector. Withih this approach a specific change in an input or an output stream would require an adjustment in one module only. The following four modules are considered (cf. Figure 3.1):

- SRP analysis
- Modelling

- Determination of theoretical bandwidth
- Determination of realistic bandwidth using RCA data

The radionuclide inventory of a single spent fuel assembly with known burn-up is, in principle, obtainable from the fuel design and reactor operating data, i.e. from the SRPs. The task of realistic bandwidths estimation requires the realistic upper and lower limits (boundary values) of each SRP. Within the SRP analysis module nine parameters are processed (cf. Table 1.2). The output provides the corresponding boundary values for each of these parameters (cf. Figure 3.2).

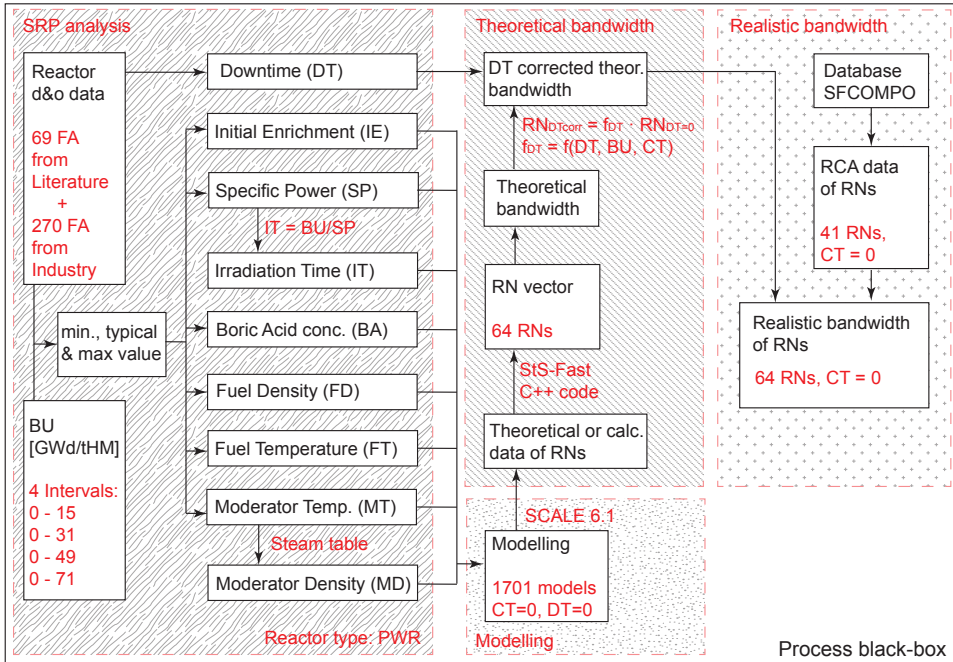


Figure 3.2: Scheme of the determination method for the RN bandwidths derived from reactor design and operating data.

The module "Modelling" defines the whole set of parameters needed for the SCALE calculations which depend on the geometry of fuel assembly and provide other software specific information related to the choice of a nuclear data library or the type of a neutron flux model. Based on these parameterization an optimal number of input files (1701) for SCALE calculations is created with the aim of the best covering of the reactor parameter variation arising from the defined SRP ranges (cf. chapter 5).

The module "Determination of theoretical bandwidths" carries out the SCALE simulations, which produce raw output files for each of 1701 models. Using the own C++

code the necessary information of each relevant radionuclide, like activity and burn-up values of each time step, is selected from these raw data files. Finally the theoretical bandwidths are created for each relevant radionuclide (cf. chapter 6.1).

The module "Determination of realistic bandwidths" prepares RCA data from SF-COMPO and carries out validations of the theoretical bandwidths and, finally, provides realistic bandwidths for each final disposal relevant radionuclide (cf. chapters 6.2-6.4).

4 SRP Analysis

Secondary Reactor Parameter (SRP) is a generic term for all physical phenomena and parameters that can influence the radionuclide composition of used nuclear fuel except for the Primary Reactor Parameters, burn-up and cooling time, that have an essential importance for the RN composition of every single fuel assembly.

There are numerous factors that can influence radionuclide composition. Table 4.1 shows the list of the important SRPs. Some of the parameters (cf. Table 4.1) are not selected for the SRP analysis of this work, because very limited information of experimental data for these parameters has been found.

Table 4.1: Secondary Reactor Parameters

Type of parameter	Name of parameter	Selected for the SRP analysis
Fuel assembly design	Initial Enrichment (IE)	yes
	Fuel Density (FD)	yes
	Impurities in the fuel matrix	no
Reactor or fuel assembly operating data	Specific Power (SP)	yes
	Downtime (DT)	yes
	Irradiation Time (IT)	yes
	Fuel Temperature (FT)	yes
	Moderator Density (MD)	yes
	Moderator Temperature (MT)	yes
	Boric Acid concentration (BA)	yes
	Effect of control rods	no
	Time-varying power load of reactor during irradiation time	no

The aims of this chapter are to identify correlations between BU and SRPs and among the different SRPs, and to determine boundary values of each independent SRP. The each correlation found between the SRPs reduces the number of the necessary SCALE calculations.

4.1 Available data of fuel assembly design and reactor operating parameters

For this work fuel assembly design and reactor operating data of 339 international PWR-UO₂ spent nuclear fuel assemblies (FA) are used, where corresponding values for the nine SRPs are available. The anonymized design and operating data for 270 of these fuel assemblies, which correspond to the German used nuclear fuel assemblies, are

provided by Industry. For the remaining 69 fuel assemblies these data are obtained from several published international technical reports (cf. Table 4.2)

A data set of nine SRPs for one single fuel assembly is usually obtained from several references (cf. Table 4.2). The main sources are primary references that in many cases come from experimental measurement programs on spent fuel samples and do not include average data of all SRPs. An important approach of this work is to reduce the number of assumptions on the fuel design and reactor operating data and to minimize incoherencies or mistakes in the original data. Therefore, the additional references of fuel design and reactor operating data are often needed to complement the SRP data sets available for specific fuel assemblies.

Table 4.2: Publicly available fuel assembly design and reactor operating data on 69 FA

Number of FA	Reactor name	Reference
3	Calvert Cliffs 1	[Radulescu et al., 2010], [Guenther et al., 1988a], [Guenther et al., 1991], [Guenther et al., 1988b]
1	GKN 2	[Radulescu et al., 2010]
1	Gösgen	[ORNL, 2003]
7	KWO	[Radulescu et al., 2010], [Barbero et al., 1980], [Guardini and Guzzi, 1982]
6	Point Beach 2	[Gauld et al., 2010]
16	Ringhals 2	[Murphy and Gauld, 2010]
14	Ringhals 3	[Murphy and Gauld, 2010]
1	Robinson 2	[Barner, 1985], [Radulescu et al., 2010]
8	San Onofre 1	[Gauld et al., 2010]
2	Takahama 3	[Radulescu et al., 2010], [Nakahara et al., 2002]
4	Trino Vercellese	[Bannella et al., 1977], [DeHart and Hermann, 1996], [Radulescu et al., 2010]
6	Turkey Point 3	[Gauld et al., 2010], [DeHart and Hermann, 1996]

All SRP data on 339 fuel assemblies are fuel assembly averaged values, which assume the averagings of two types. One type relates to the averaging over the entire irradiation time of FA. Each of nine SRP includes these values, so that for one single used FA one set of nine SRP values is given. The other type relates to the averaging over one reactor operating cycle. In this study this type of averaging is marked with index *i*. In general, the reactor operating cycle values are completely available only for SP, IT and DT. Therefore, in this work mainly the fuel assembly averaged and entire irradiation time averaged SRP variability values are considered.

For the SRP analysis a uniform distribution of assemblies for the entire burn-up range is assumed.

4.2 Correlations between SRPs

The aim here is to find linear relations between BU and SRPs and between SRPs themselves. This information is required for obtaining realistic variability ranges of those SRPs, which are dependent on the burn-up. Moreover, the correlations between the SRPs reduce the number of required calculations (cf. chapter 5). It is important also to check original data for correlations. Some SRPs such as $MT \sim MD$ and $BU \sim (SP, IT)$ naturally correlate with each other, however, it is important to show that these correlations are present within the original data. Table 4.3 shows the corresponding correlation coefficients between BU and SRPs and between SRPs themselves. Thereby, the correlation coefficients, which assigned the index i , correspond to the SRP values per reactor operating cycle, while the coefficients, which don't have such an index, correspond to SRP values averaged over the entire irradiation time experienced by the fuel assembly.

Table 4.3: Correlation coefficients between BU and SRPs and between different SRPs.

	IE –	SP SP_i	IT IT_i	BA BA_i	FD –	FT FT_i	MD MD_i	MT MT_i	DT DT_i
BU	0.75	0.28	0.29	0.00	0.10	0.14	0.30	0.30	0.03
BU_i	–	0.90 _i	0.00 _i	0.03 _i	–	0.38 _i	0.78 _i	0.78 _i	0.05 _i
IE	–	0.14	0.27	0.04	0.05	0.07	0.11	0.10	0.07
–	–	–	–	–	–	–	–	–	–
SP		–	0.16	0.04	0.22	0.14	0.41	0.39	0.01
SP_i			0.05 _i	0.08 _i	–	0.52 _i	0.76 _i	0.77 _i	0.03 _i
IT			–	0.06	0.03	0.01	0.00	0.00	0.01
IT_i				0.01 _i	–	0.00 _i	0.17 _i	0.16 _i	0.00 _i
BA				–	0.05	0.01	0.00	0.00	0.00
BA_i					–	0.12 _i	0.02 _i	0.03 _i	0.02 _i
FD					–	0.23	0.22	0.22	0.01
–						–	–	–	–
FT						–	0.43	0.45	0.00
FT_i							0.18 _i	0.18 _i	0.00 _i
MD							–	0.99	0.00
MD_i								0.98 _i	0.10 _i
MT								–	0.00
MT_i									0.09 _i
DT									–
DT_i									–

Correlation between BU and SRPs

This subsection provides a more detailed description of the correlations between BU and SRPs, which are expressed as the values of the correlation coefficients in the first

row of Table 4.3. The first line in the first row shows the correlation coefficients between BU and SRPs which are averaged over the entire irradiation time, while the second line shows the analogous data for the averaging over the reactor operating cycle (these values are marked with the index i). In the case of the entire irradiation time averaging the quasi linear relation between BU and initial enrichment (IE) is clearly observed (the correlation coefficients is equal to 0.75). Thus, the limits and typical values of IE depend on BU. Consequently, these values must be determined according to the BU (cf. section 4.3).

The low value of the correlation coefficient of 0.28 (the second box in the first row) shows that the SP values are almost independent of the BU. However, the reactor operating cycle values show very high linear relation to BU (the correlation coefficient is 0.90). These relationships can be clearly understood. Generally, BU is the product of SP and IT. Thus, for reactor operating cycle values the following equation is fulfilled:

$$BU_i = SP_i \cdot IT_i \quad (4.1)$$

Note that the typical reactor operating cycle time is about 300 days with relatively small variety. Here, the 339 FA database contains about 1200 irradiation time values per reactor operating cycle (IT_i) and more than 95 % of these values are between 250 and 350 days. Thus, in this case the irradiation time is approximately a constant and, therefore, BU_i depends essentially on the SP_i . This explains the correlation coefficient of 0.90 between BU_i and SP_i in equation 4.1.

The weak correlation between BU and SP for entire irradiation time averaged values can be also explained, because total BU of a single FA is build-up in several operating cycles (cf. equation (4.2)), which can correspond to very different irradiation times and to very different specific power values. Typically one FA can have between 2 and 5 reactor operating cycles, while SP_i can vary between 5 and 60 MW/ t_{HM} . It is often observed that for most cycles the FA experiences a high specific power in the middle of reactor core, while for one or two cycles the same FA is placed at the periphery of reactor core, where the specific power is low. Thus, in this case, the IT cannot be considered as a constant, while it plays the same role as the SP in building-up the BU. This also applies to the similar correlation coefficients between BU and SP and between BU and IT, which are given by 0.28 and 0.29, respectively. Therefore, the relation between BU and SP is non-linear.

Based on this analysis the limits and typical values of SP are set dependent on the burn-up values, similarly to that for IE (cf. section 4.3), while the IT values are calculated from BU and SP.

$$\underbrace{\sum_{i=1}^n BU_i}_{BU} = \underbrace{\sum_{i=1}^n (SP_i \cdot IT_i)}_{SP} / \underbrace{\sum_{i=1}^n IT_i}_{IT} \cdot \underbrace{\sum_{i=1}^n IT_i}_{IT}, \quad n \text{ is number of FA cycles} \quad (4.2)$$

Good linear correlations are observed between BU_i and MD_i , MT_i , but not between BU_i and FT_i (cf. Table 4.3, first row, boxes 6-8). However, these SRPs include values per reactor operating cycle for a small number of fuel assemblies only. The "averaged"

values of these SRPs show low correlation to BU. Therefore, the values for these SRPs are fixed and assumed independent of burn-up.

The remaining SRPs have very small values of the correlation coefficients what implice the weak dependens on BU. This is observed both for the entire irradiation time averaged values and for the operating cycle averaged values. Thus, the limits and typical values for these SRPs are fixed for the entire range of burn-up.

Correlation amongst the SRPs

This subsection provides a more detailed description of the correlations between SRPs themselves, which are expressed as the values of the correlation coefficients in rows 2-10 of Table 4.3.

The correlation coefficients show that IE has no relation to all other SRPs (cf. second row in Table 4.3).

The correlation coefficients per reactor operating cycle between SP_i and MD_i , MT_i and FT_i show very close behaviour like by BU_i (cf. first and third row in Table 4.3). This is also understandable, because SP_i determines BU_i (cf. equation (4.1)). However, only the SRP data per reactor operating cycle show this very well correlation that correspond to a small number of FA data. Thus, SP are defined as no correlated to MD, MT and FT.

The low values of correlation coefficients of BA and FD suggest that these SRPs do not significantly depend on any of SRPs (cf. fifth and sixth rows accordingly in Table 4.3).

The correlation coefficients of FT of about 0.45 show that this SRP is only weakly dependent on MT/MD (cf. seventh row in Table 4.3). However, these coefficients are too small to be significant. Thus, FT are defined as not correlated to MD, MT.

Good linear correlation is observed between MT and MD, which is also consistent with the thermohydraulic law. Thus, in this work the limits and typical values of MT are determined from the FA database (i.e. from 339 FA data), while the MD range was fixed via steam table correlation.

The correlation coefficients of DT show no dependens on the other SRPs.

Consequently, among the SRPs, BU correlates to IE; IT is calculated from BU and SP, while BU is independent on the other SRPs. Moreover, seven SRPs do not correlate to each other (IE, SP, FD, FT, BA, MT and DT), while MD correlates to MT. Thus, the boundaries and typical value of IE and SP are adapted to BU, while the boundaries and typical values of FD, FT, BA and MT are fixed for entire range of BU. The DT is set to zero (cf. section 4.4).

4.3 Boundaries and typical values of SRPs

The aim of this section is to determine the boundaries (or the minimum/maximum values) and typical values of the independent SRPs using the set of 339 FA data. The typical value depending on the type of the SRP is defined either as a average of all

available FA data or as a median value between the minimum and maximum. Because BU correlates to IE and SP, it is necessary to divide BU in several ranges. To optimize the number of models (or calculations) the BU range is divided in the following four ranges:

- low burn-up 0 – 15 GWd/t_{HM},
- middle burn-up 0 – 31 GWd/t_{HM},
- high burn-up 0 – 49 GWd/t_{HM},
- very high burn-up 0 – 71 GWd/t_{HM},

Table 4.4 summarizes the boundaries and typical values for each SRP and for each of the defined BU ranges. A more detailed explanation to these values is discussed below.

Table 4.4: Variability ranges of SRP values.

BU [GWd/t _{HM}]	IE [wt % ²³⁵ U]			SP ¹ [MW/t _{HM}]			BA [ppm]			FD [g/cm ³]			FT [K]			MT ² [K]		
	min.	typ.	max.	min.	typ.	max.	min.	typ.	max.	min.	typ.	max.	min.	typ.	max.	min.	typ.	max.
0 – 15	1.0	1.9	5.0	14	20	25	260			9.46			640			540		
0 – 31	1.9	3.0	5.0	14	25	39	500			10.4			773			585		
0 – 49	3.0	4.4	5.0	25	39	48	820			10.85			1140			605		
0 – 71	4.4	–	5.0	39	43	48												

DT [days] is zero for all model configurations, i.e. DT = 0

¹ IT [days] relates to the BU and SP via equations (4.1) or (4.2)

² MD [g/cm³] correlates to MT via steam table

Boundaries and typical values of IE

The initial uranium enrichment is a basic parameter of uranium oxide (UO₂) fuel. It is important to have the information of uranium isotopic distribution that should include ²³⁴U, ²³⁵U, ²³⁶U and ²³⁸U. The minor uranium isotope ²³⁴U is present in natural uranium and its content increases in the enrichment process together with ²³⁵U. The isotope ²³⁶U does not exist naturally, but it is introduced during fuel processing when reprocessed uranium is mixed with natural uranium. Some experimental programs do not report ²³⁶U, because this information is considered sensitive. Experimental reports often provide only the initial ²³⁵U enrichment, while the values for the other minor isotopes of ²³⁴U and ²³⁶U are not available. Moreover, it is important to note that the initial concentrations of ²³⁴U and ²³⁶U can be highly dependent on origin of the

fuel, as different countries use different amounts of reprocessed fuel in fuel production. Thus, because of the lack of information, the focus of this study is put on the uranium composition that includes only ^{235}U and ^{238}U . The initial concentrations of ^{234}U and ^{236}U are set to zero. The effect of this unknown initial uranium composition will be discussed in chapter 6.

The [Henkel, 2008] contains a discretized representation data of BU-IE distribution for more than 90000 PWR commercial spent nuclear fuel assemblies (cf. Figure 4.1). Here, the numbers of assemblies are shown in a colour-coded format. The colour indicates the number of assemblies with burn-up and enrichment falling within each bin, as indicated in the legend. The black points in the Figure 4.1 correspond to 339 fuel assemblies discussed in this work, where each point represents one fuel assembly. The data from 339 FA database covers very well the possible range of IE distribution. This gives a good indication to that the distribution ranges of all other SRPs are probably wide. Using of BU-IE distribution data for more than 90000 FA the boundaries and typical value of IE can be determined more realistically. This idea has been used by this work.

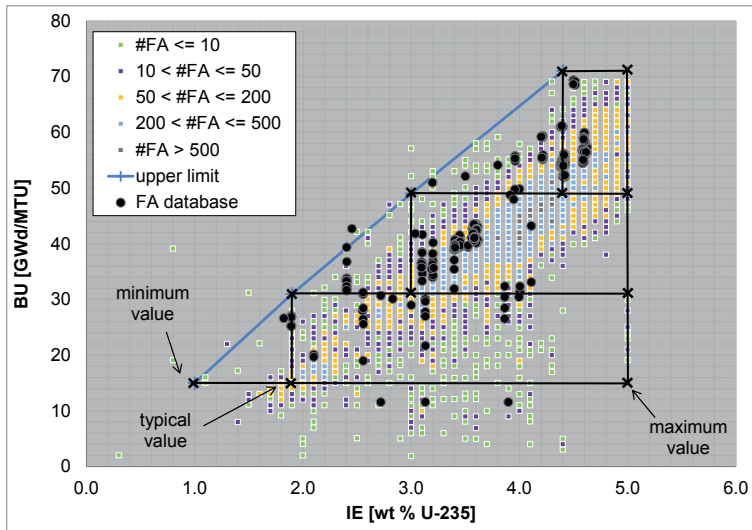


Figure 4.1: BU vs. IE. Here, the IE boundaries are defined according to the maximum burn-up of 15, 31, 49 and 71 GWd/ t_{HM} . The coloured points correspond to real and for the higher burn-up data projected PWR fuel assemblies [Henkel, 2008]. Each coloured point indicates the number of fuel assemblies between less than 10 (green points) and more than 500 (dark gray points). The black points correspond to 339 fuel assemblies from this work, where each point represents one fuel assembly.

Using the BU-IE distribution of 90000 FA the boundaries of four BU ranges that are discussed on beginning of this section are set such that the necessary number of the

future calculations is minimized. For example, the typical value of IE from the low BU range corresponds to the minimum value of IE from the middle BU range etc. (cf. Figure 4.1). Typical value here is a value, which represents the largest number of existing fuel assemblies within this BU range, e.g. for low BU range the typical value of IE (cf. Figure 4.1 blue point) corresponds to number of fuel assemblies between 200 and 500.

Thus, the boundaries and the typical values for each burn-up range can be well defined (cf. Table 4.4). The maximum value of each BU range is set to 5.0 wt % ^{235}U , in order to include the fuel assemblies with high IE and low BU, which correspond to early shutdowns of NPPs. This is particularly relevant for Germany. For the very high BU interval up to 71 GWd/t_{HM} the typical and maximum values of IE coincide at the same value of 5.0 wt % ^{235}U .

Boundaries and typical values of SP/IT

In general, the SP values are provided by reactor operators and are obtained using neutronic core simulation codes. However, the level of documentation in reference reports may be very inconsistent to each other. Modern experimental programs often report very detailed time-dependent power values for the analysed fuel samples. However, some older programs report only the assembly averaged burn-up at the end of each operating cycle. Knowing the cycle length, this information can be used to derive the cycle-averaged assembly power for each assembly. For this work this information is very important.

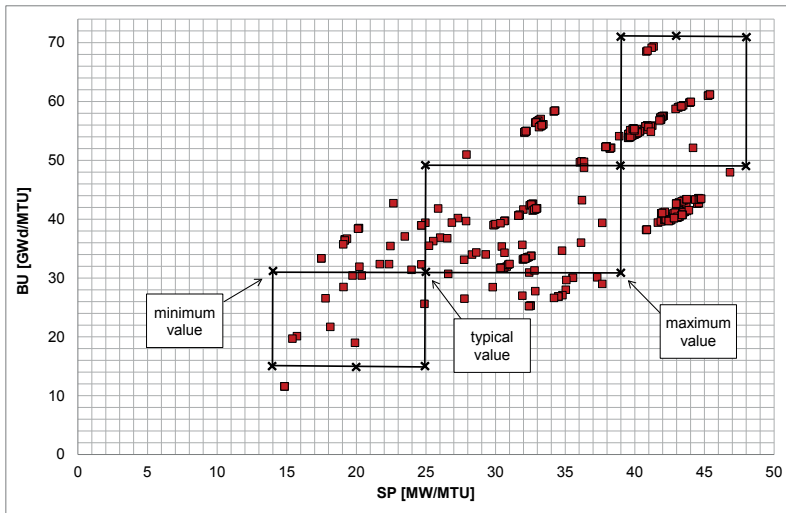


Figure 4.2: BU vs. SP. Definition of SP boundaries and typical value for each BU interval

Similarly to the case of IE, the ranges and the typical values of SP are adapted to BU. Thus, for each BU interval three values are defined: the minimum, the maximum

and the typical value (cf. Table 4.4). These values are selected such that the number of required calculations is minimized (cf. Figure 4.2). The IT values are calculated according to equation (4.2).

Boundaries and typical values of BA

The presence of dissolved boron in the moderator of a PWR changes the neutron flux spectrum in the fuel and therefore influences the plutonium production and concentrations of highly absorbing isotopes. The critical boron concentration is an important parameter for reactor operation and its value during each cycle is normally available from the operator. In cases where the detailed time variation of boron concentration is not available, the use of cycle-average concentrations gives similar results for depletion modelling.

Start-up to full power operation of the reactor typically requires one or two days of low power operation for testing, during which the critical boron concentration is very high. The boron concentration then exhibits an abrupt decrease because of the build-up of ^{135}Xe in the first few days of operation. After that, the decrease is very linear and proportional to fuel reactivity decrease due to the depletion of fissile atoms and the build-up of fission products and other neutron absorbers.

Because the detailed time variation of boron concentration are not available for most of 339 FA data, the cycle-average concentrations are used in this work. The boundaries and the typical values are obtained from 339 FA data accordingly to the entire BU range (cf. Table 4.4).

Boundaries and typical values of FD

The volumetric fuel pellet density is usually given as an absolute or a relative density to the theoretical density (TD). The required value of fuel density balances the advantage of the increased fuel loading in the reactor for longer cycle operation and the need to keep some void fraction in the pellet for limiting the effects of swelling due to gas fission production. The fuel pellet is usually fabricated with a dishing and chamfer that effectively reduces the density compared to the full fuel volumetric density. It is this effective fuel density that is usually used in neutronics codes. It is important to clearly identify, if possible, if the fuel density value is the actual density or the effective (linear) density.

Fuel linear density may be available in the experimental reports. When details of the pellet dimensions (dishing etc.) are not provided, it may be possible to estimate the effective fuel density using the active fuel (stack) length and the mass of fuel in the stack (rod or assembly). For UO_2 fuels, the as-fabricated nominal pellet density is typically 94-97 % of the theoretical density, where $\text{TD} = 10.96 \text{ g/cm}^3$.

The majority of the FD values from the 339 FA database are centered at the value of 10.4 g/cm^3 and not exceed 10.44 g/cm^3 . For the conservative approach the maximum value of FD is set as 99 % of theoretical density (cf. Table 4.4).

Boundaries and typical values of FT

Fuel temperature is not measured in commercial reactors but is calculated with codes, using either simplified models created solely for the radial temperature or more detailed and complex thermo-mechanical models. In most cases the fuel temperature will be given by the plant operator as a volume-average temperature or as neutron-absorption equivalent (effective) temperature.

The fuel temperature gradient between pellet centre and pellet surface is directly proportional to the linear power with limited dependence on the pellet radius. For fresh UO_2 fuel a typical value of fuel pellet temperature gradient is $350\text{ }^\circ\text{C}$ for a linear power of 200 W/cm while for highly irradiated fuel a gradient of $550\text{ }^\circ\text{C}$ is more representative.

The most significant variable affecting fuel temperature apart of the linear power is the fuel matrix thermal conductivity. Therefore, there is a significant difference between a UO_2 rod, a mixed oxide rod or a gadolinium fuel rod. The fuel conductivity is highly affected by the build-up of other chemical fission product species and hence the gradient increases with fuel burn-up.

The temperature of the fuel pellet surface is also strongly influenced by the fuel and clad gap that varies in width during irradiation. The gap exists at low irradiation of the fuel that leads to a pellet-surface to coolant gradient of $150\text{ }^\circ\text{C}$ at 200 W/cm . At higher irradiation the gap is completely closed due to swelling of the fuel and the gradient decreases to about $100\text{ }^\circ\text{C}$.

A typically uncertainty for the reported fuel temperature is $50\text{ }^\circ\text{C}$ at the level of one standard deviation. When fuel temperature data are not given and must be estimated, the uncertainty should be increased significantly, e.g. $100\text{ }^\circ\text{C}$.

The typical values of FT are obtained from average values of 339 FA and the minimum and maximum values from 339 FA data per operational cycle in order to take more conservative approach (cf. Table 4.4).

Boundaries and typical values of MT/MD

The moderator temperature and moderator density are correlated to each other via thermohydraulic law. The neutron spectrum in the fuel is very dependent on the MT/MD and has a impact on the nuclide composition in the fuel. For PWRs the reactor pressure is fixed and the MT variations between the inlet and outlet of the core are only due to the MD change. If the only information available is the core inlet water temperature, the corresponding temperature and density at sample location can be accurately estimated by a simple heat balance between core inlet and sample position knowing the axial power distribution in core [Delette et al., 2004].

The typical values of MT are obtained from average values of 339 FA and the minimum and maximum values from data per operational cycle in order to take more conservative approach (cf. Table 4.4). The MD values are determined via steam table accordingly.

Boundaries and typical values of DT

The downtime is a reactor operating parameter and can have significant impact of some radionuclides. For this work the DT is able to eliminate and so the values are set to zero. The method of DT elimination is described in next section 4.4.

4.4 Downtime analysis

Downtime (DT) of a single FA is the time, where this FA is taken out from a reactor core between two operating cycles. Typically this time is between consecutive operating cycles and corresponds to a rather short time of one or two months. However, it is often that a FA is being out of reactor core for one or more operating cycles, and that causes a much longer intermittent down time that comprises longer decay time of radionuclides for this FA. The reload and management of the FAs in the reactor core results from the operational conditions of the NPP. Therefore, DT can vary very widely, and this can have a significant effect on the concentration of some radionuclides.

The correlation analysis has shown that DT has no interdependencies with BU and the other SRPs (cf. Table 4.3). Thus, the DT impact on radionuclide composition can be analysed separately from the other SRPs.

The aim of the downtime analysis is to show that the determination of theoretical bandwidths can be made using a model with zero DT. The theoretical bandwidths with zero downtime calculations are used as a reference for the bandwidths and must be corrected for those radionuclides that are significantly affected by DT variations.

The 339 FA database provides a burn-up averaged DT value and DT_i values per operational cycle for each fuel assembly (cf. Figure 4.3). The average DT per fuel assembly (red dots in the Figure 4.3) corresponds to the wide interval between 13 and 1400 days, while the average DT for all 339 FAs is about 120 days. The DT_i per reactor operational cycle (blue dots in the Figure 4.3) may vary within an even wider range between a few days and almost 3000 days. However, these cases are not very frequent.

The Figure 4.4 shows the DT_i distribution for all 339 FAs that corresponds to 900 DT_i values. A short downtime up to a few months corresponds to 84 % of all 339 FAs and is a typical time for the usually applied reload and fuel assembly management. A short DT_i is distributed fairly equally between first, second and third cycles. The majority DT_i values of the fourth and fifth cycles correspond also to the short downtime. The downtime of about 400 days corresponds to the 10 % of all 339 FAs. This time comprises typically one reactor operation cycle, during which the FA is discharged from the core into a cooling pool. These values mostly correspond to the second cycle. Less than 4 % of all 339 FAs have downtime of about 750 days. These FAs experience down times covering two operational cycles, in which these FA were placed into the cooling pool. These downtimes are distributed fairly equally between all cycles with exception of the fifth one. A very long downtime of more than 800 days corresponds to 2 % of all 339 FAs. These DT_i values correspond to the second or third cycles. This long DT_i includes more than two operational cycles, in which these FAs are placed in the cooling

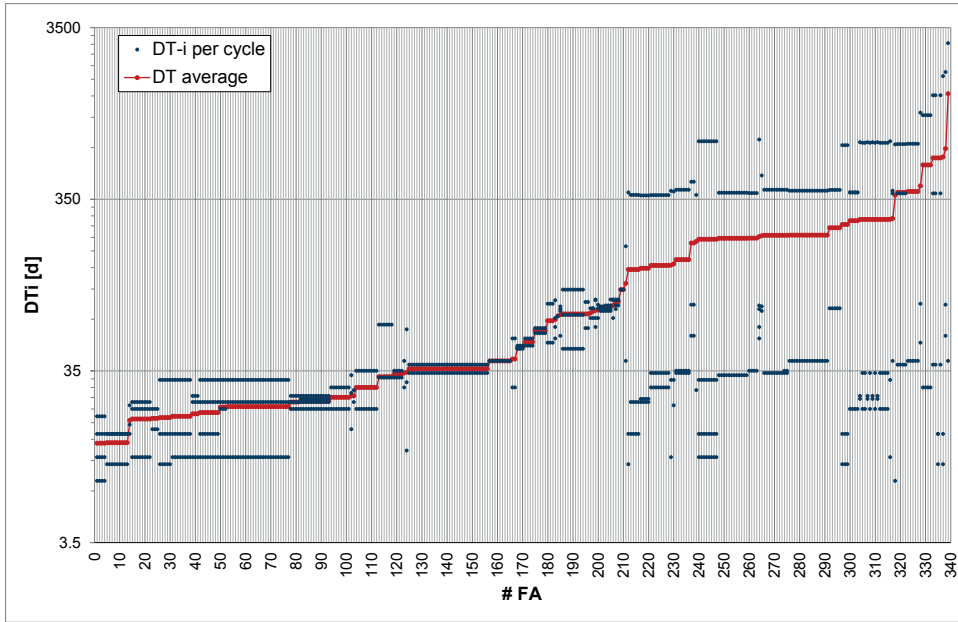
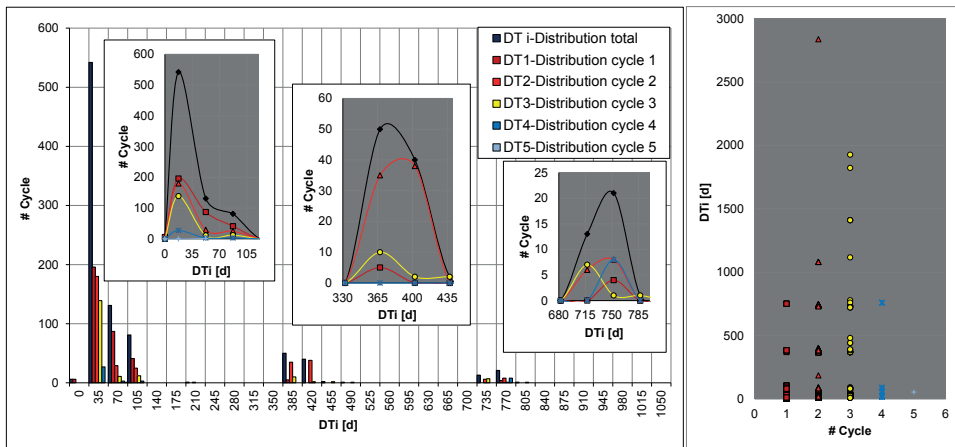


Figure 4.3: DT distribution.

Figure 4.4: DT_i distribution per reactor operational cycle.

pool. The Table 4.5 summarizes the DT_i pre-analysis of 339 FAs, which is aimed to determine the input conditions for the DT modelling analysis. Of course this particular

DT_i distribution may not be applied to general case. However, the task of the first step is to determine the conservative and realistic DT_i that covers possibly more than 90 % of the FAs. Thus, the value of $DT_i=400$ days was chosen as the best representative value for the modelling.

Table 4.5: DT_i distribution

100 % or 900 DT_i	84 %	60 %	$DT_i < 35$ d	fairly equally distributed between first, second and third cycles
		24 %	$35 \text{ d} < DT_i < 105$ d	first cycle dominant
	10 %		$DT_i \sim 400$ d	second cycle dominant
	4 %		$DT_i \sim 750$ d	fairly equally distributed between first, second, third and fifth cycles
	2 %		$800 \text{ d} < DT_i < 3000$ d	occurs by second and third cycles

The analysis performed at the first stage suggests that the operation history of a typical FA can be modelled under the assumption of only one durable period (DT_i), which can be set the value of 400 days. The other DT_i periods within the operation history could be modelled as short intervals of 50 days each. The next (second) stage is to determine at which position within the operational history this durable period ($DT_i=400$ days) makes the largest impact on the final RN composition. The pre-analysis based on all 339 FAs shows that this durable period of downtime corresponds most frequently to the second cycle (cf. Table 4.5). This observation, however, might not hold in general. The impact of the position of the longest DT_i within the operational history is analysed here using simulations, where $DT_i=400$ days is placed on the different position, assuming the FA operational history for burn-up of 65 GWD/ t_{HM} . Additionally, a simplified reference model is investigated, where the $DT_i=400$ days is placed after each operational cycle. Table 4.6 provides model properties for SCALE simulations, which correspond to this analysis. The results of the second stage show that the location of the longest DT_i at the end of the fuel assembly operating history makes the largest impact on the RN composition. Comparing this particular model with the simplified model shows that deviations between these two models do not exceed 10 – 15 %. Thus, the further DT analysis of theoretical bandwidths assumes the simplified model, which corresponds to the most conservative case.

In general the DT impact on the radionuclide composition is a complex process, which must be considered separately for each radionuclide. Here, it is important to understand the behaviour of the radionuclides due to the variation of the realistic downtime and to understand consequences of the approximations in downtime modelling on the further results. In the next stage the influences of the downtime on each RN concentrations are determined and their magnitudes are characterized. These magnitudes are computed with aid of SCALE calculations applied to the cases of $DT=0$ and $DT=400$ days. Table 4.6 gives the initialization of input data as averaged values on each SRP, which are necessary for this analysis.

The determination of the magnitude using the averaged DT impact of $DT=400$ days

Table 4.6: Model of DT analysis

Geometry	16×16 AFA 3G [NEI, 2004]
Neutron flux modeling	newt 2D
Data library	ENDF-B/VII.0
Burn-up	0 – 65 GWd/t _{HM}
Specific Power	36 MW/t _{HM}
Initial Enrichment	4.0 % wt. ²³⁵ U
Fuel Temperature	900 K
Moderator Temperature	580 K
Fuel Density	10.408 g/cm ³
Moderator Density	0.73 g/cm ³
Boric Acid concentration	460 ppm
Downtime	400 d

gives the best conservative estimate, which covers at least 94 % of all 339 FAs. The magnitude of the DT impact, denoted as the multiplication DT-correction factor f_{DT} , is generally a function of downtime, burn-up and cooling time (cf. equation (4.3)).

$$RN_{DT_{corr}} = f_{DT}(DT, BU, CT) \cdot RN_{DT=0} \quad (4.3)$$

Referring to the magnitude of this impact all radionuclides can be split into the three groups (cf. Table 4.7):

- RNs independent of DT (31 RNs), i.e. the deviations in comparison to calculations with DT=0 constitute 2 % or less.
- RNs conservative by DT=0 (17 RNs), i.e. the DT impact has decreasing effect on RN concentration in comparison to calculations with DT=0. In this case the multiplication factor $f_{DT_{max}}$ is applied to the lower limit of the theoretical bandwidth (cf. Table 4.7).
- RNs underestimated by DT=0 (16 RNs), i.e. the DT impact has increasing effect on RN concentration in comparison to calculations with DT=0. In this case the multiplication factor $f_{DT_{max}}$ is applied to the upper limit of the theoretical bandwidth (cf. Table 4.7).

Table 4.7 summarizes the DT effect on the radionuclides' contained in the PWR-UO₂ used nuclear fuel. There are 31 RNs that are independent of DT. The values of 17 RNs are overestimated within this analysis. Thus, the values could be considered conservative in the calculations with DT=0. These RNs represent fission products (β^- decay). The maximum difference between DT=0 and DT=400 days of 60 % is observed for ¹⁴⁴Ce and ¹⁴⁴Pr. Note that these differences correspond to high burn-up up to 65 GWd/t_{HM} are independent of CT. For burn-up less than 65 GWd/t_{HM} these differences

decrease. 16 RNs, which represent the actinides and ^{152}Eu and ^{93}Mo with β^+ decay, are underestimated by calculations with $\text{DT}=0$. Here the maximum difference of 450 % is observed for ^{226}Ra . The maximum differences for most RNs are obtained for $\text{CT}=0$. At increase in CT these differences tend to zero. Only for two RNs (^{238}Pu and ^{234}U) the differences increase with increasing CT . The detailed results for each RN will be discussed in chapter 6.4 in the context of the determination of realistic bandwidths.

Table 4.7: Multiplication DT-correction factor for averaged $\text{DT}=400$ days, $\text{BU}=[0,65]$ GWD/t_{HM} and $\text{CT}=[0,5]$ years

RNs independent of DT $f_{\text{DT}} = 1$	RNs conservative by DT=0			RNs underestimated by DT=0		
	RN	$f_{\text{DT,max}}$	Remark	RN	$f_{\text{DT,max}}$	Remark
$^{108\text{m}}\text{Ag}$, ^{243}Am , ^{14}C , ^{249}Cf , ^{251}Cf , ^{244}Cm , ^{245}Cm , ^{246}Cm , ^{247}Cm , ^{248}Cm , ^{154}Eu , ^{155}Eu , ^3H , ^{129}I , ^{237}Np , ^{107}Pd , ^{239}Pu , ^{240}Pu , ^{241}Pu , ^{242}Pu , ^{243}Pu , ^{244}Pu , ^{103}Ru , ^{124}Sb , ^{79}Se , ^{126}Sn , ^{99}Tc , ^{235}U , ^{236}U , ^{238}U , ^{93}Zr	$^{110\text{m}}\text{Ag}$	0.9		^{227}Ac	4.1 2.4	by $\text{BU}=65$, $\text{CT}=0$ by $\text{BU}=65$, $\text{CT}=5$
	^{144}Ce	0.6	by $\text{BU}=[30,65]$	^{241}Am	1.6 1.08	by $\text{CT}=0$ by $\text{CT}=5$
	^{134}Cs	0.8		$^{242\text{m}}\text{Am}$	1.7	
	^{135}Cs	0.97 1	by $\text{BU}=[55,65]$ by $\text{BU}=[0,55]$	^{242}Cm	1.8 1.7	by $\text{BU}=[0,45]$ by $\text{BU}=65$
	^{137}Cs	0.94 0.97	by $\text{BU}=65$ by $\text{BU}=30$	^{243}Cm	1.7 1.5	by $\text{BU}=[0,45]$ by $\text{BU}=65$
	^{85}Kr	0.8	by $\text{BU}=65$	^{152}Eu	1.3 1	by $\text{BU}=25$ by $\text{BU}=65$
	^{94}Nb	0.8		^{93}Mo	1.05	
	^{95}Nb	0.95		^{231}Pa	2.2 2.15	by $\text{BU}=65$, $\text{CT}=0$ by $\text{BU}=65$, $\text{CT}=5$
	^{147}Pm	0.8		^{238}Pu	1.17 1.2	by $\text{CT}=0$ by $\text{CT}=5$
	^{144}Pr	0.6	by $\text{BU}=[30,65]$	^{226}Ra	4.5 2.5	by $\text{BU}=65$, $\text{CT}=0$ by $\text{BU}=65$, $\text{CT}=5$
	^{106}Rh	0.66	by $\text{BU}=65$	^{229}Th	3.4	by $\text{BU}=65$
	^{106}Ru	0.66	by $\text{BU}=65$	^{230}Th	2.1 1.55	by $\text{BU}=65$, $\text{CT}=0$ by $\text{BU}=65$, $\text{CT}=5$
	^{125}Sb	0.7	by $\text{BU}=65$	^{232}Th	1.12 1.09	by $\text{CT}=0$ by $\text{CT}=5$
	^{151}Sm	0.96	by $\text{BU}=[40,65]$	^{232}U	1.6 1.13	by $\text{BU}=65$, $\text{CT}=0$ by $\text{BU}=65$, $\text{CT}=5$
	^{90}Sr	0.93	by $\text{BU}=[40,65]$	^{233}U	1.2 1.13	by $\text{BU}=65$, $\text{CT}=0$ by $\text{BU}=65$, $\text{CT}=5$
	^{90}Y	0.93		^{234}U	1.09 1.13	by $\text{BU}=65$, $\text{CT}=0$ by $\text{BU}=65$, $\text{CT}=5$
	^{95}Zr	0.95				

5 Modelling

The task of modelling is to optimize the number of calculations and to create the corresponding SCALE input files (cf. Figure 3.2). Simulations are carried out with the burn-up code SCALE 6.1 [ORNL, 2011] using the nuclear data library ENDF/B-VII.0 [Chadwick et al., 2006]. A two dimensional model of a PWR-UO₂ fuel assembly is assumed. The setup of these simulations initializes the required input parameters including the values of the SRPs (cf. Table 5.1).

Table 5.1: Model of RN analysis

Geometry	18×18 Westinghouse Sweden [NEI, 2004]
Neutron flux modelling	newt 2D
Data library	ENDF-B/VII.0
Cooling time	0
BU, IE, SP, IT, BA, FD, FT, MD, MT and DT	cf. Table 4.4

The first step of optimization implies the minimization of the number of required calculations. This process is carried out in parallel with the SRP and downtime analyses. Seven out of the nine SRPs were found independent of each other. Moreover, for these SRPs the DT can be discarded, i.e. set to zero (cf. chapter 4.2 and 4.4). Table 5.2 represents minimization of the number of calculations. The first row shows the number of BU intervals and the three values (minimum, typical and maximum) of each independent SRP, respectively. This first optimization step reduces the number of theoretically possible combinations of 78732 to 2916 SCALE input files.

In the next step of optimization the limiting values of the BU intervals for IE and SP were selected such that one of the limiting values of a higher BU interval coincided (overlapped) with the typical value of the next lower BU interval (cf. Figures 4.1 and 4.2). The scheme of the overlap and of the duplication of the models is shown in Figure 5.1. The optimization occurred due to discarding the duplicating models. Thus, the number of calculations is reduced from 2916 to 1701 models, i.e. to 1701 SCALE input files, which are further used for the determination of theoretical bandwidths.

Table 5.2: Optimization of the number of models

Step	Description	Number of models
1 st	$\underbrace{4}_{\text{BU}} \cdot \underbrace{3}_{\text{IE}} \cdot \underbrace{3}_{\text{SP\&IT}} \cdot \underbrace{3}_{\text{BA}} \cdot \underbrace{3}_{\text{FT}} \cdot \underbrace{3}_{\text{FD}} \cdot \underbrace{3}_{\text{MT\&MD}} \cdot \underbrace{1}_{\text{DT}}$	2916
2 nd	cf. Figure 5.1	1701

BU: 0 - 15 [GWd/tHM]	IE: [wt % U-235]	SP: [MW/tHM]	
(1.0) (1.9) (5.0)	(14) (20) (25) (14) (20) (25) (14) (20) (25)	(14) (20) (25) (14) (20) (25) (14) (20) (25)	$4 \cdot \left(\underbrace{3}_{BA} \cdot \underbrace{3}_{FT} \cdot \underbrace{3}_{FD} \cdot \underbrace{3}_{MT\&MD} \cdot \underbrace{1}_{DT} \right) = 4 \cdot 81$
(1.9) (3.0) (5.0)	(14) (25) (39) (14) (25) (39) (14) (25) (39)	(14) (25) (39) (14) (25) (39) (14) (25) (39)	$4 \cdot \left(\underbrace{3}_{BA} \cdot \underbrace{3}_{FT} \cdot \underbrace{3}_{FD} \cdot \underbrace{3}_{MT\&MD} \cdot \underbrace{1}_{DT} \right) = 4 \cdot 81$
(3.0) (4.4) (5.0)	(25) (39) (48) (25) (39) (48) (25) (39) (48)	(25) (39) (48) (25) (39) (48) (25) (39) (48)	$4 \cdot \left(\underbrace{3}_{BA} \cdot \underbrace{3}_{FT} \cdot \underbrace{3}_{FD} \cdot \underbrace{3}_{MT\&MD} \cdot \underbrace{1}_{DT} \right) = 4 \cdot 81$
(4.4) (5.0) (5.0)	(39) (43) (48) (39) (43) (48) (39) (43) (48)	(39) (43) (48) (39) (43) (48) (39) (43) (48)	$1 \cdot \left(\underbrace{3}_{SF\&IT} \cdot \underbrace{3}_{BA} \cdot \underbrace{3}_{FT} \cdot \underbrace{3}_{FD} \cdot \underbrace{3}_{MT\&MD} \cdot \underbrace{1}_{DT} \right) = 1 \cdot 243$ $\Rightarrow 12 \cdot 81 + 1 \cdot 243 = 972 + 243 = 1215$

Figure 5.1: Second optimization step of the number of models.

6 Realistic bandwidths of PWR-UO₂ RN inventory

6.1 Theoretical bandwidths of RNs

The first block of theoretical bandwidths module is to perform 1701 SCALE calculations and, thus, to provide output files for the build-up of theoretical bandwidths. The most important information needed for this task is saved in binary files named *ft71f001* containing isotopic concentrations for more than 2000 nuclides in units gram-atoms [ORNL, 2011, p. 1371]. All these data are associated with a given time step. Thus, the first block of calculations provides 1701 *ft71f001* files.

The tasks of the next block (cf. Figure 3.2) are to read all the *ft71f001* binary files and to select the required information for the 64 relevant radionuclides and to build-up the corresponding theoretical bandwidths. This block uses the tool developed by [Schneider, 2014], which has been expanded for the application within this work. The results yield the theoretical bandwidths of the activity vs. burn-up for the corresponding radionuclides.

The main purpose here is to determine the lower/upper limits of the theoretical bandwidths and, additionally, to classify each RN according to its sensitivity on varying the SRP values. Tentatively, the considered RNs can be divided into four groups (cf. Figure 6.1):

- RN independent of all SRPs (cf. Figure 6.1 (a) top left), i.e. the magnitude of the bandwidth does not exceed 2 % of the averaged value between upper and lower limits. These RNs depend only on the primary reactor parameter BU and CT.
- RN dependent on all SRPs (cf. Figure 6.1 (b) top right), i.e. the magnitude of the bandwidth is "equally" for each SRP. Therefore, an additional and detailed sensitivity analysis is required to substantiate an accurate statement of each SRP.
- RN strongly dependent on IE (cf. Figure 6.1 (c) bottom left), i.e. IE has the largest effect on the bandwidth magnitude compared to other SRPs. All other SRPs have only a small or negligible impact on the bandwidth.
- RN strongly dependent on IE and SP (cf. Figure 6.1 (d) bottom right), i.e. IE and SP has the largest effect on bandwidth magnitude compared to other SRPs. All other SRPs have only a small or negligible impact on the bandwidth.

Some RNs cannot be definitely associated with one of these four groups. Such RNs are placed into the second group (b), which characterizes the most general behaviour, and for these RNs additional and detailed analyses are required. The separation of the RNs into the four groups is very useful for the task of reverse specification, i.e. the determination of the SRPs values from a given RN inventory. There are some

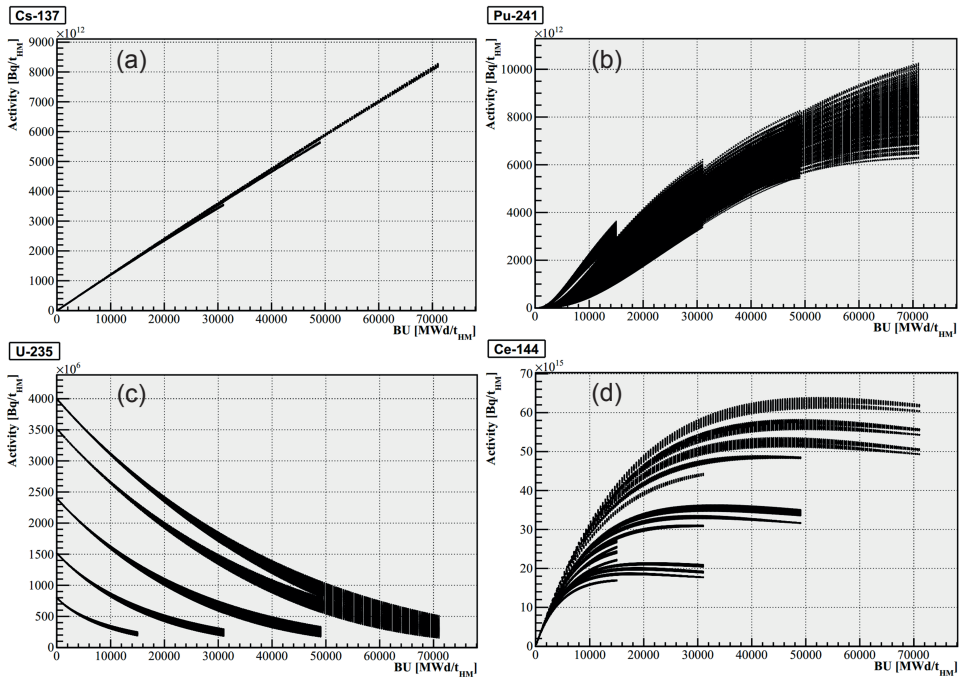


Figure 6.1: Example of RN sensitivity by variation of SRPs. There are four groups: (a) RN independent of all SRPs, (b) RN dependent on all SRPs, (c) RN strongly dependent on IE and (d) RN strongly dependent on IE and SP.

radionuclides with particular behaviour on the SRPs sensitivity, like ^{137}Cs , ^{235}U etc. (cf. Table 6.4) that could potentially be used as "key nuclides" for this task. The possible range of the values of important parameters, like burn-up, cooling time, IE, SP and DT can be reduced by the use of such "key nuclides" taking advantage from their specific dependence or sensitivity behaviour on SRPs. E.g. ^{137}Cs is independent of all SRPs and its bandwidth is very small, moreover it is linear with the burn-up, thus, burn-up can be well determined. Using this information and that of the strong dependence of ^{235}U on IE (the impact from other SRPs can be neglected) we can derive the corresponding IE, and so on. It is very challenging to recurse all parameters from the individual nuclides without an addition of extra information. This work provides estimates of SRP values and their interdependences, despite a detailed quantitative assessment of the SRP dependences was beyond the scope of this thesis. Nonetheless, it can be done as an extension in the future.

The last block of the theoretical bandwidth module is to consider the effect of DT (cf. chapter 4.4). The calculated theoretical bandwidths include lower and upper limits depending on the BU for each RN. The bandwidth calculations were carried out assuming

zero downtime (DT=0) during the irradiation. For those RNs that depend on DT, the DT correction are implemented as shown in Table 4.7. The bandwidth limits are expanded accordingly to the determined multiplication correction factor f_{DT} . This factor is determined as the maximum ratio between the RN concentrations calculated for DT=0 and DT=400 days, which is obtained for burn-up between 0 and 65 GWd/t_{HM} and for cooling time between 0 and 5 years. The corresponding DT effects are discussed in more detail in section 6.4.

The next section deals with available experimental data that are essentially important for the determination of the realistic bandwidths.

6.2 Available experimental or RCA data

The theoretical bandwidths are not necessarily realistic bandwidths. It is important to validate theoretical results with experimental data. Therefore, the destructive radiochemical assay (RCA) data are taken from the public Spent Fuel Isotopic Composition Database (SFCOMPO), which is maintained by the OECD Nuclear Energy Agency [NEA, 2015b]. This database includes RCA data for more than 600 spent fuel samples from 8 different reactor designs. The PWR data comprise measurements for more than 300 fuel samples with an associated burn-up range between 3 and 75 GWd/t_{HM}. These RCA data cover 41 final disposal relevant radionuclides (cf. Table 6.1). However, for some of these RNs only a few measurements are available. It is desired to continue development of this database.

The theoretical bandwidths together with the measurements build-up the realistic bandwidth of the theoretically predicted spent fuel radionuclide inventories. The individual bandwidths of these RNs are discussed in the section 6.4.

Most of measurements from SFCOMPO correspond to zero post-irradiation cooling time (CT=0), but some measurements correspond to various cooling times, which do not exceed 10 years. To compare calculations with measured data from the SFCOMPO database the latter have to be corrected for the indicated cooling times as is done in this work. All 64 RNs are analysed with respect on their behaviour to post-irradiation cooling time and bases on this analysis are subdivided into the three groups (cf. Table 6.1):

- RNs independent of CT (32 RNs), i.e. the results of the calculations with CT=0 and CT=10 years yield less than 1 % deviation.
- RNs overestimated by CT=0 (24 RNs), i.e. the CT impact has a negative effect on the RN concentration relative to the calculations with CT=0. Thus, the measurements affected by CT up to 10 years show lower activity values than the calculated bandwidth at zero CT.
- RNs underestimated by CT=0 (8 RNs), i.e. the CT impact has a positive effect on RN concentration as calculations with CT=0. Thus, the measurements affected by CT up to 10 years show higher activity values than the calculated bandwidth at zero CT.

Table 6.1: Available RCA data from SFCEMPO and RNs behaviour up to 10 years of post-irradiation cooling time; (n: number of measurement data points).

RNs independent of CT			RNs overestimated by CT=0			RNs underestimated by CT=0		
RN	n	BU range [GWd/t _{HM}]	RN	n	BU range [GWd/t _{HM}]	RN	n	BU range [GWd/t _{HM}]
^{108m} Ag	0	–	^{110m} Ag	3	30.71 – 52.43	²²⁷ Ac	0	–
^{242m} Am	58	6.92 – 59.66	¹⁴⁴ Ce	24	14.30 – 75.00	²⁴¹ Am	108	6.92 – 75.00
²⁴³ Am	99	6.92 – 75.00	²⁴² Cm	71	8.30 – 52.43	²²⁶ Ra	0	–
¹⁴ C	15	12.92 – 46.83	²⁴³ Cm	25	14.30 – 59.66	²³⁰ Th	0	–
²⁴⁹ Cf	0	–	²⁴⁴ Cm	109	6.92 – 75.00	²³² Th	0	–
²⁵¹ Cf	0	–	¹³⁴ Cs	62	6.92 – 75.00	²³² U	13	6.92 – 52.43
²⁴⁵ Cm	27	14.30 – 59.66	¹³⁷ Cs	118	6.92 – 75.00	²³³ U	5	45.90–55.00
²⁴⁶ Cm	27	14.30 – 75.00	¹⁵² Eu	0	–	²³⁴ U	180	3.34 – 75.00
²⁴⁷ Cm	8	30.17 – 52.43	¹⁵⁴ Eu	81	6.92 – 75.00			
²⁴⁸ Cm	0	–	¹⁵⁵ Eu	41	27.35 – 75.00			
¹³⁵ Cs	30	18.68 – 75.00	³ H	0	–			
¹²⁹ I	12	14.58 – 52.50	⁸⁵ Kr	0	–			
⁹³ Mo	0	–	⁹⁵ Nb	0	–			
⁹⁴ Nb	0	–	¹⁴⁷ Pm	4	29.07 – 59.66			
²³⁷ Np	85	6.33 – 75.00	¹⁴⁴ Pr	0	–			
²³¹ Pa	0	–	²⁴¹ Pu	255	3.34 – 75.00			
¹⁰⁷ Pd	0	–	¹⁰⁶ Rh	0	–			
²³⁸ Pu	174	6.92 – 75.00	¹⁰³ Ru	1	75.00			
²³⁹ Pu	259	3.34 – 75.00	¹⁰⁶ Ru	44	6.92 – 75.00			
²⁴⁰ Pu	259	3.34 – 75.00	¹²⁴ Sb	0	–			
²⁴² Pu	255	3.34 – 75.00	¹²⁵ Sb	27	6.92 – 59.66			
²⁴³ Pu	0	–	⁹⁰ Sr	14	18.68 – 59.66			
²⁴⁴ Pu	2	52.50 – 59.66	⁹⁰ Y	0	–			
⁷⁹ Se	9	18.68 – 46.46	⁹⁵ Zr	0	–			
¹⁵¹ Sm	49	17.69 – 75.00						
¹²⁶ Sn	9	18.68 – 46.46						
⁹⁹ Tc	38	16.02 – 74.00						
²²⁹ Th	0	–						
²³⁵ U	259	3.34 – 75.00						
²³⁶ U	248	3.34 – 75.00						
²³⁸ U	225	3.34 – 59.66						
⁹³ Zr	0	–						

6.3 Available RN inventory of international PWR-UO₂ SNF

The presently available experimental data are insufficient for validating the bandwidths for all radionuclides of interest for waste management. It is however possible to perform a comprehensive verification by comparing the theoretical bandwidths with other reference inventory calculations, which have been performed in several countries for the needs of long-term safety assessments, spent fuel transportation and storage, and other applications. In this work, predicted theoretical isotope bandwidths are compared to the calculated RN inventories from USA, Switzerland, Sweden and Germany (cf. Table 6.2).

Table 6.2: Properties of calculated international RN inventory

Available information	[SKB, 2010] (Sweden)	[Peiffer et al., 2011] (Germany)	[NAGRA, 2014] (Switzerland)	[ORNL, 2016] (USA)
Number of RN	44	64	64	59
BU [GWd/t _{HM}]	44.8	55	32.9 – 56.6	7 – 53
CT [years]	35 (on year 2045)	0	60 days	on year 2020
Fuel impurities (FI)	yes	yes	yes	no ¹

¹ FI only for Co with 30.2 ppm

The Oak Ridge National Laboratory (ORNL) provided calculated inventories (for 59 final disposal relevant RNs) for approximately 2000 US PWR-UO₂ spent fuel assemblies with a burn-up range between 7 and 53 GWd/t_{HM} [ORNL, 2016]. Each FA corresponds to the individual CT for year 2020 and does not exceed 35 years.

The "Nationale Genossenschaft für die Lagerung radioaktiver Abfälle" (NAGRA) calculated inventories of fuel assembly families that represent average data for approximately 3300 Swiss PWR-UO₂ SNF [NAGRA, 2014]. These fuel assembly families correspond to an average burn-up between 32.9 and 56.6 GWd/t_{HM} and CT of 60 days. All 64 final disposal relevant RNs have been analyzed.

In Sweden, the "Swedish Nuclear Fuel and Waste Management Co" (SKB) calculated the total radionuclide inventory from the total number of assemblies with an averaged burn-up of 44.8 GWd/t_{HM} (PWR spent fuel) [SKB, 2010]. The calculated inventories provide the total mean activity values for 44 final disposal relevant radionuclides. The RN activity values in the report [SKB, 2010] correspond to the total RN inventory based on the number of fuel assemblies (total number of PWR FA: 6016 with 464 kg per one FA) with calculation for the year 2045 (i.e. CT=35 years). Thus, the RN activity values have to be normalized on the factor $2791.424 = 6016 \cdot 464 / 1000$ and have to be corrected for the cooling time of 35 years.

In Germany the "Gesellschaft für Anlagen- und Reaktorsicherheit (GRS) mbH" compiled the radioactive waste specification [Peiffer et al., 2011]. The activity in Bq per t_{HM} of all 64 final disposal relevant radionuclides was calculated on the basis of a model fuel

assembly with a burn-up of 55 GWd/t_{HM}, cooling time 0 and an initial enrichment of 4.4 wt % ²³⁵U.

For realistic modelling of the huge amount of fuel assemblies it is important to know the initial fuel composition (particularly for ²³⁴U and ²³⁶U) and the fuel impurity data. When the SRP analysis was performed this information has not been assembled and its importance was not fully recognized, and, therefore, the analysis of these data is not included in the thesis (cf. chapter 4). Consequently, the concentrations of ²³⁴U and ²³⁶U are set to zero in the initial composition and the fuel impurities are not considered in the theoretical bandwidths calculations. However, after a more complete information on averaged values of the initial fuel composition has been collected additional calculations of the theoretical bandwidths of ²³⁴U and ²³⁶U have been performed. Table 6.3 shows the fuel impurity concentrations, which are used in the modelling of international RN inventories.

Table 6.3: Fuel impurities.

Elem. ⁵	SWE ¹ [ppm]	DEU ² [ppm]	CHE ³ [ppm]	USA ⁴ [ppm]	Elem.	SWE [ppm]	DEU [ppm]	CHE [ppm]	USA [ppm]
Ag	0.05	5	1	0	Li	0.05	1	1	0
Al	6	21	40	0	Lu			0.3	0
Ar			0.1	0	Mg	1	5	2	0
As			0.3	0	Mn	2	1	2	0
Au			0.1	0	Mo	5	5	5	0
B	0.05	0.5	0.6	0	N	14	30	25	0
Ba			10	0	Na		5	15	0
Be			0.1	0	Nb			1	0
Bi	0.5	5	0.4	0	Ni	5	3.5	25	0
Br			0.5	0	O	133621		134314	0
C	8.4	4	50	0	Os			0.1	0
Ca	3	10	40	0	P		5	35	0
Cd	0.233		0.5	0	Pb	0.6	5	1	0
Ce			1	0	Pt			0.1	0
Cl	2	4.5	5	0	Re			0.1	0
Co	0.5	5	1	30.2	Ru			0.1	0
Cr	1	3	4	0	S			10	0
Cu	0.5	5	1	0	Sb			1	0
Dy	10		0.3	0	Sc			10	0
Er			0.3	0	Se			2	0
Eu	0.02		0.3	0	Si	10	6	40	0
F	2	4	5	0	Sm	0.04		0.3	0
Fe	5	15	55	0	Sn	0.8	5	1	0
Ga			0.3	0	Ta		5	1	0
Gd	0.06		0.3	0	Tb			0.3	0
Ge			0.3	0	Te			1	0
H			0.3	0	Th		5		0
H ₂ O		2		0	Ti	10	5	1	0
Hf			1	0	Tl			0.1	0
Hg			0.1	0	Tm			0.3	0
Ho			0.3	0	V	0.3	5	1	0
In	0.3		1	0	W	0.2	5	2	0
Ir			0.1	0	Yb			0.3	0
K		10	10	0	Zn	25	5	5	0
La			1	0					

¹ [SKB, 2010] (Sweden)² [Peiffer et al., 2011] (Germany)³ [NAGRA, 2014] (Switzerland)⁴ [ORNL, 2016] (USA)⁵ empty values are not specified

6.4 Realistic bandwidths of RN

This chapter shows the results of realistic bandwidths calculations and their particular build-up for each radionuclide. The sensitivity of realistic bandwidths to the variation of the SRPs needs to be discussed. Each SRP contributes to the magnitude of realistic bandwidth in a different way. Table 6.4 lists the most important effects, which significantly contribute to the RN's realistic bandwidths:

- Cooling time (CT). The exact knowledge of CT is very important for interpreting the measured and calculated inventory data and for providing the realistic bandwidths.
- Downtime (DT) is important for a set of DT-sensitive fission products and actinides.
- Fuel impurities (FI) are important for light elements and some fission products.
- Initial composition (IC) is important for ²³⁴U.
- Modelling and nuclear ORIGEN library data, e.g. addnux, branching factors, cross sections (Lib) can have significant effects on concentrations of some radionuclides.
- Initial enrichment (IE) and specific power (SP) are the basic SRPs, which have a dominant effect on some radionuclides.

Most of the data used for the build-up or for the comparison of realistic bandwidths are affected with cooling time. For this work the effect of the cooling time is investigated up to 35 years. To take the cooling time into account the affected radionuclide data should be recalculated according to the discharge time of the assembly (i.e. to the time zero). For the light radionuclides and fission products the cooling time influences only their own decay functions and, therefore, its effect can be relatively easily taken into account. For most actinides the behaviour of mother-daughter radionuclides cannot be neglected.

The radionuclides marked in red (cf. Table 6.4) are characterized by the longest half-life times in the corresponding decay chains. All other RNs in the corresponding decay chain attain the secular equilibrium with the main RN. Consequently, it is most important to compute the bandwidth for main RN, because bandwidths of the remaining RNs are the same (cf. discussion of ²⁴²Cm bandwidth, Figure 6.37).

The radionuclides marked in green (cf. Table 6.4) were not originally included into the list of 64 final disposal relevant radionuclides. However, these RNs are also important for safety analyses. For these RNs the calculations yielded zero concentrations for the entire burn-up range. There are two types of such RNs:

- Light radionuclides, for which the fuel impurities were not considered in the calculations of the theoretical bandwidths (cf. Table 4.1). They are produced by the activation process and not by fission processes during the irradiation time. Hence, there are no processes within the model, which could lead to increased concentrations of these RNs.

- Actinide ²⁵²Cf, for which the zero activity is attributed to the so called "modelling properties". This could be attributed to bugs in the SCALE version 6.1.0 possibly related to reading the library data for ²⁵²Cf (cf. section 2.2). The recommendation here is to test this possibility using additional simulation with the most recent SCALE version.

The blue-marked radionuclides are the actinides, which are not included in the list of final disposal relevant RNs (cf. Table 1.1), although they are required for the correct calculation of the cooling time effect on some RNs, which are included in this list, e.g. the concentration of ²⁴⁹Cf depends on ²⁴⁹Bk (cf. Figure 6.58).

6.4.1 Realistic bandwidths of fission products and light radionuclides

For the cooling time up to 35 years twelve radionuclides (^{108m}Ag , ^{14}C , ^{135}Cs , ^{129}I , ^{93}Mo , ^{94}Nb , ^{107}Pd , ^{79}Se , ^{151}Sm , ^{126}Sn , ^{99}Tc and ^{93}Zr) could be accepted as CT independent (cf. Figure 6.2 and Table 6.4). For the remaining radionuclides the CT correction is required for building-up the realistic bandwidths and for comparing them with calculated international inventory data. In the following the realistic bandwidths are discussed in alphabetical order.

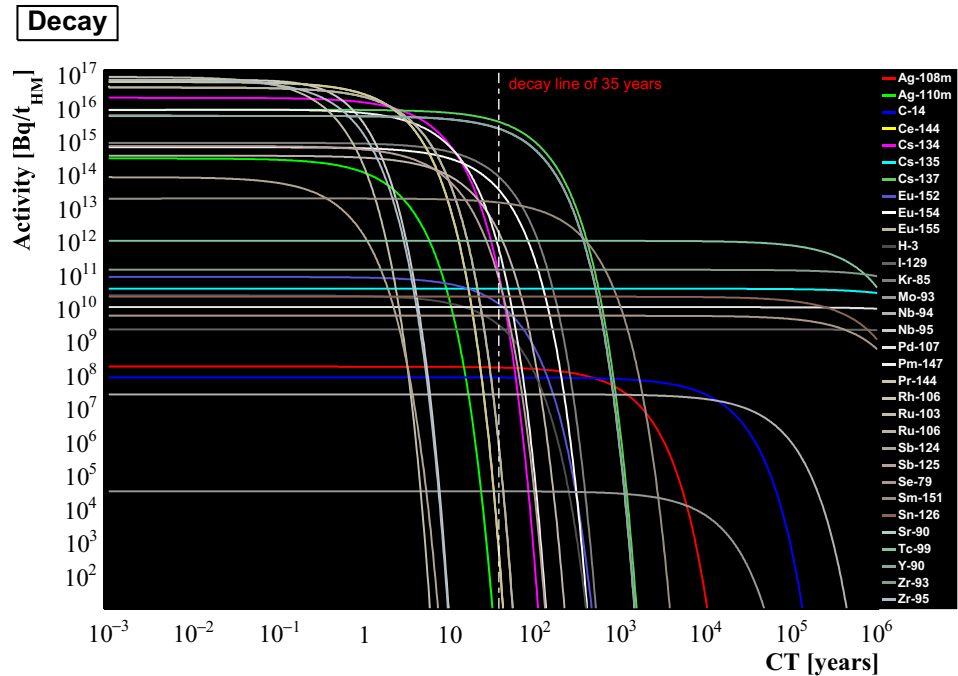


Figure 6.2: Decay of fission products and light radionuclides.

^{108m}Ag

^{108m}Ag is a direct fission product (it is shielded by the stable nuclide ¹⁰⁸Pd). During irradiation time it is built-up by direct fission and activation processes. For this radionuclide there are no measurements in SFCOMPO. This RN is mostly sensitive to IE, which variation makes the most significant contribution to the bandwidth (cf. Figure 6.3). However, on the basis of calculated international data and the available information of fuel impurities (cf. Table 6.3) the impact from the latter is by about two orders larger than the common effect of the other SRPs (cf. Figure 6.3). Hence, the FI is a dominant factor determining the bandwidth of this radionuclide. The impact of all other SRPs can be neglected.

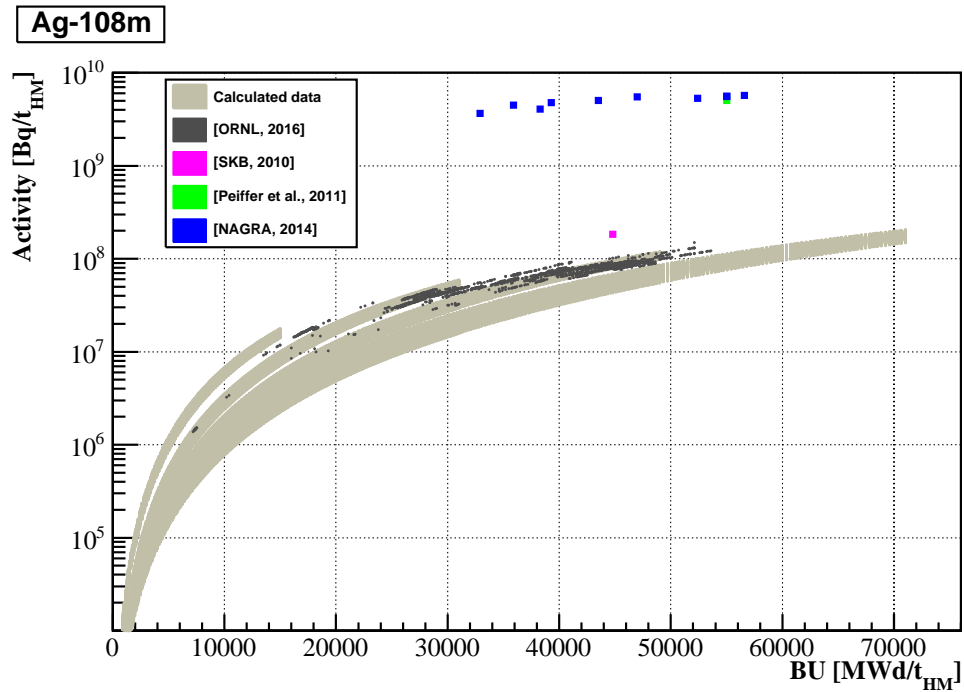


Figure 6.3: Theoretical bandwidth of ^{108m}Ag and effect of fuel impurities.

^{110m}Ag

^{110m}Ag is a direct fission product (it is shielded by the stable nuclide ¹¹⁰Pd). During irradiation time it is built-up by direct fission and activation processes. For this radionuclide there are some measurements available. The SRP analysis shows different SRP behaviour than for ^{108m}Ag, the dependencies on DT, IE and SP are stronger. These SRPs make the most significant contribution to the bandwidth (cf. Figure 6.4). The theoretical bandwidth considers DT correction as of Table 4.7, which is in a good agreement with experimental and calculated international data.

Note that calculated international data values from USA and Germany have different build-up rates than all other values. This may be caused using different ORIGEN libraries.

Moreover, in contrast to ^{108m}Ag, ^{110m}Ag shows no sensitivity to fuel impurities. However, the natural abundancies of the stable isotopes ¹⁰⁷Ag and ¹⁰⁹Ag are almost equal and, therefore, they should be formed in approximately equal ratios. This difference in the behaviour of the two isotops requires a further understanding.

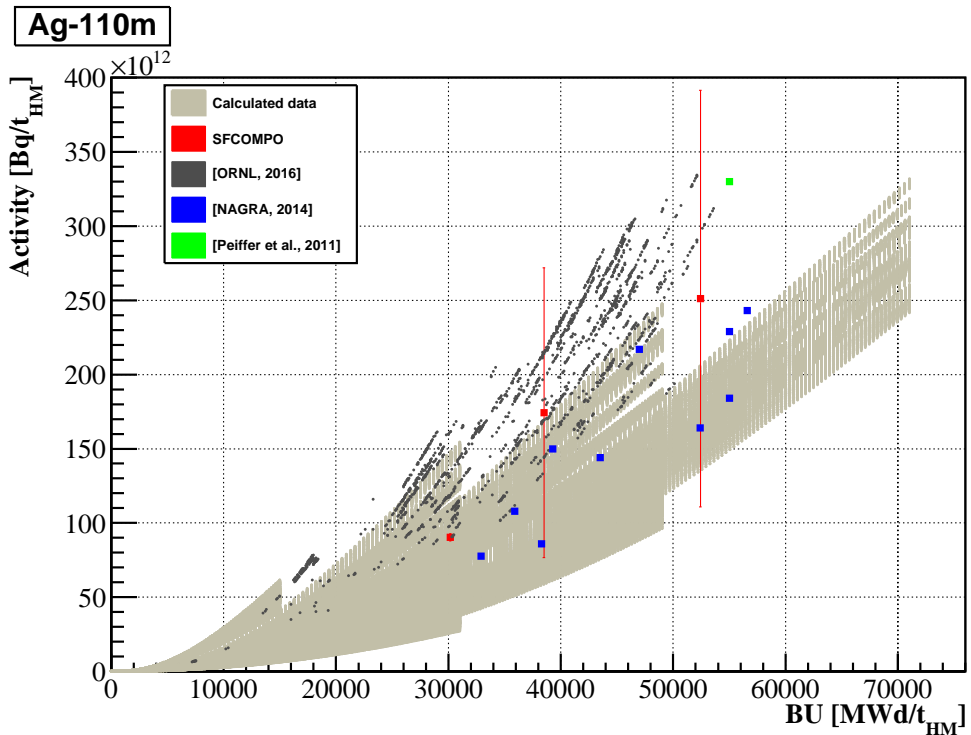


Figure 6.4: Realistic bandwidth of ^{110m}Ag.

¹⁴C

¹⁴C is a light radionuclide. During irradiation time it is built-up by activation processes. There are three ways, which leads to the production of ¹⁴C:

- ¹⁴N $\xrightarrow{(n,p)}$ ¹⁴C
- ¹⁷O $\xrightarrow{(n,\alpha)}$ ¹⁴C
- ¹³C $\xrightarrow{(n,\gamma)}$ ¹⁴C

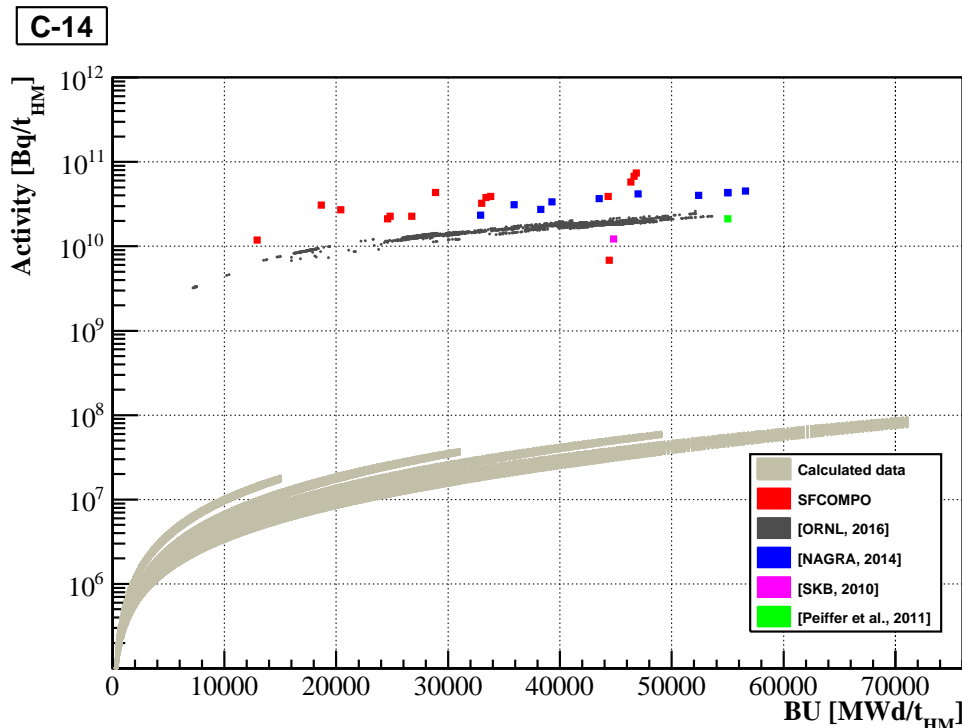


Figure 6.5: Theoretical bandwidth of ¹⁴C and effects of fuel impurities and of model properties.

This RN is mostly sensitive to IE, which variation makes the most significant contribution to the bandwidth (cf. Figure 6.5). However, the difference between the theoretical bandwidth and the aggregate of the available experimental and calculated international data is up to the factor of 1000 larger than the common effect of the other SRPs (cf. Figure 6.5). From literature it is known that the reaction ¹⁴N $\xrightarrow{(n,p)}$ ¹⁴C has the largest effect on the composition of ¹⁴C during the irradiation in a reactor core. Based on the fuel impurities information it is not clear, why calculated data values from US match the experimental values and other calculated international values well, although US modelling does not include any impurities except Co (cf. Table 6.3). This discrepancy needs to be

better understood. This discrepancy cannot be attributed to the different *addnux* levels (the levels 2 and 4 tested here) in the calculations with SCALE 6.1.0 version (cf. also section 2.2). Indeed, the switch between the two levels of the *addnux* parameter leads only to a switch between the data libraries, while the JEFF multigroup and ENDF/B libraries are (usually) very similar.

The previous conclusion shows that FI, then the model properties (i.e. the SCALE version) and then IE are the dominant factors determining the bandwidth of the content of this radionuclide in the PWR-UO₂ spent fuel. The impact of all other SRPs can be neglected.

^{144}Ce (^{144}Pr)

^{144}Ce is a fission product. During irradiation time it is built-up by fission and activation processes. This RN is mostly sensitive to DT, IE and SP, while the variation in IE makes the most significant contribution to the bandwidth (cf. Figure 6.6). The theoretical bandwidth as shown in Figure 6.6 corresponds to the DT corrected bandwidth with the considered average DT of 400 days. The DT correction factor is given in Table 4.7. The theoretical bandwidth is in a good agreement with experimental and calculated international data.

However, the use of the US data in this comparison rises a point of concern. The half-life of ^{144}Ce of 285 days implies that the activity will definitely begin to saturate after several operation cycles as seen in all other calculated international and experimental data. On the contrary, all of the ORNL data appear to be effectively linear with the burn-up showing no saturation. The discrepancy with the ORNL data needs to be better understood.

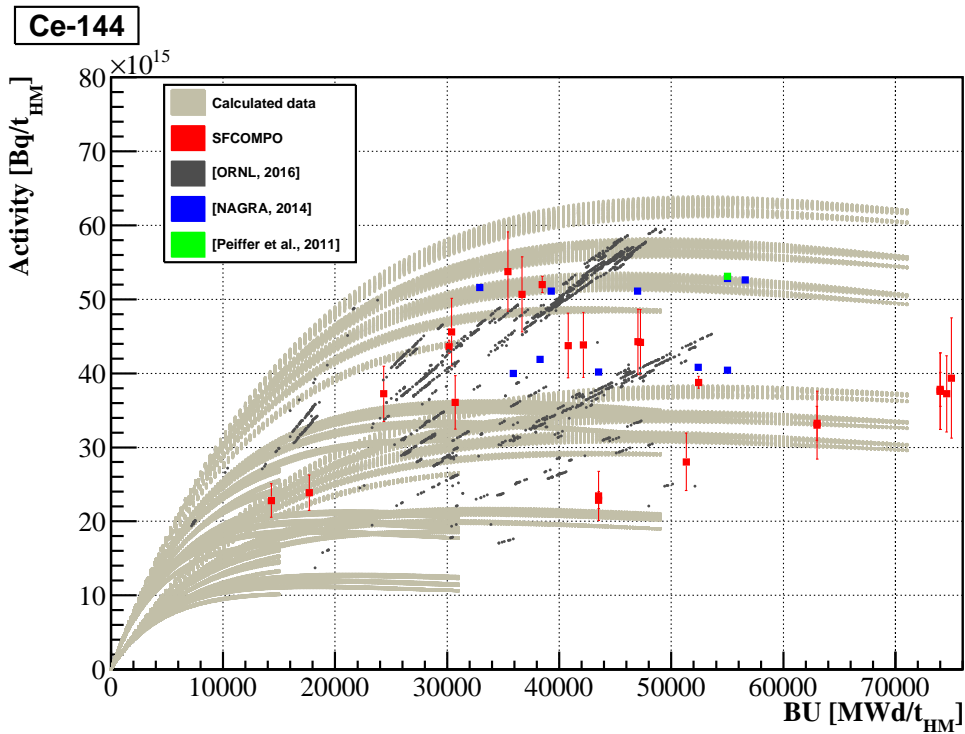


Figure 6.6: Realistic bandwidth of ^{144}Ce .

¹³⁴Cs

¹³⁴Cs is a fission product. During irradiation time it is built-up by fission and activation processes. This RN is mostly sensitive to DT, which variation makes the most significant contribution to the bandwidth (cf. Figure 6.7). The theoretical bandwidth in Figure 6.7 corresponds to the DT corrected bandwidth considering the average DT of 400 days. The DT correction factor is given in Table 4.7. The theoretical bandwidth is in a good agreement with the experimental and calculated international data.

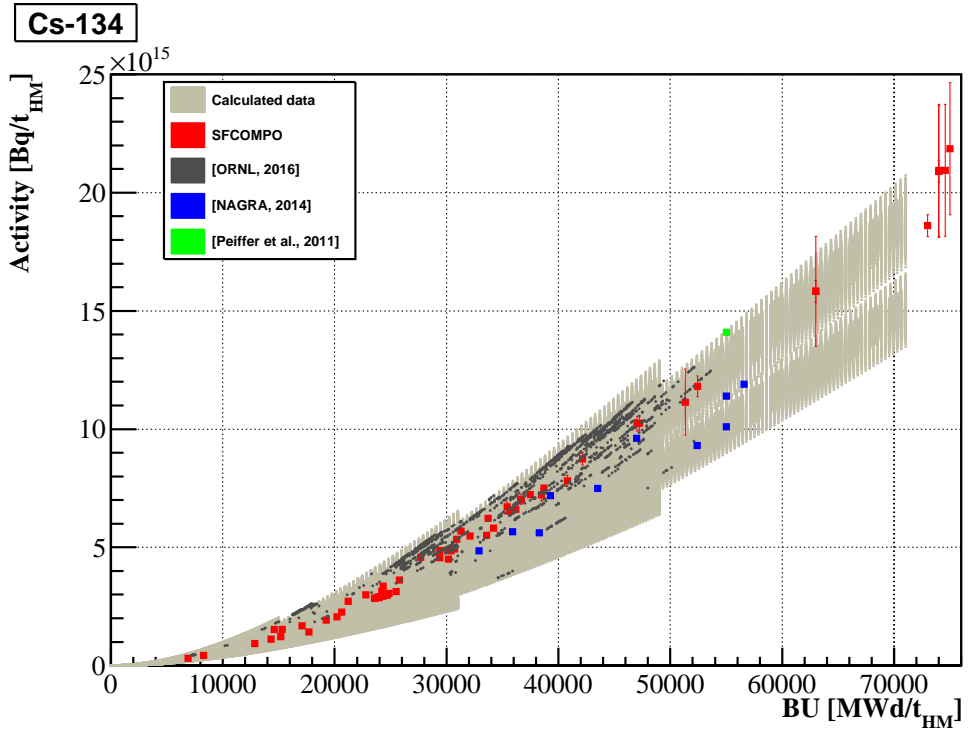
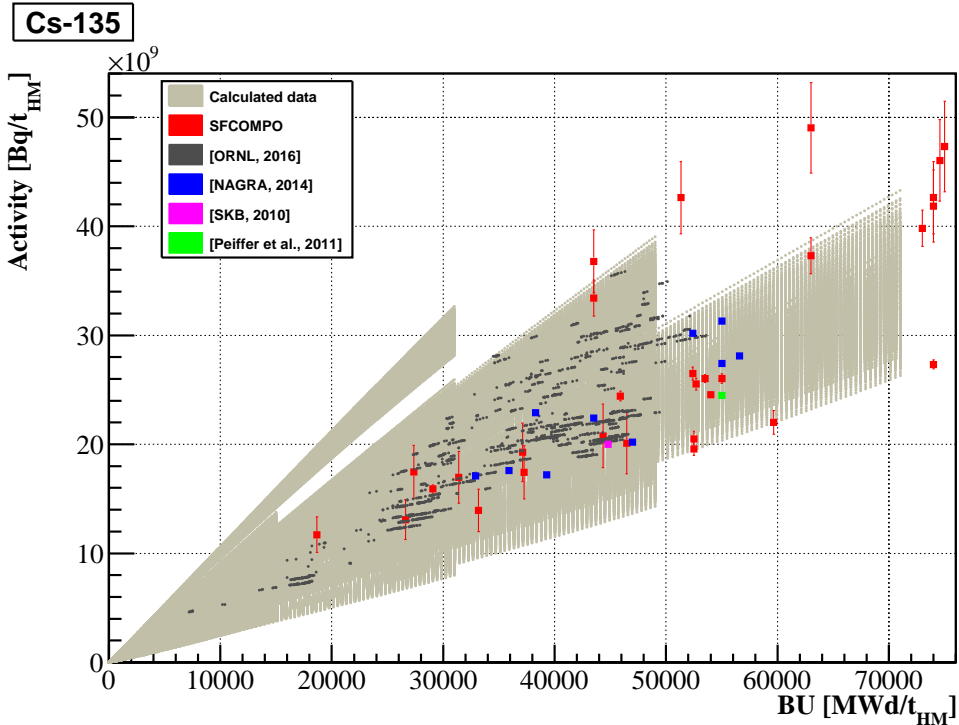


Figure 6.7: Realistic bandwidth of ¹³⁴Cs.

¹³⁵Cs

¹³⁵Cs is a fission product. During irradiation time it is built-up by fission and activation processes. This RN is mostly sensitive to IE and then to DT and the variations in these SRPs make the most significant contributions to the bandwidth (cf. Figure 6.8). The theoretical bandwidth considering the DT correction (cf. Table 4.7) is in a good agreement with the experimental and calculated international data.

Figure 6.8: Realistic bandwidth of ¹³⁵Cs.

¹³⁷Cs

¹³⁷Cs is a direct fission product. Its production is linear with the irradiation time. This RN is mostly sensitive to DT, which variation makes the most significant contribution to the bandwidth (cf. Figure 6.9). The theoretical bandwidth in Figure 6.9 corresponds to the DT corrected bandwidth considering the average DT of 400 days. The theoretical bandwidth is in a good agreement with the experimental and calculated international data.

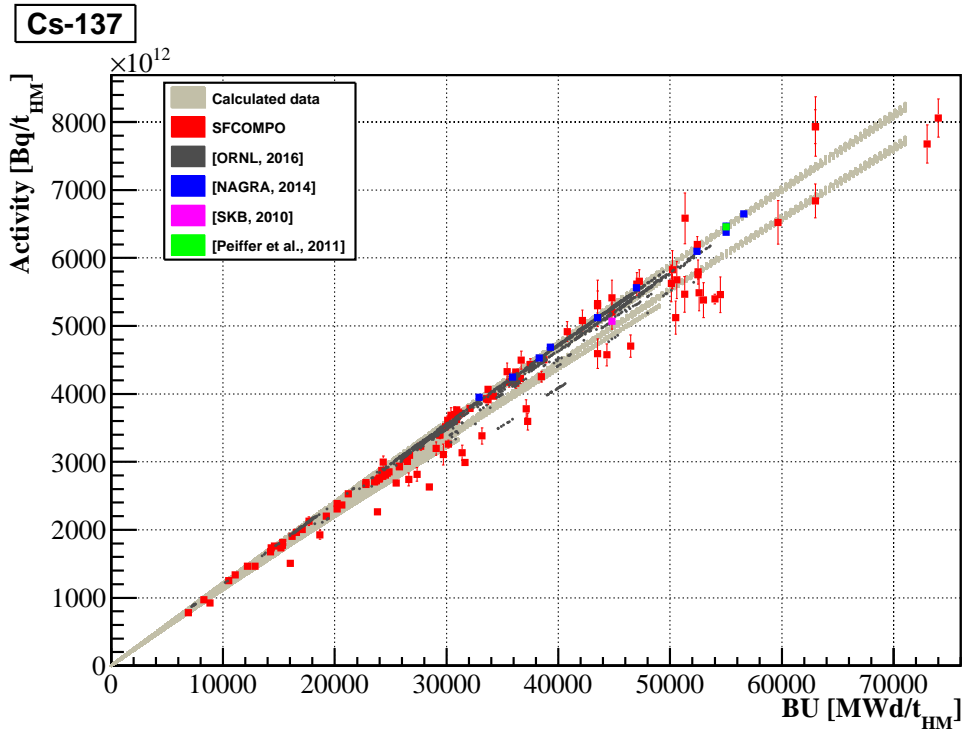


Figure 6.9: Realistic bandwidth of ¹³⁷Cs.

¹⁵²Eu

¹⁵²Eu is a fission product. During irradiation time it is built-up by fission and activation processes. This RN is sensitive on all SRPs, while the variations in IE and DT make the most significant contributions to the bandwidth (cf. Figure 6.10). There are no measurements in SFCOMPO for this radionuclide. The theoretical bandwidth considering DT correction is in a good agreement with the calculated international data. The slightly higher values from NAGRA and SKB can be attributed to the fuel impurities. However, these values are still within the theoretical bandwidth, therefore, this RN is not classified as FI sensitive.

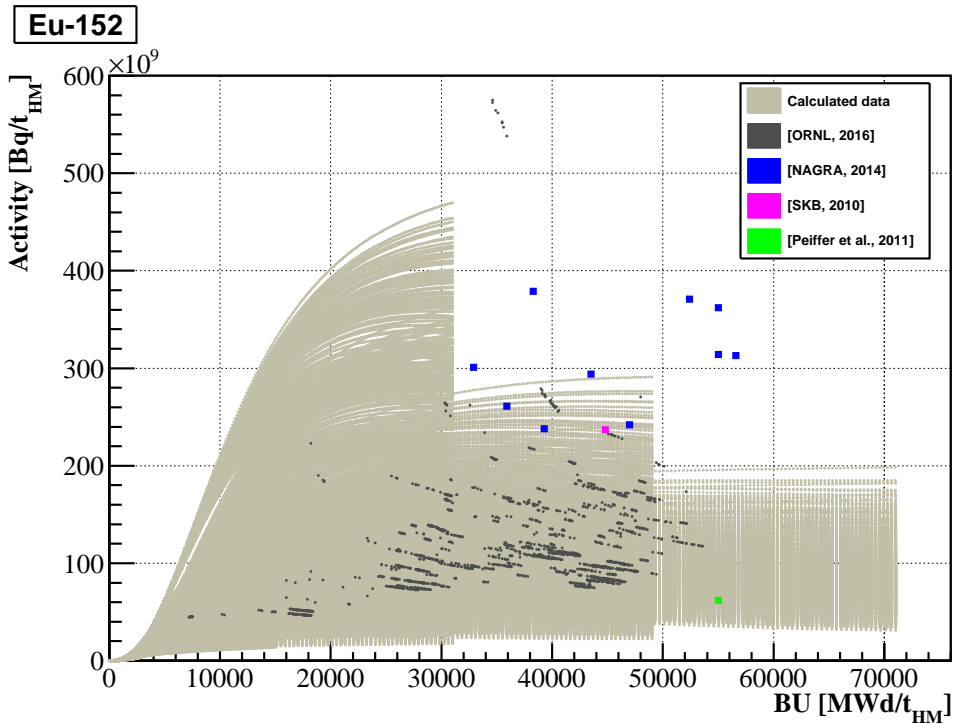


Figure 6.10: Realistic bandwidth of ¹⁵²Eu.

¹⁵⁴Eu

¹⁵⁴Eu is a fission product. During irradiation time it is built-up by fission and activation processes. This RN does not show strong dependency on any SRP (cf. Figure 6.11). The theoretical bandwidth is in a good agreement with the experimental and calculated international data.

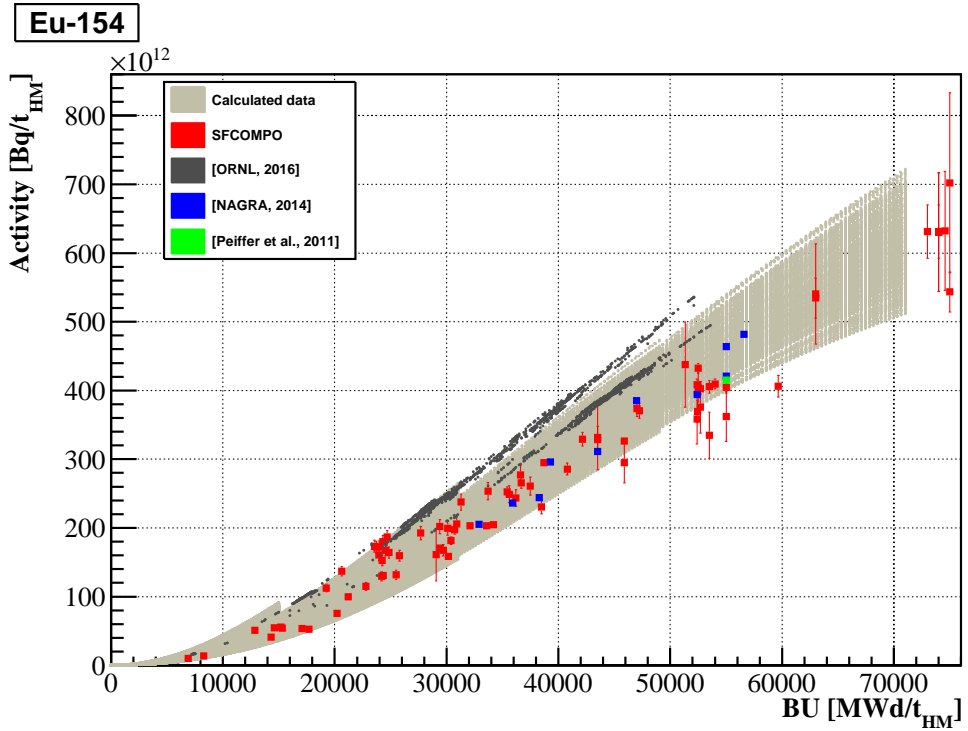


Figure 6.11: Realistic bandwidth of ¹⁵⁴Eu.

¹⁵⁵Eu

¹⁵⁵Eu is a fission product. During irradiation time it is built-up by fission and activation processes. This RN is mostly sensitive to IE, which variation makes the most significant contribution to the bandwidth (cf. Figure 6.12). The theoretical bandwidth is in a good agreement with the experimental and calculated international data.

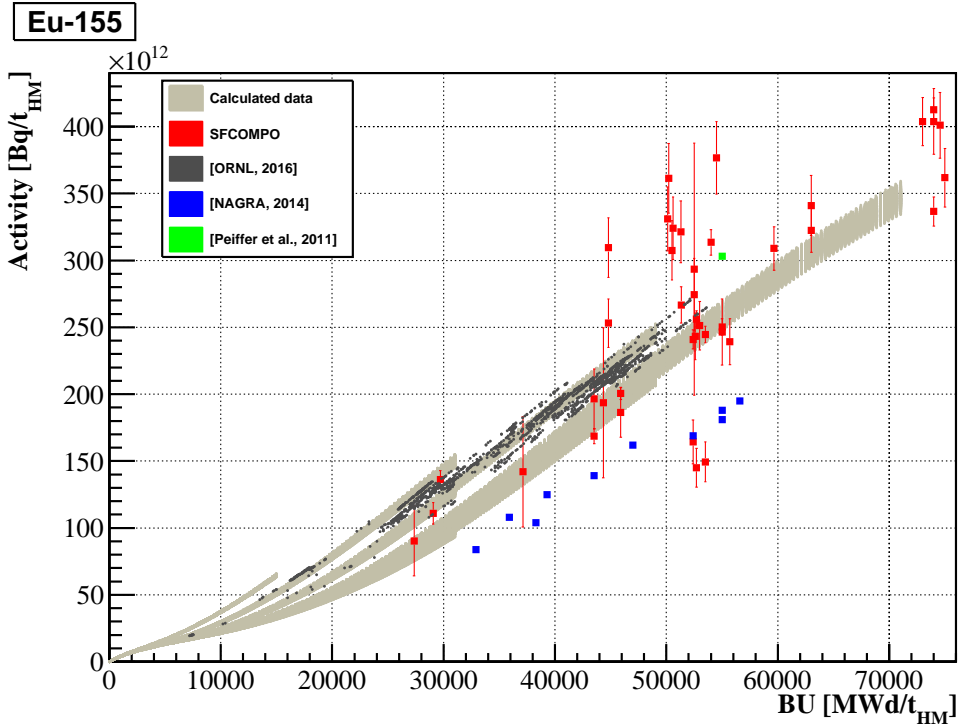


Figure 6.12: Realistic bandwidth of ¹⁵⁵Eu.

³H

³H is a light radionuclide. During irradiation time it is built-up by activation and fission processes. For this radionuclide any measurements in SFCOMPO are missing. This RN is mostly sensitive to IE, which variation makes the most significant contribution to the bandwidth (cf. Figure 6.13). However, the difference between the calculated international data and theoretical bandwidth is by a factor of 1000 larger than the effect of the IE (cf. Figure 6.13). This could be explained by the use of the SCALE version 6.1.0. The problems related to this version are discussed in section 2.2. A small difference between NAGRA, GRS and US, SKB values is caused by different fuel impurities (cf. Table 6.3).

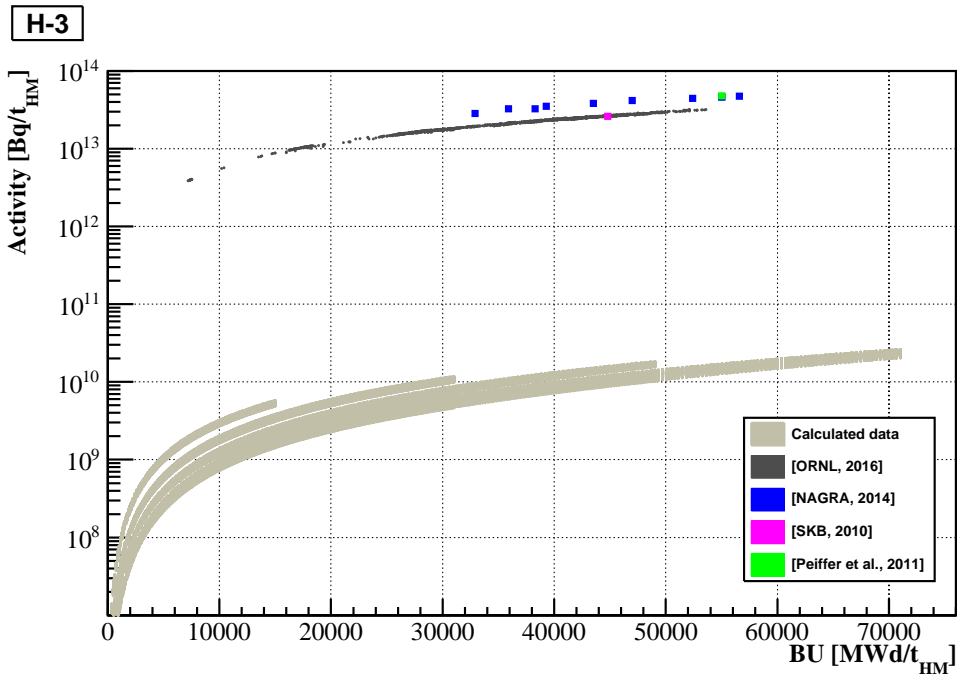


Figure 6.13: Theoretical bandwidth of ³H and effects of fuel impurities and of model properties.

¹²⁹I

¹²⁹I is a fission product. During irradiation time it is built-up by fission and activation processes. This RN is mostly sensitive to IE, which variation makes the most significant contribution to the bandwidth (cf. Figure 6.14). The theoretical bandwidth is in a good agreement with the experimental and calculated international data.

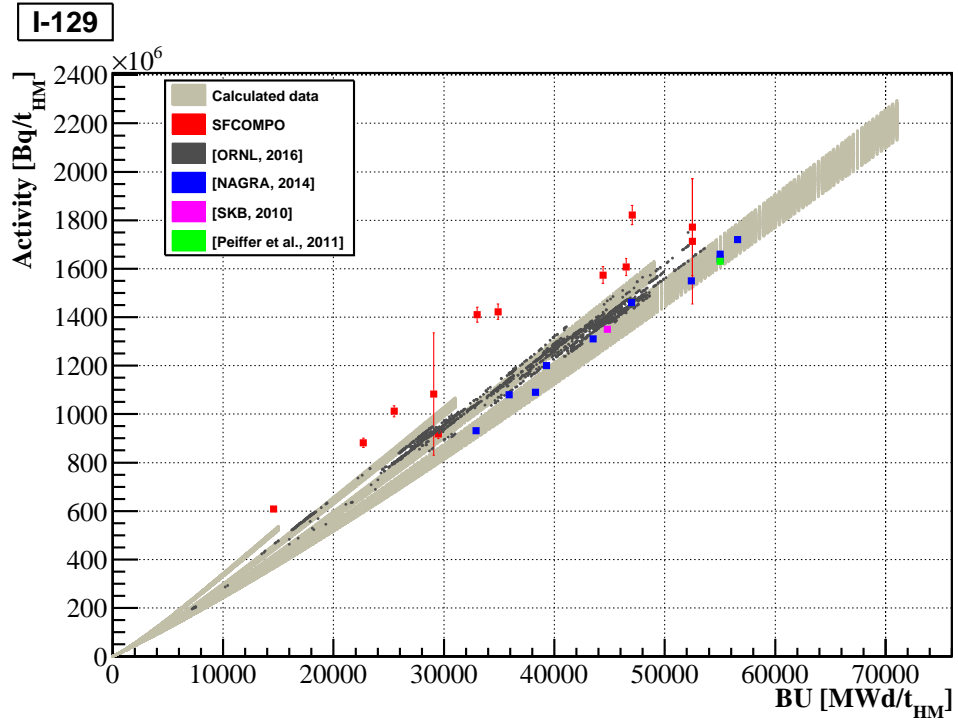


Figure 6.14: Realistic bandwidth of ¹²⁹I.

⁸⁵Kr

⁸⁵Kr is a fission product. During irradiation time it is built-up by fission and activation processes. This RN is mostly sensitive to IE, which variation makes the most significant contribution to the bandwidth (cf. Figure 6.15). There are no measured values in SFCOMPO for this radionuclide. The theoretical bandwidth considering the DT correction is in a good agreement with the calculated international data.

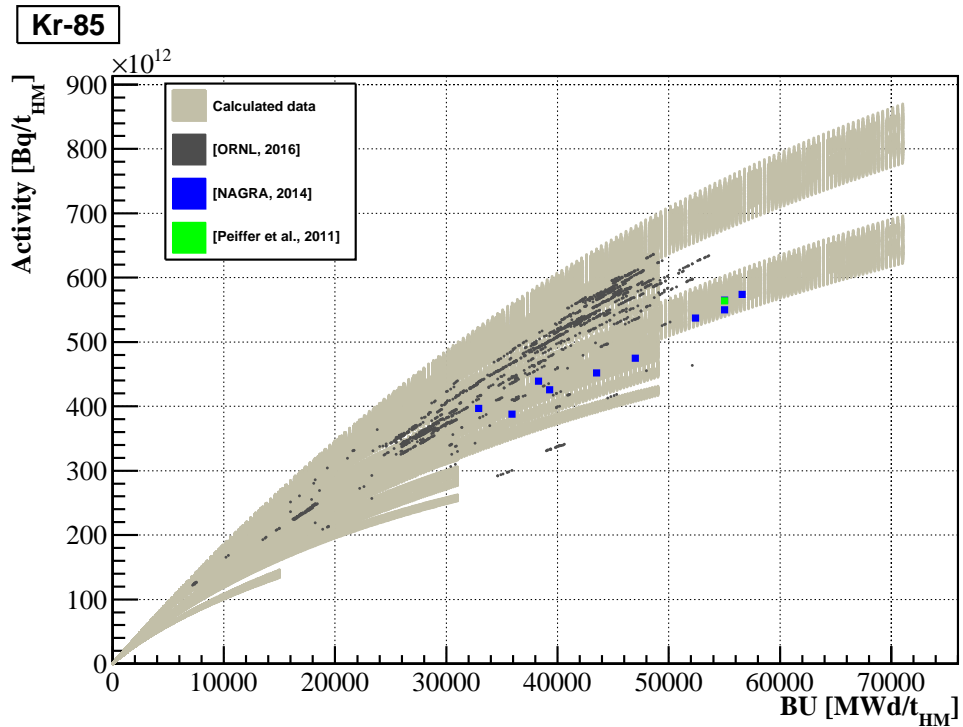


Figure 6.15: Realistic bandwidth of ⁸⁵Kr.

⁹³Mo

⁹³Mo is a fission product. During irradiation time it is built-up by fission and activation processes. This RN is mostly sensitive to IE and DT, while variation in IE makes the most significant contribution to the bandwidth (cf. Figure 6.16). However, the difference between the calculated international data and theoretical bandwidth is by a factor of 1000 larger than the effect of the IE (cf. Figure 6.16). This is caused by the fuel impurities. Particular in each of the considered sources of calculated international data the initial composition of Mo was set to 5 ppm. Note that there are no measured values in SFCOMPO and no calculated data at ORNL for this RN.

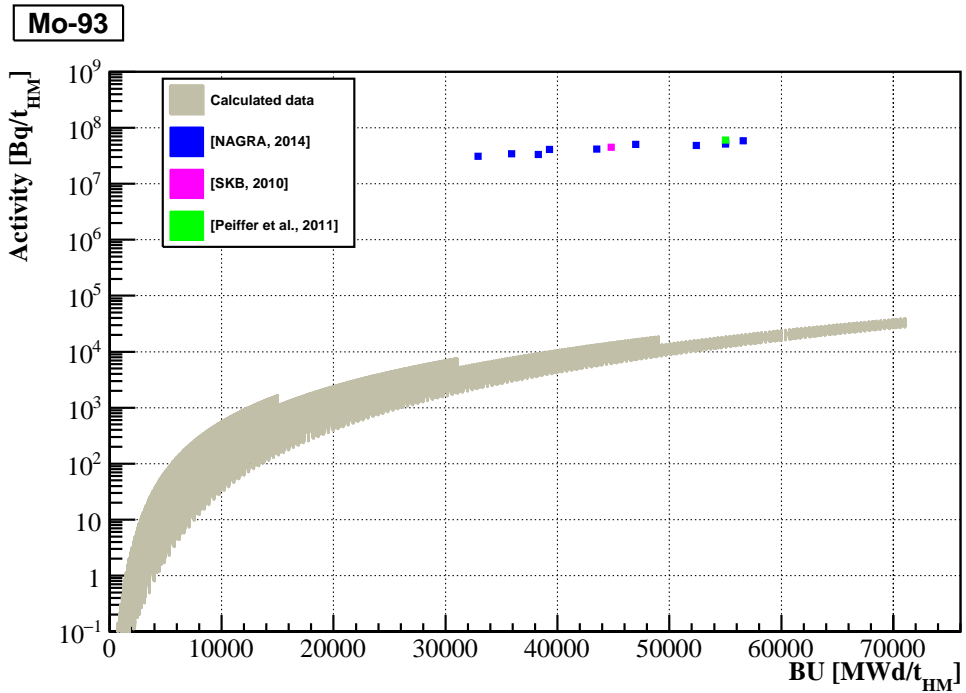


Figure 6.16: Theoretical bandwidth of ⁹³Mo and effect of fuel impurities.

⁹⁴Nb

⁹⁴Nb is a fission product. During irradiation time it is built-up by fission and activation processes. This RN is mostly sensitive to DT, which variation makes the most significant contribution to the bandwidth (cf. Figure 6.17). However, on the basis of calculated Swiss data [NAGRA, 2014] there is a large impact from FI to the bandwidth. The calculated Swiss data assume 1 ppm of Nb. Thus, this parameter gives the most important contribution to the realistic bandwidth. Note that there are no experimental data in SFCOMPO for this RN.

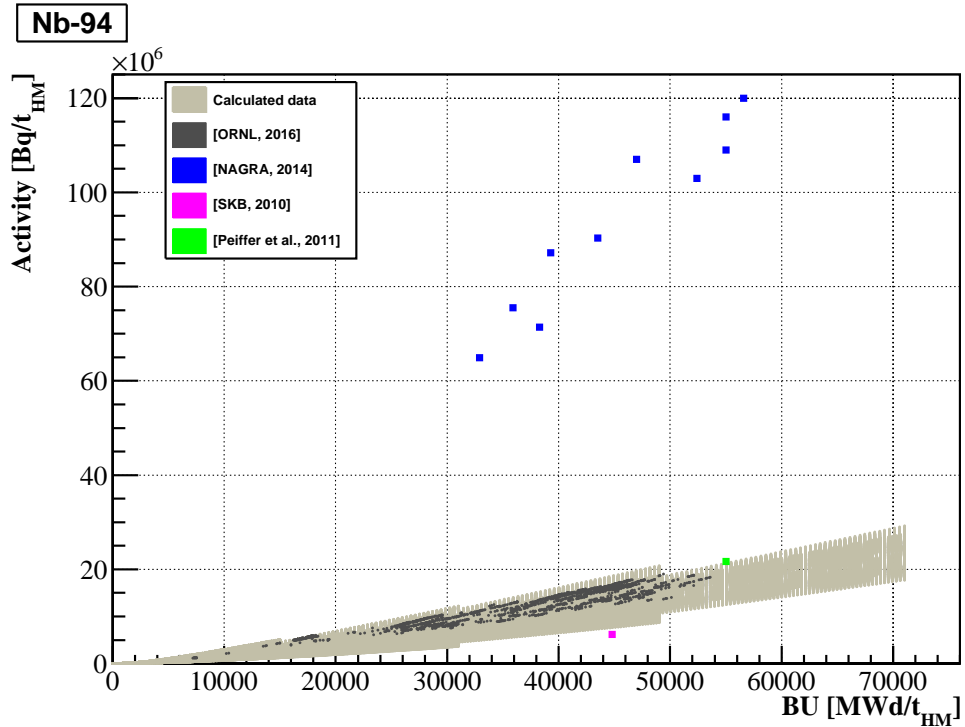


Figure 6.17: Theoretical bandwidth of ⁹⁴Nb and effect of fuel impurities.

^{95}Zr (^{95}Nb)

^{95}Zr is the main radionuclide in the decay chain $^{95}\text{Zr} \rightarrow ^{95}\text{Nb}$, i.e. the concentration of ^{95}Nb is determined by secular equilibrium with ^{95}Zr . However, because the information on FI of Zr is not considered by the calculated international data, while the calculated Swiss data consider 1 ppm of Nb, the ^{95}Nb bandwidth is more interesting in the frame of this study. Therefore, Figure 6.18 shows the bandwidth only for ^{95}Nb . The both radionuclides are fission products. During irradiation time they are built-up by fission and activation processes. These RNs are mostly sensitive to IE, SP and DT, while variations in IE and SP make the most significant contribution to the bandwidths (cf. Figure 6.18). The result reveals no impact from FI, i.e. the calculated Swiss and German data agree with the theoretical bandwidth. The theoretical bandwidth in Figure 6.18 corresponds to the DT corrected bandwidth considering the average DT of 400 days. There are no experimental data in SFCOMPO for these RNs.

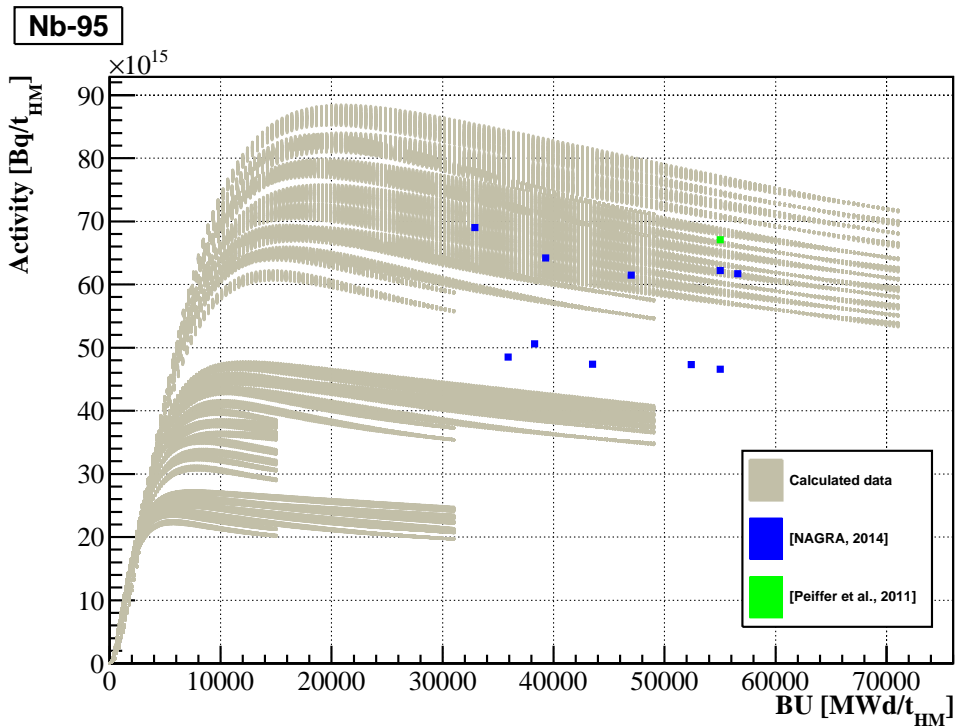


Figure 6.18: Realistic bandwidth of ^{95}Nb .

¹⁰⁷Pd

¹⁰⁷Pd is a fission product. During irradiation time it is built-up by fission and activation processes. There are no experimental data in SFCOMPO for this RN. This RN is mostly sensitive to IE, which variation makes the most significant contribution to the bandwidth (cf. Figure 6.19). The theoretical bandwidth is in a good agreement with the calculated international data.

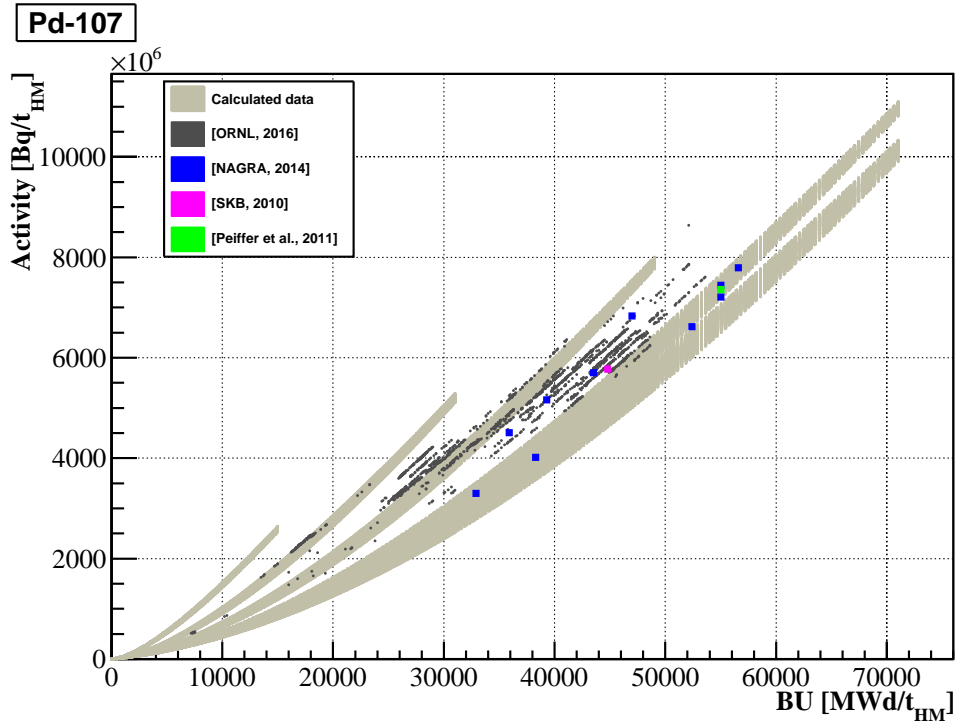


Figure 6.19: Realistic bandwidth of ¹⁰⁷Pd.

¹⁴⁷Pm

¹⁴⁷Pm is a fission product. During irradiation time it is built-up by fission and activation processes. This RN is mostly sensitive to IE, SP and DT, while variations of IE and SP make the most significant contribution to the bandwidth (cf. Figure 6.20). The theoretical bandwidth is in a good agreement with the experimental and calculated international data.

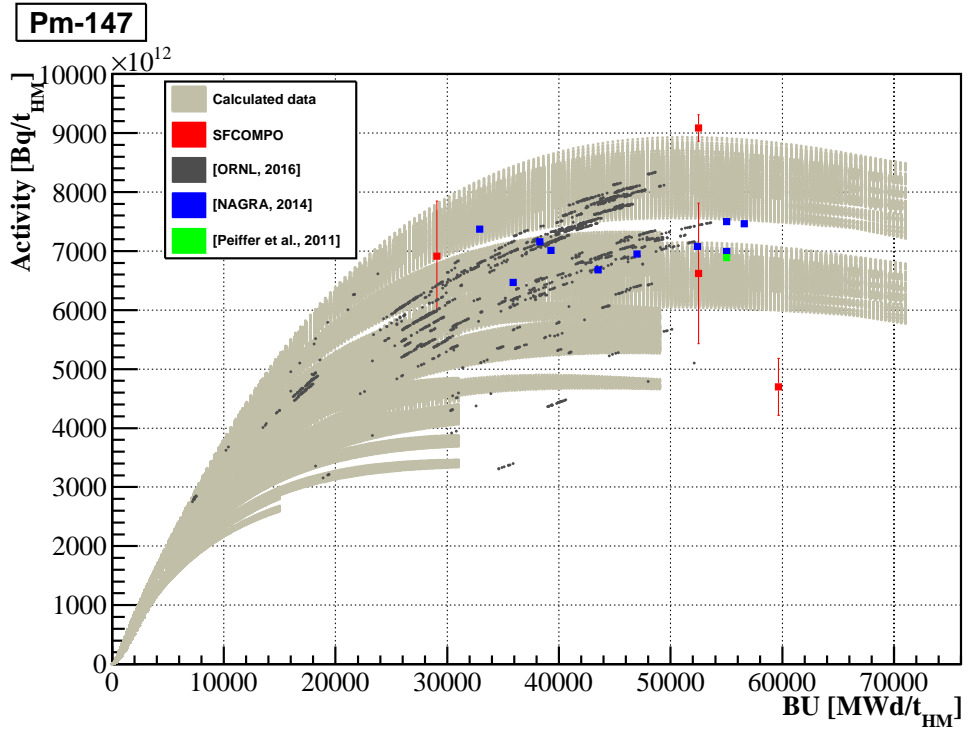


Figure 6.20: Realistic bandwidth of ¹⁴⁷Pm.

^{106}Ru (^{106}Rh)

^{106}Ru is a fission product. During irradiation time it is built-up by fission and activation processes. This RN is mostly sensitive to DT, IE and SP, while variation in IE makes the most significant contribution to the bandwidth (cf. Figure 6.21). The theoretical bandwidth in Figure 6.21 corresponds to the DT corrected bandwidth considering the average DT of 400 days. The theoretical bandwidth is in a good agreement with the experimental and calculated international data.

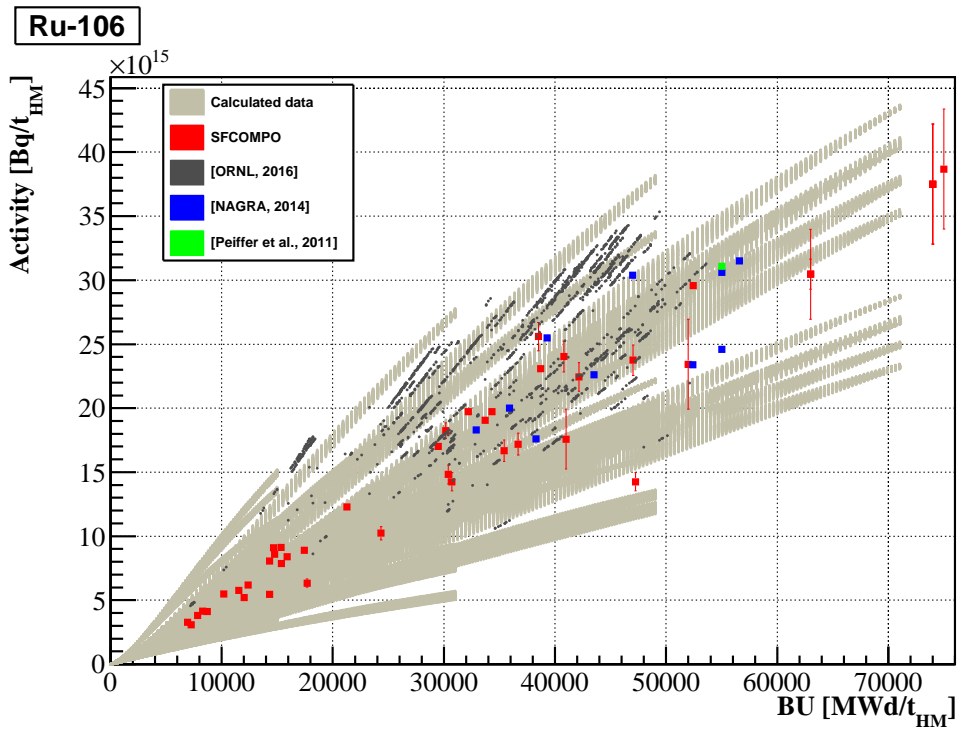


Figure 6.21: Realistic bandwidth of ^{106}Ru .

¹⁰³Ru

¹⁰³Ru is a fission product. During irradiation time it is built-up by fission and activation processes. This RN is mostly sensitive to IE and SP, which variations make the most significant contribution to the bandwidth (cf. Figure 6.22). The theoretical bandwidth is in a good agreement with the experimental and calculated international data.

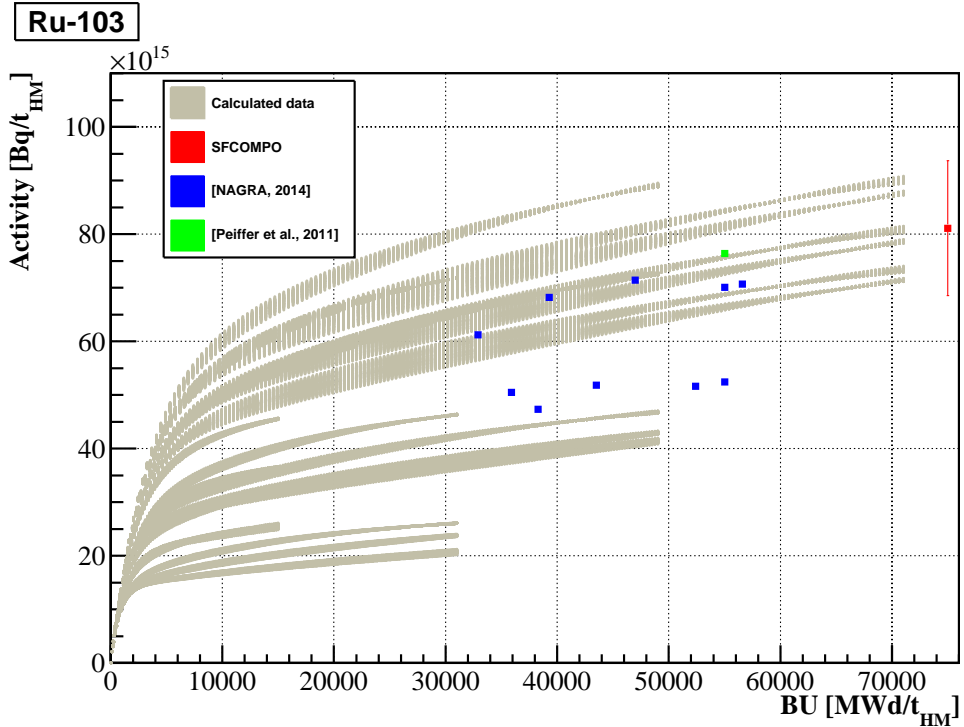


Figure 6.22: Realistic bandwidth of ¹⁰³Ru.

¹²⁴Sb

¹²⁴Sb is a fission product. During irradiation time it is built-up by fission and activation processes. There are no experimental data in SFCOMPO for this RN. This RN is sensitive to all SRPs, while variation in IE makes the most significant contribution to the bandwidth (cf. Figure 6.23). The theoretical bandwidth is in a good agreement with the calculated international data.

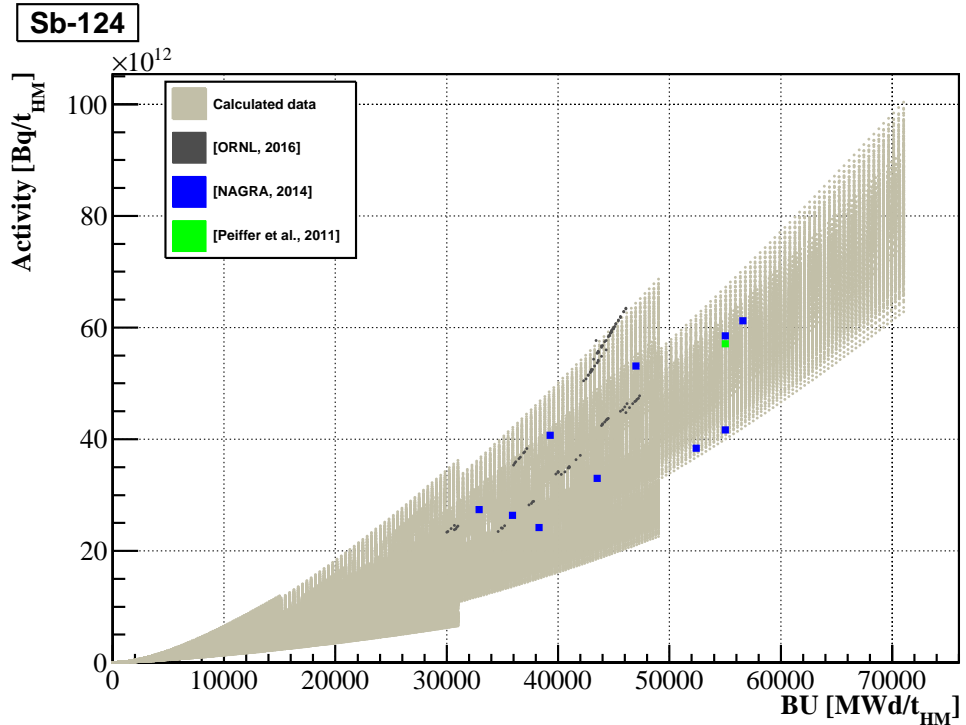


Figure 6.23: Realistic bandwidth of ¹²⁴Sb.

¹²⁵Sb

¹²⁵Sb is a fission product. During irradiation time it is built-up by fission and activation processes. This RN is mostly sensitive to DT, IE and SP, while the variation in IE makes most significant contribution to the bandwidth (cf. Figure 6.24). The theoretical bandwidth in Figure 6.24 corresponds to the DT corrected bandwidth considering the average DT of 400 days. The theoretical bandwidth is in a good agreement with the experimental and calculated international data.

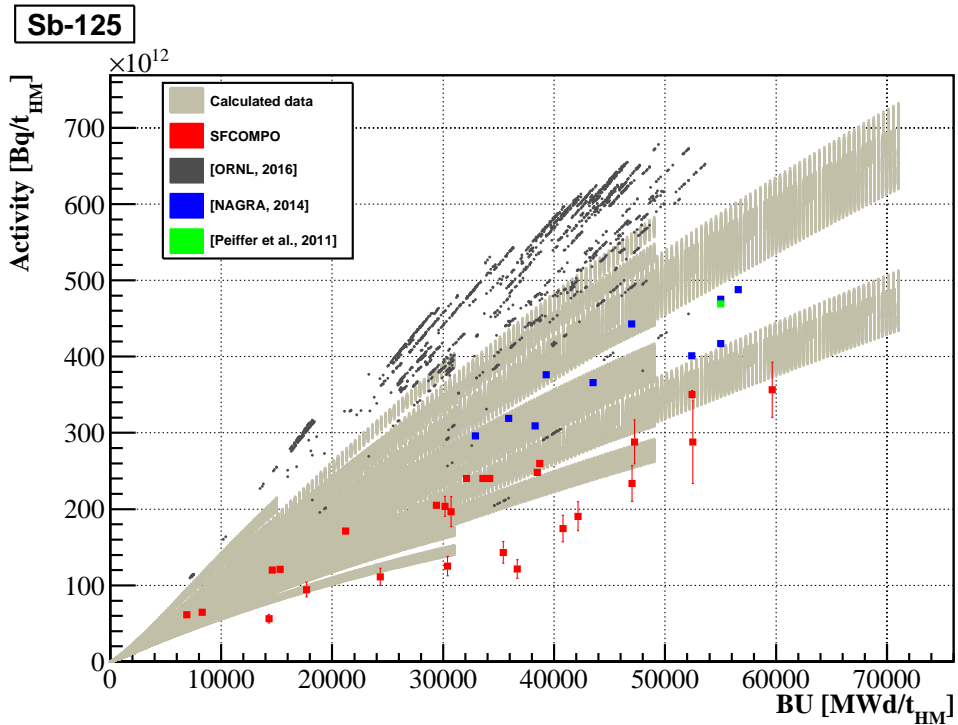


Figure 6.24: Realistic bandwidth of ¹²⁵Sb.

⁷⁹Se

⁷⁹Se is a fission product. During irradiation time it is built-up by fission and activation processes. This RN is practically insensitive to any of the SRPs (cf. Figure 6.25). The theoretical bandwidth is in a good agreement with the experimental and calculated international data.

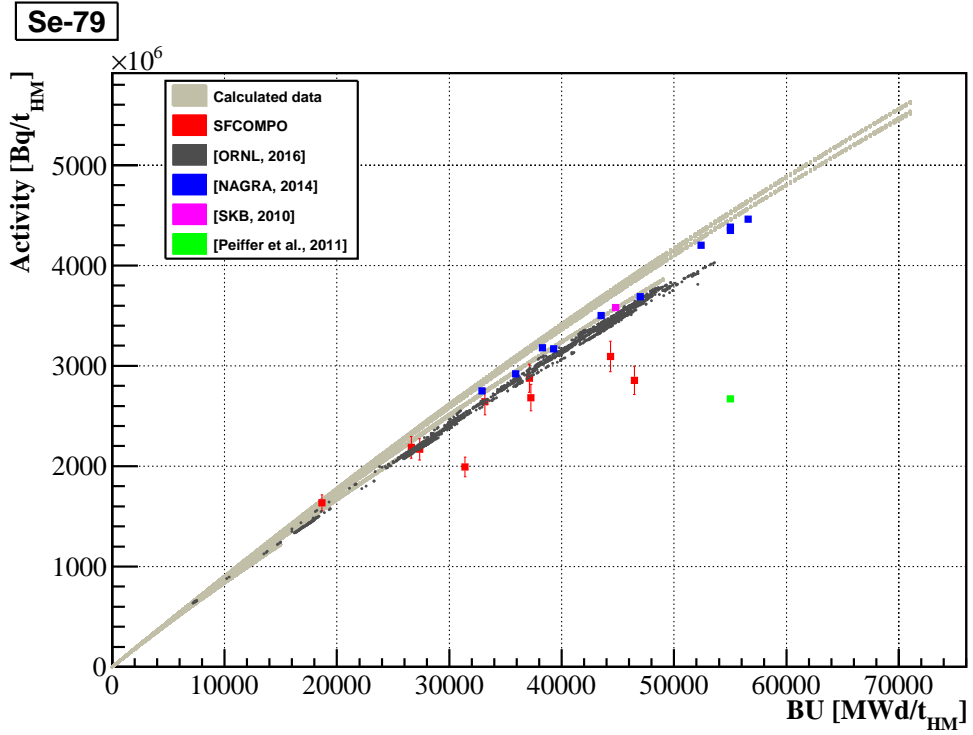


Figure 6.25: Realistic bandwidth of ⁷⁹Se.

¹⁵¹Sm

¹⁵¹Sm is a fission product. During irradiation time it is built-up by fission and activation processes. This RN is sensitive to all SRPs, while the variation in IE makes the most significant contribution to the bandwidth (cf. Figure 6.26). The theoretical bandwidth in Figure 6.26 corresponds to the DT corrected bandwidth considering the average DT of 400 days. The slightly higher values of calculated Swiss and Swedish data correspond to the impurities of Sm in the fuel. However, these values are still within the theoretical bandwidth, therefore, these impurities have no significant impact on this RN activity. The theoretical bandwidth is in a good agreement with the experimental and calculated international data.

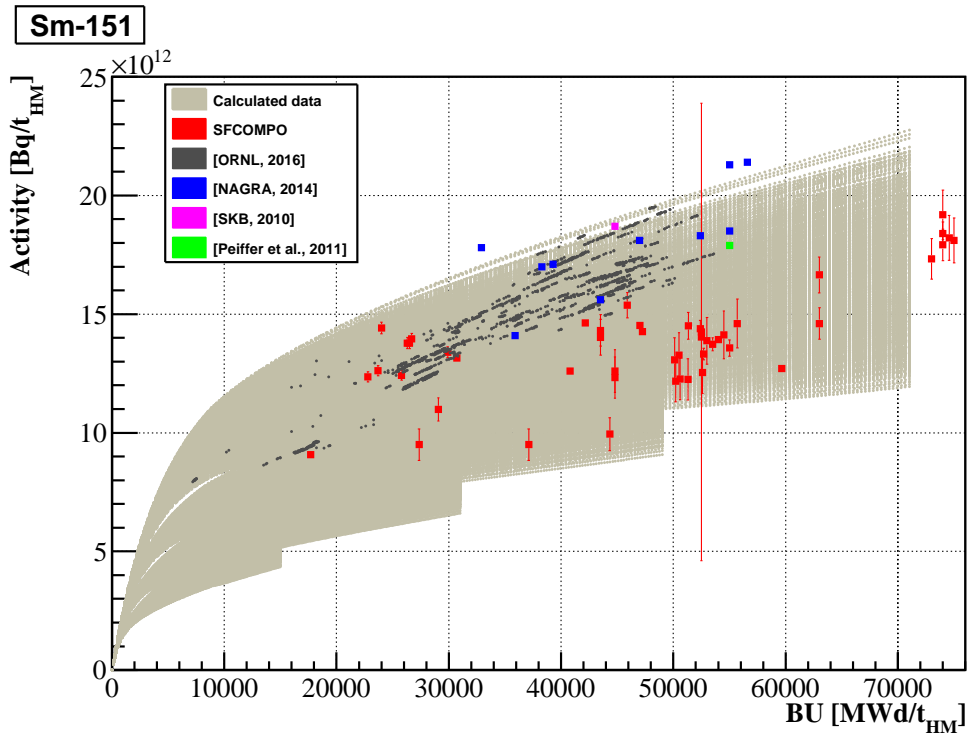


Figure 6.26: Realistic bandwidth of ¹⁵¹Sm.

¹²⁶Sn

¹²⁶Sn is a fission product. During irradiation time it is built-up by fission and activation processes. This RN is mostly sensitive to IE, which variation makes the most significant contribution to the bandwidth (cf. Figure 6.27). The theoretical bandwidth is in a good agreement with the experimental and calculated data from ORNL. The reason for the difference to the other calculated international data can be attributed to fuel impurities (cf. Table 6.3). Thus, FI and then IE are the most important SRPs for the ¹²⁶Sn content in the PWR-UO₂ spent fuel. The impact of all other SRPs can be neglected.

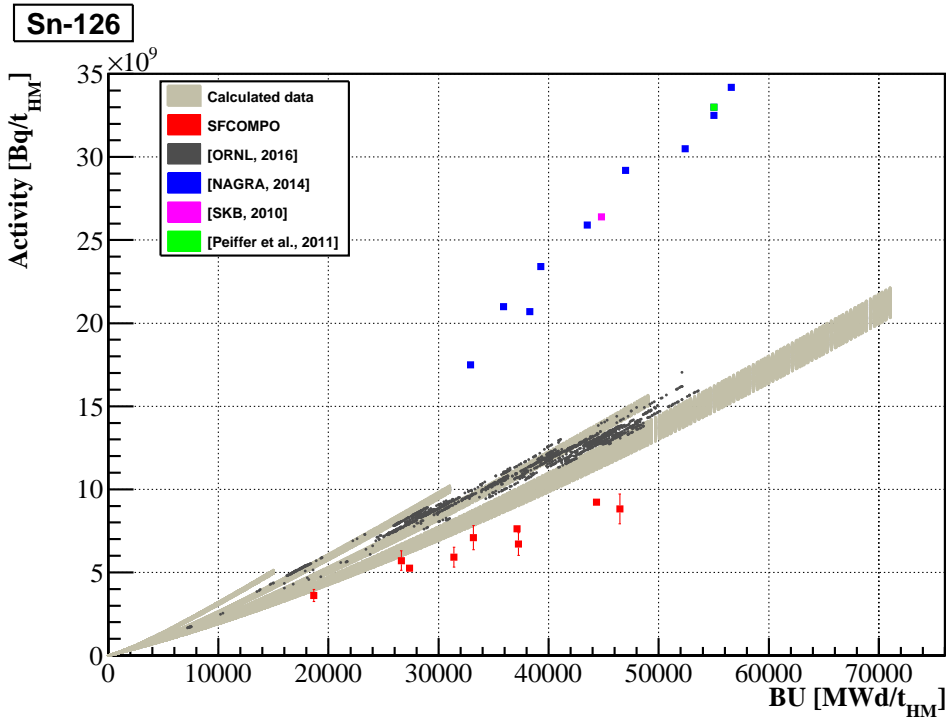


Figure 6.27: Realistic bandwidth of ¹²⁶Sn.

⁹⁰Sr (⁹⁰Y)

⁹⁰Sr is a fission product. During irradiation time it is built-up by fission and activation processes. This RN is mostly sensitive to DT and IE, while the variation in IE makes the most significant contribution to the bandwidth (cf. Figure 6.28). The theoretical bandwidth in Figure 6.28 corresponds to the DT corrected bandwidth considering the average DT of 400 days. The theoretical bandwidth is in a good agreement with the experimental and calculated international data.

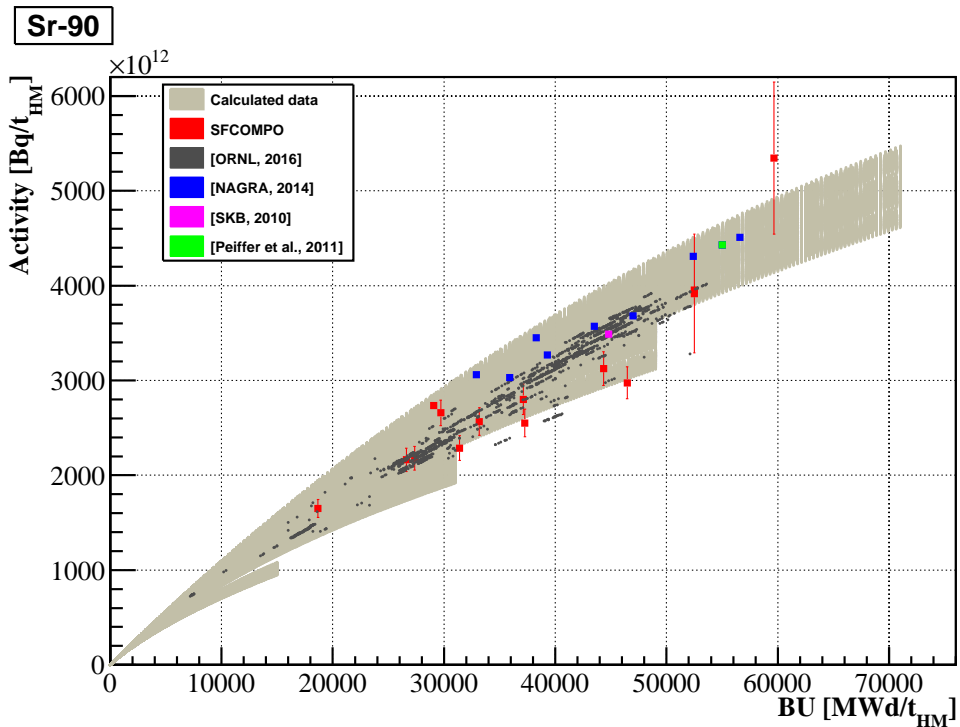


Figure 6.28: Realistic bandwidth of ⁹⁰Sr.

⁹⁹Tc

⁹⁹Tc is a fission product. During irradiation time it is built-up by fission and activation processes. This RN is practically insensitive to any of the SRPs (cf. Figure 6.29). The theoretical bandwidth is in a good agreement with the experimental and calculated international data.

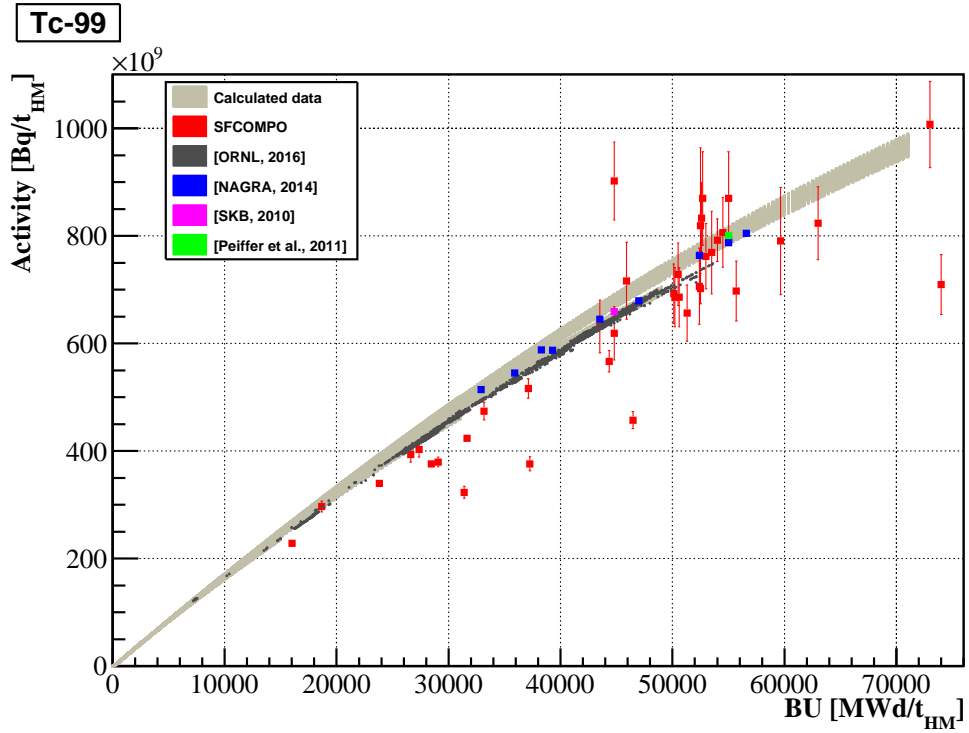


Figure 6.29: Realistic bandwidth of ⁹⁹Tc.

^{93}Zr

^{93}Zr is a fission product. During irradiation time it is built-up by fission and activation processes. There are no experimental data in SFCOMPO for this RN. This RN is mostly sensitive to IE, which variation makes the most significant contribution to the bandwidth (cf. Figure 6.30). The theoretical bandwidth is in a good agreement with the calculated international data.

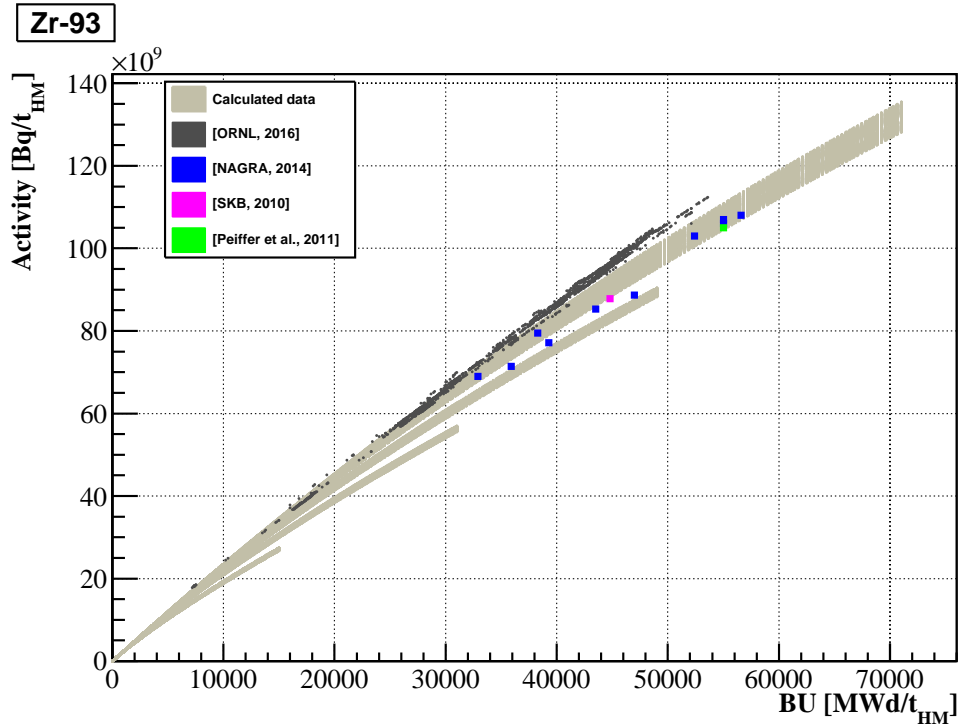


Figure 6.30: Realistic bandwidth of ^{93}Zr .

6.4.2 Realistic bandwidths of actinides

For most of the actinides their mother-daughter behaviour is important for the cooling time correction up to 35 years. Each radionuclide is discussed in relation to its own decay chain. In each decay chain there is a main radionuclide, i.e. all the other radionuclides from this chain attain the secular equilibrium with this RN. This radionuclide has the largest half-life time in the chain. The main RNs are marked in red (cf. Figure 6.31 and Table 4.7).

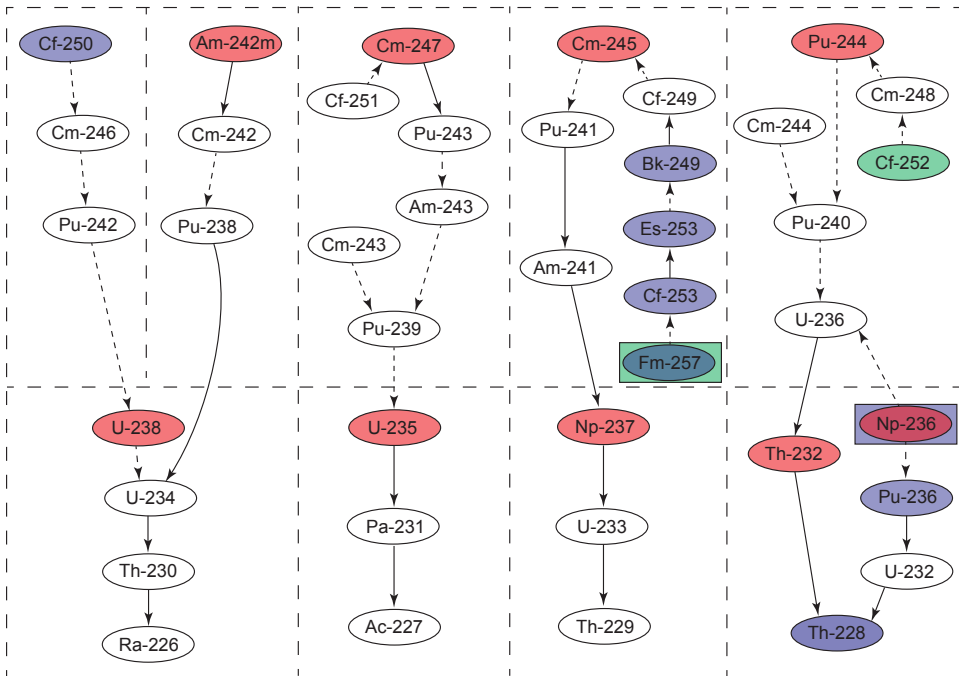


Figure 6.31: Chart of actinide's mother-daughter behaviour: actinides marked in red are the main radionuclides in their decay chains. Actinides marked in blue are a "new" radionuclides that are not included in the list of final disposal relevant RNs. Actinides marked in green are the radionuclides with zero concentrations. Dashed arrows indicate that for CT of up to 35 years the mother radionuclide has no impact on the concentration of the daughter radionuclide. Solid arrows show that for CT of up to 35 years the impact of the mother radionuclide decay must be considered to correct the concentration of the daughter radionuclide.

The Figure 6.31 gives an overview of the mother-daughter relation of actinides and shows the importance of approximations and assumptions for the cooling time correction.

The association of a radionuclide with a given decay chain depends on the considered cooling time. For this work the relevant upper cooling time of CT=35 years is the time correction to the discharge date, which is assumed in the calculated SKB inventory data. The chart 6.31 illustrates the decay dependencies of actinides. Below the realistic bandwidths of the actinides a discussed in relation to the decay chains the belong.

The decay chain: $^{250}\text{Cf} \xrightarrow{\alpha} ^{246}\text{Cm} \xrightarrow{\alpha} ^{242}\text{Pu}$

Parent-daughter relations do not affect significantly the activities of the individual members of this decay chain. Therefore, the activities of these RNs are determined by their own individual decays. Because of its short half-life and small concentration, ^{250}Cf is not relevant for the analysis of realistic bandwidth. Anyway, ^{250}Cf is not included in the list of relevant radionuclides (cf. Table 1.1).

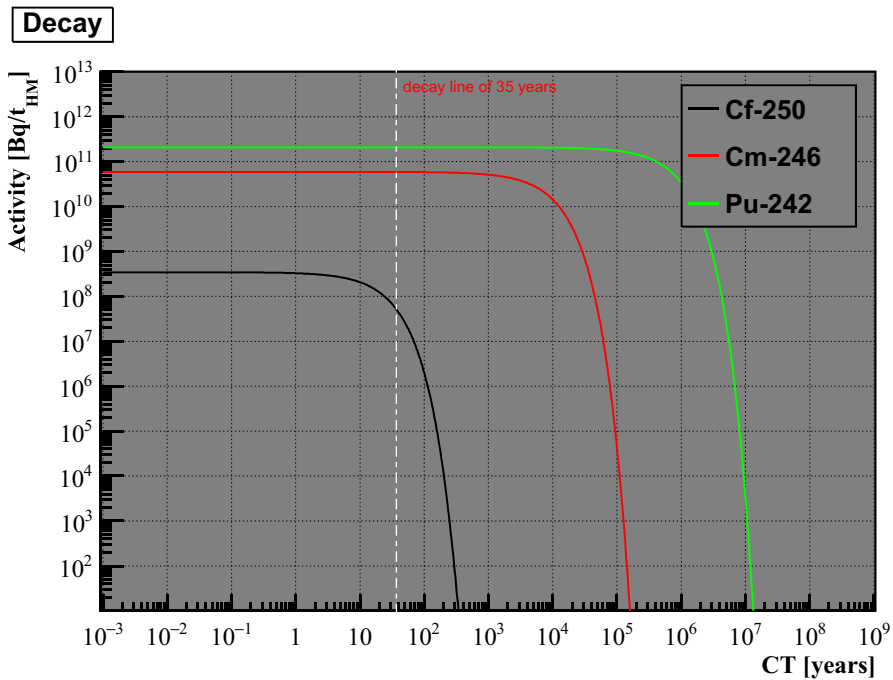


Figure 6.32: Decay chain of ^{250}Cf .

²⁴⁶Cm

During irradiation time ²⁴⁶Cm is built-up by activation processes. This RN is mostly sensitive to IE, which variation makes the most significant contribution to its bandwidth (cf. Figure 6.33). The theoretical bandwidth is in a good agreement with the experimental and calculated international data.

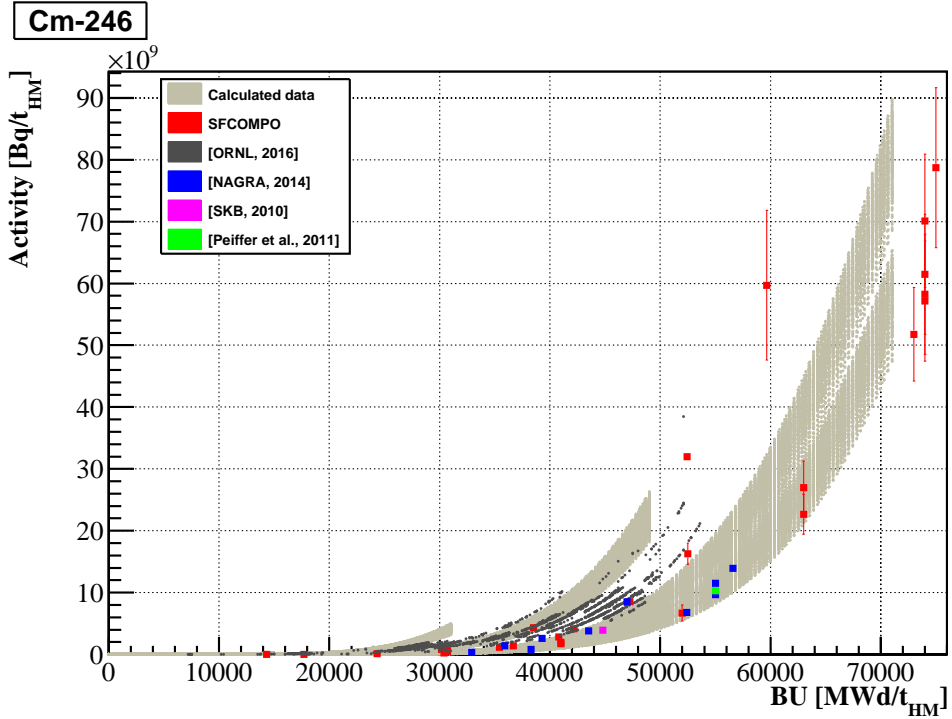


Figure 6.33: Realistic bandwidth of ²⁴⁶Cm.

^{242}Pu

During irradiation time ^{242}Pu is built-up by activation processes. This RN is mostly sensitive to IE, which variation makes the most significant contribution to its bandwidth (cf. Figure 6.34). The theoretical bandwidth is in a good agreement with the experimental and calculated international data.

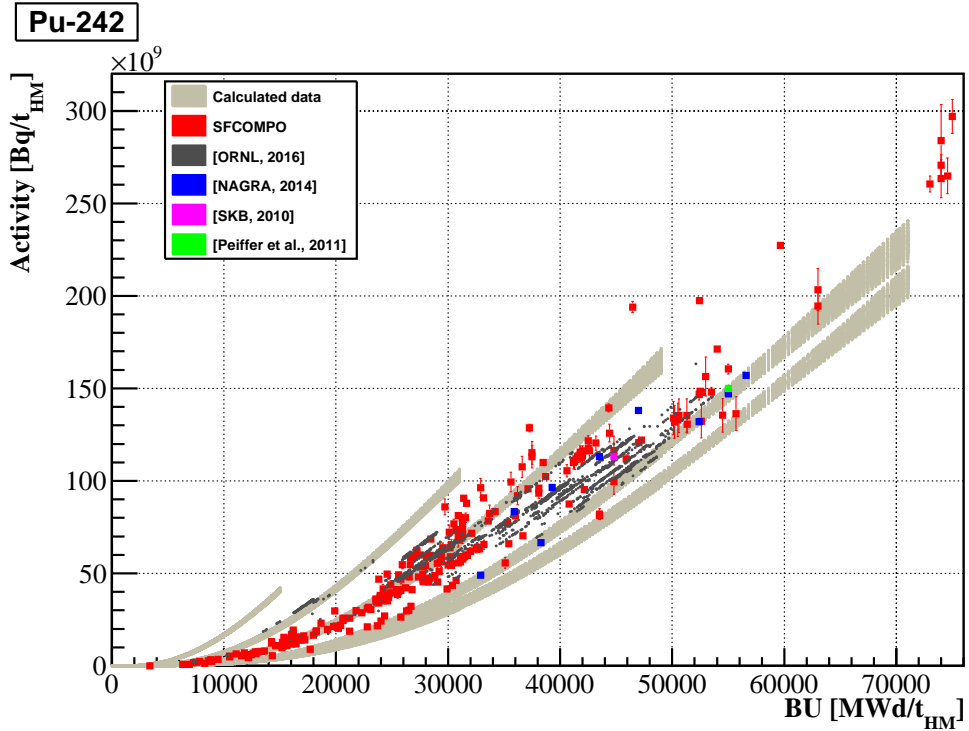


Figure 6.34: Realistic bandwidth of ^{242}Pu .

The decay chain: $^{242\text{m}}\text{Am} \xrightarrow{\beta^-} ^{242}\text{Cm} \xrightarrow{\alpha} ^{238}\text{Pu}$

The particular property of this decay chain is that ^{242}Cm is a short-lived radionuclide, which activity is greatly decreased after about seven years. After about ten years its activity is determined by the secular equilibrium with $^{242\text{m}}\text{Am}$ (cf. Figure 6.35). Thus, for long cooling times (the cases of the US and the SKB data) the correction for the discharge date requires an additional information on the concentration at an earlier (below seven years) discharge time. Because these data are not available such corrections were not performed (cf. Figure 6.37). Therefore, the comparison of the theoretical bandwidths with some experimental and calculated international data were not possible.

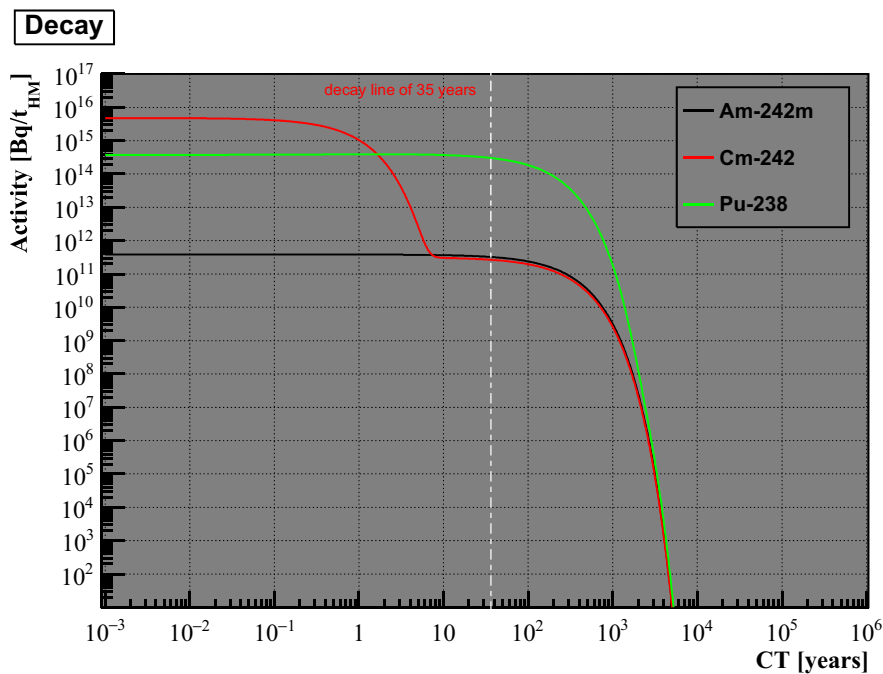


Figure 6.35: Decay chain of $^{242\text{m}}\text{Am}$.

^{242m}Am

During irradiation time ^{242m}Am is built-up by activation processes. This RN shows dependency on all SRPs, while variation in DT makes the most significant contribution to the bandwidth (cf. Figure 6.36). Particularly, the concentration of ^{242m}Am builds-up with the downtime and decreases with the cooling time (cf. Table 6.4). The theoretical bandwidth in Figure 6.36 corresponds to the DT corrected bandwidth considering the average DT of 400 days. Several calculated US data points correspond to the assemblies, which experienced cycle maximum DTs of up to 5-6 years, i.e. the DT correction factor should be approximately 5-6 times higher than it is listed in the Table 4.7. This effect of large DT can be seen in the Figure 6.36, where the US data points exceed the theoretical bandwidth. The additional correction on DT of up to 5-6 years shows that all calculated US data are well within the theoretical bandwidth. Thus, the theoretical bandwidth is in a good agreement with the experimental and calculated international data.

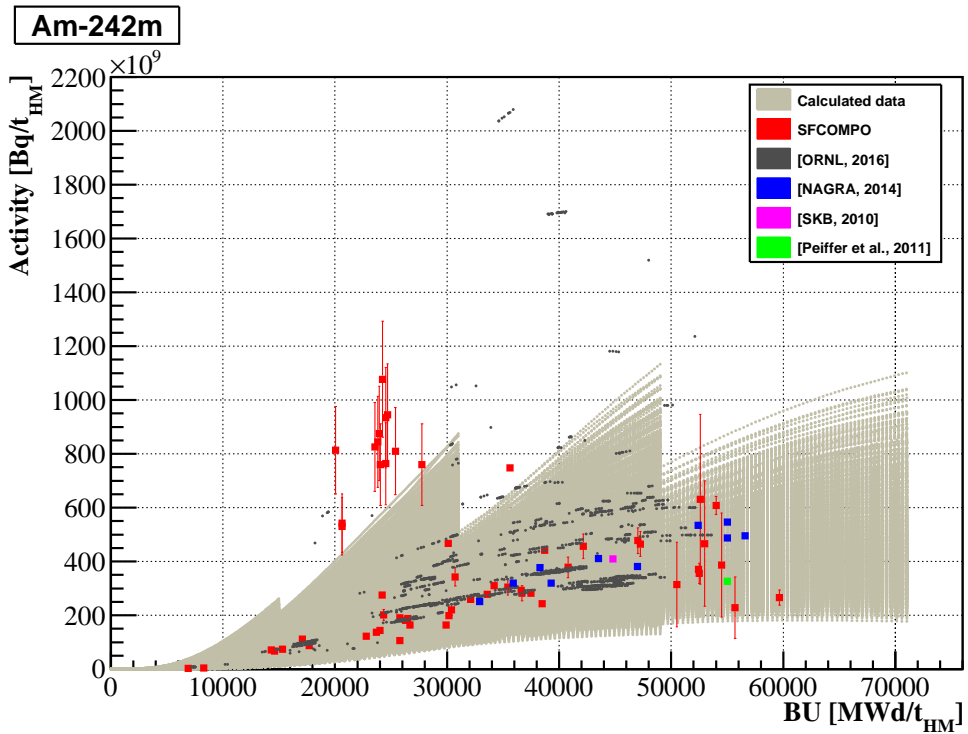


Figure 6.36: Realistic bandwidth of ^{242m}Am.

²⁴²Cm

During irradiation time ²⁴²Cm is built-up by an activation process and by decay of precursor radionuclide. This RN shows dependency on all SRPs, while variation in the DT makes the most significant contribution to the bandwidth (cf. Figure 6.37). ²⁴²Cm is short-lived RN. Therefore, the cooling time correction can be made only in cases, where the secular equilibrium between ^{242m}Am and ²⁴²Cm is not achieved. The ORNL and SKB provide the concentration values only for the cases, where such an equilibrium has been achieved (i.e. for the cooling times between 25 and 35 years). Therefore, the comparison of the theoretical bandwidths for this RN with these calculated international data were not possible. For similar reasons the comparison with some of the available experimental data was also not performed.

The theoretical bandwidth in Figure 6.37 corresponds to the DT corrected bandwidth considering the average DT of 400 days. The theoretical bandwidth is in a good agreement with the experimental and calculated international data.

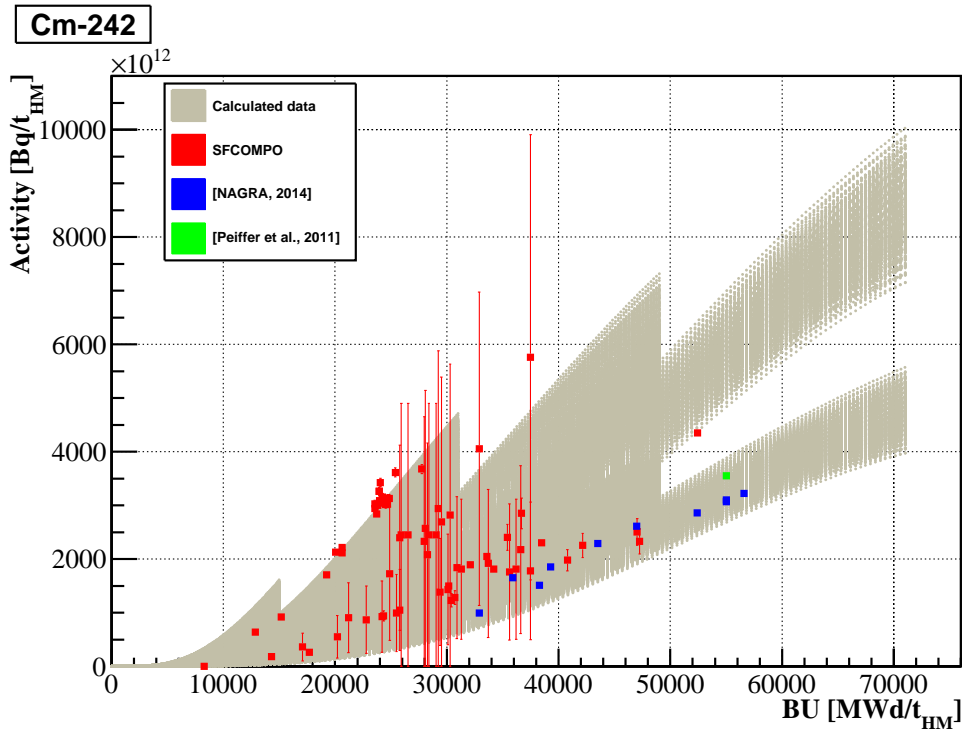


Figure 6.37: Realistic bandwidth of ²⁴²Cm.

²³⁸Pu

During irradiation time ²³⁸Pu is built-up by an activation process and decay of ²⁴²Cm. This RN is mostly sensitive to DT, which variations makes the most significant contribution to its bandwidth (cf. Figure 6.38). Particularly ²³⁸Pu concentration builds-up with downtime and decreases with the cooling time (cf. Table 6.4). The theoretical bandwidth in Figure 6.38 corresponds to the DT corrected bandwidth considering the average DT of 400 days. Several calculated US data points correspond to the assemblies, which experienced the cycle maximum DT of up to 5-6 years, i.e. the DT correction factor should be approximately 5-6 times higher than that in the Table 4.7. This effect of large DT can be seen in the Figure 6.38, where the US data points are exceed the theoretical bandwidth. The additional correction on DT of up to 5-6 years shows that all calculated US data are well within the theoretical bandwidth.

Slightly higher activities of the calculated US data correspond to the effect of burnable absorber exposure that is considered in the ORNL modelling.

The theoretical bandwidth is in a good agreement with the experimental and calculated international data.

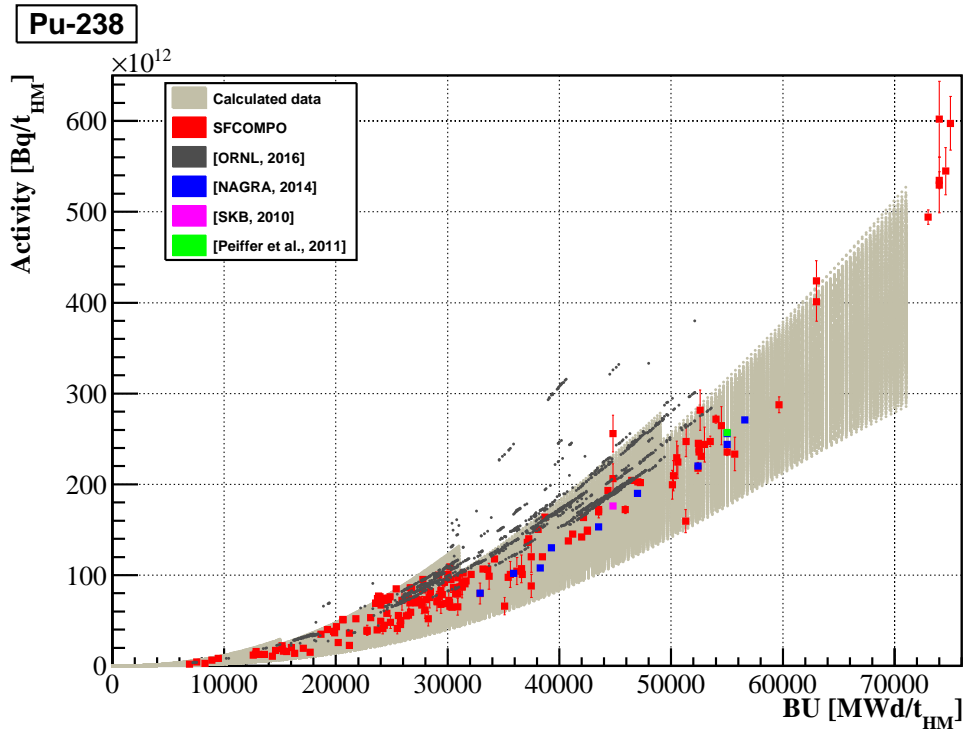


Figure 6.38: Realistic bandwidth of ²³⁸Pu.

The decay chain: $^{238}\text{U} \xrightarrow{\alpha} ^{234}\text{U} \xrightarrow{\alpha} ^{230}\text{Th} \xrightarrow{\alpha} ^{226}\text{Ra}$

Figure 6.39 shows that the decay of ^{238}Pu in the decay chain of ^{238}U has a significant impact on the concentration of ^{234}U and consequently on the concentrations of the daughter radionuclides. ^{238}U is not influenced by its parent radionuclide ^{242}Pu and, thus, remains constant for more than 10^9 years. This Figure shows the activities computed for the case, where the initial composition of ^{234}U was set equal to zero. On the other hand, the results of experimental and calculated international data show that the realistic initial content of ^{234}U is not zero (cf. Figure 6.42). Additional simulations with realistic initial concentrations of the uranium isotopes as given in [Cerne et al., 1987] provide a factor of 10 higher activity values for ^{234}U and the correspondingly higher activity values for ^{230}Th and ^{226}Ra . The concentrations of the latter two isotopes are by a factor of 100 higher than in the case of zero initial concentration of ^{234}U (cf. Figure 6.40).

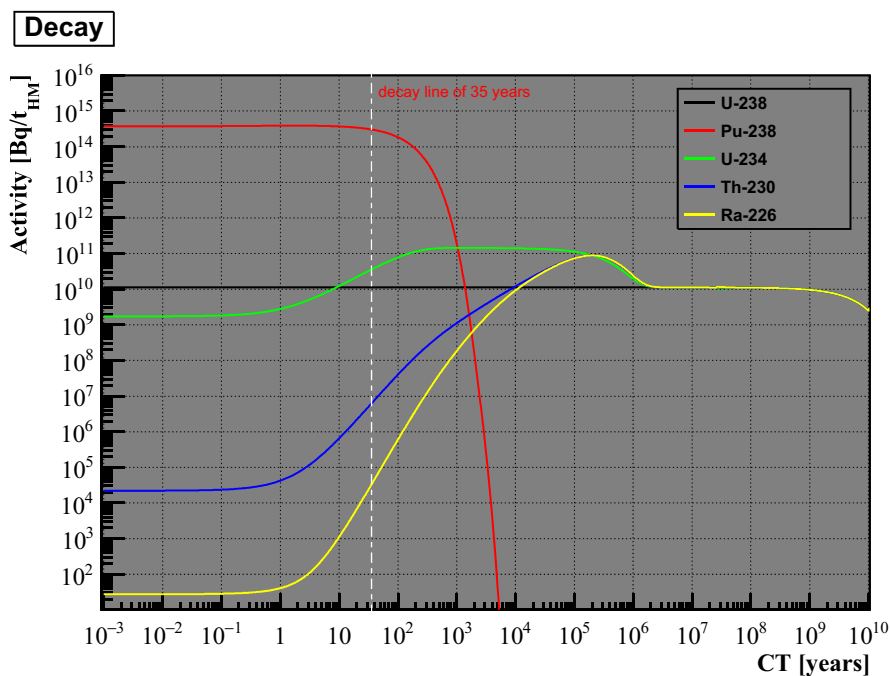


Figure 6.39: Decay chain of ^{238}U with initial composition of ^{234}U equal zero.

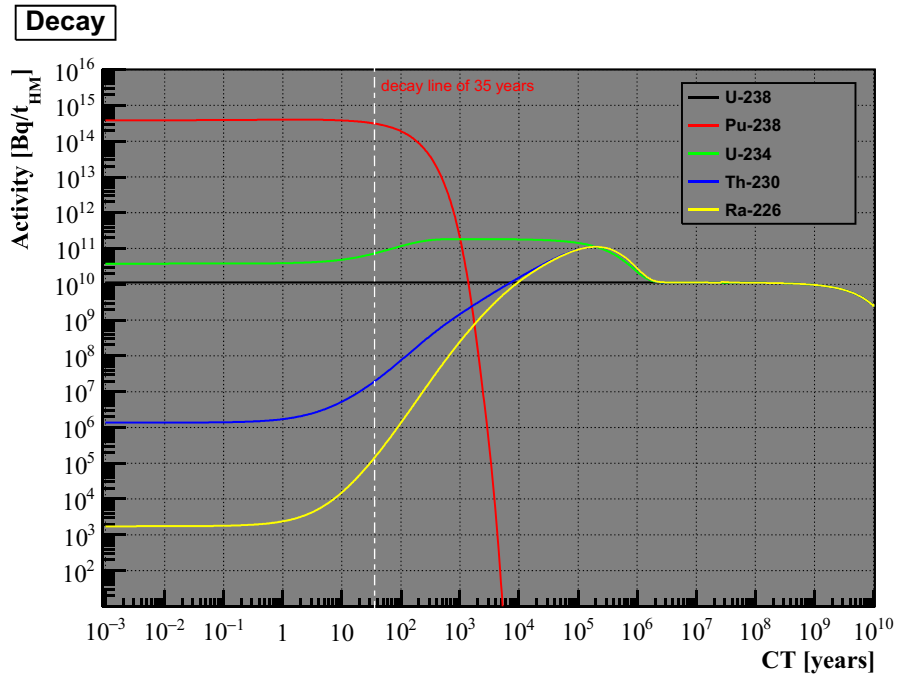


Figure 6.40: Decay chain of ²³⁸U with considered initial composition of ²³⁴U as of [Cerne et al., 1987].

²³⁸U

During irradiation time ²³⁸U is depleted by the irradiation process. This RN shows the dependence on IE, which variation makes the most significant contribution to the bandwidth (cf. Figure 6.41). The theoretical bandwidth is in a good agreement with the experimental and calculated international data.

The stronger negative gradient of all calculated US data points can be attributed to control rod effects (the ORNL modelling considers the burnable absorber exposure). Due to the effect of the thermal neutron consumption the neutron capture by ²³⁸U is increased, what leads to an increase in Pu production (cf. Figure 6.51).

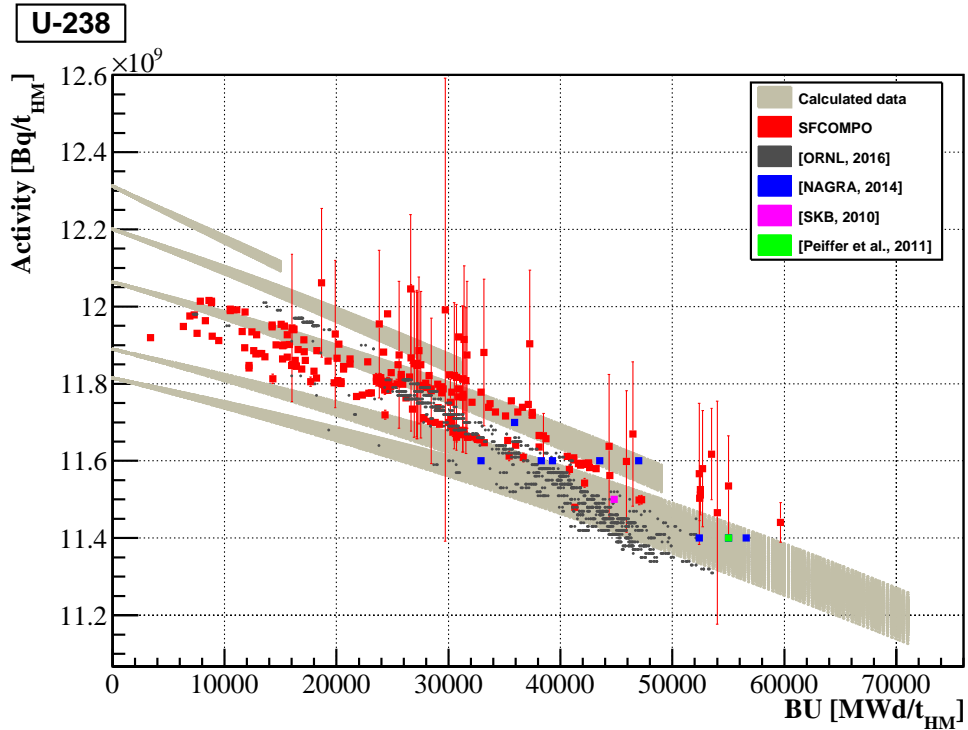


Figure 6.41: Realistic bandwidth of ²³⁸U.

²³⁴U

During irradiation time ²³⁴U is built-up by activation and decay processes. This RN depends both on DT and IE, while the IE makes the most significant contribution to the bandwidth (cf. Figure 6.42).

However, the activity of ²³⁴U is strongly dependent on the initial composition (IC) of this RN in the fuel. At the time when the SRP analysis has been performed the importance of this information was not realized because of the lack of available data, and therefore, its effect was not taken into account (i.e. initial concentration of ²³⁴U was set equal to zero). Figure 6.42 shows that this assumption led to a factor of 10 difference between the theoretical bandwidth and the experimental data or calculated international data, while the latter two sources of information were in a good agreement with each other. Additional simulations with the initial uranium isotopic content from [Cerne et al., 1987] provided a very good agreement with these data.

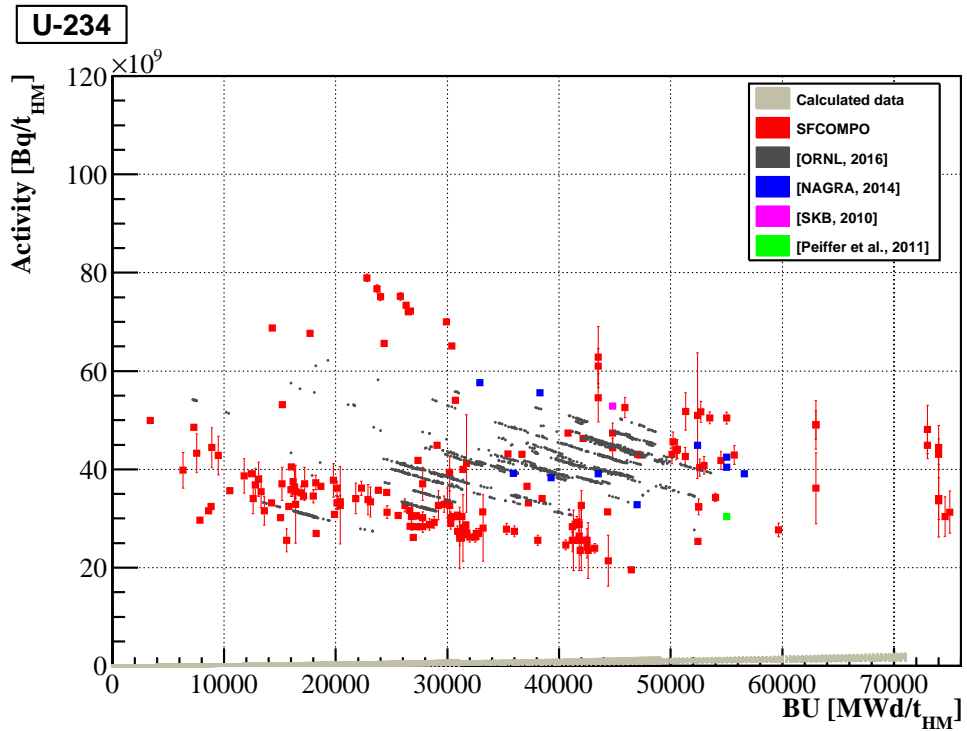
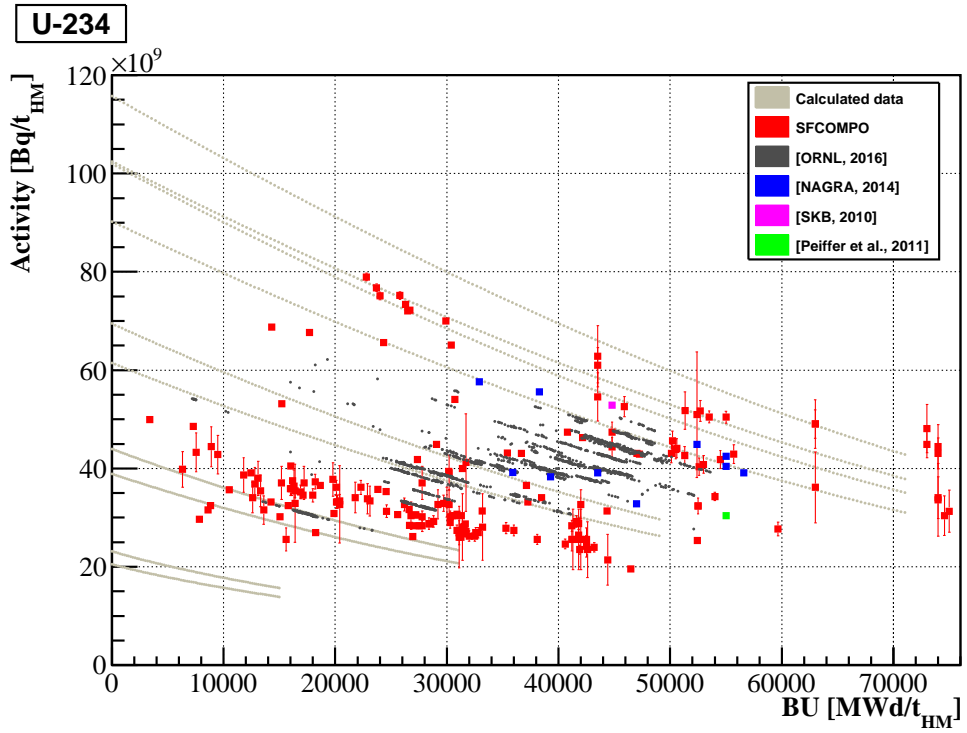


Figure 6.42: Effect of initial composition on ²³⁴U concentration.

Figure 6.43: Realistic bandwidth of ²³⁴U.

²³⁰Th

During irradiation time ²³⁰Th is built-up by activation and decay processes. This RN depends on DT and IE, while the DT makes the most significant contribution to the bandwidth.

However, ²³⁰Th is quite sensitive to the initial composition of ²³⁴U. An assumption of zero initial concentration of ²³⁴U may lead to discrepancies between the theoretical bandwidth and the available calculated international data to a factor of 100. Figure 6.44 shows the bandwidth corrected for the initial concentration. The theoretical bandwidth is in a good agreement with the calculated international data. However, the positive slope of the theoretical bandwidth on burn-up is not consistent with the negative slope revealed by the calculated international data. These deviations could be related to the problems in the SCALE version 6.1.0, which are discussed in the section 2.2.

There are no experimental data in SFCOMPO for this RN.

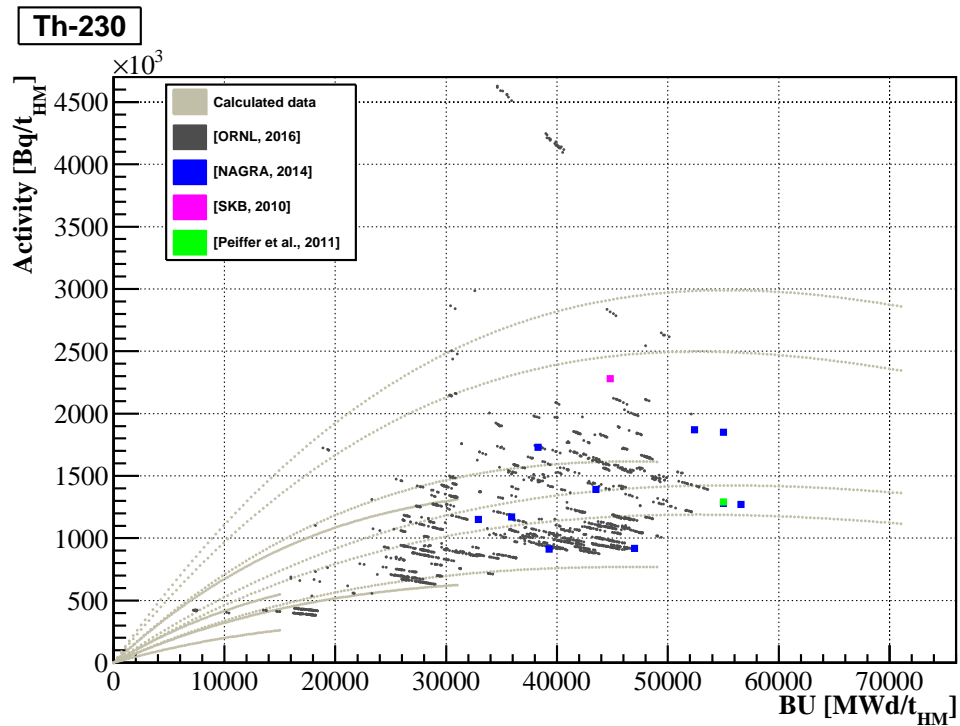


Figure 6.44: Realistic bandwidth of ²³⁰Th, corrected to the initial composition of ²³⁴U.

²²⁶Ra

During irradiation time ²²⁶Ra is built-up by activation and decay processes. This RN depends on DT and IE, while the DT makes the most significant contribution to the bandwidth.

In analogy to ²³⁰Th the initial composition of ²³⁴U gives the largest contribution to the theoretical bandwidth with a maximum discrepancy factor of 100. Figure 6.45 shows the bandwidth corrected for the initial concentration. The theoretical bandwidth is in a good agreement with the calculated NAGRA and GRS data. The calculated US and SKB data provide slightly higher activity values.

There are no experimental data in SFCOMPO for this RN.

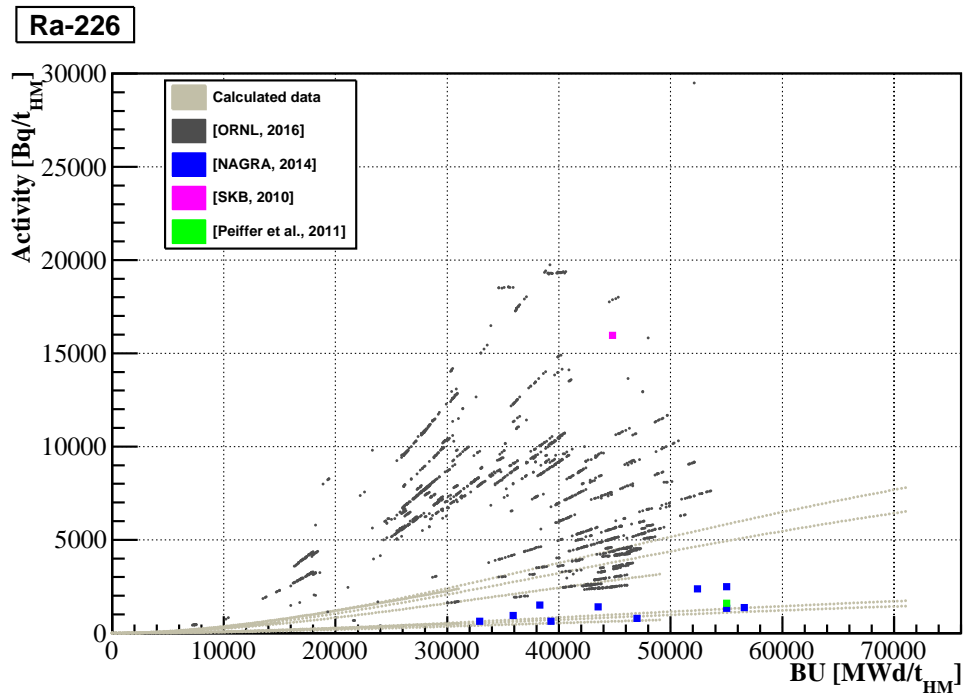
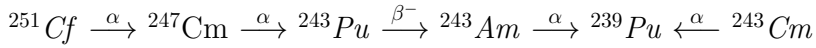


Figure 6.45: Realistic bandwidth of ²²⁶Ra, corrected to the initial composition of ²³⁴U.

The decay chain:



The decay chain of ${}^{247}\text{Cm}$ includes six radionuclides: ${}^{251}\text{Cf}$, ${}^{247}\text{Cm}$, ${}^{243}\text{Pu}$, ${}^{243}\text{Am}$, ${}^{243}\text{Cm}$ and ${}^{239}\text{Pu}$. All these radionuclides can be assumed to be cooling time independent (for CT = 35 years) except for the short-lived radionuclides ${}^{243}\text{Pu}$ and ${}^{243}\text{Cm}$ (cf. Figure 6.46). ${}^{243}\text{Pu}$ achieves the secular equilibrium with ${}^{247}\text{Cm}$ in a few days. Therefore, the realistic bandwidth of ${}^{243}\text{Pu}$ is determined by the realistic bandwidth of ${}^{247}\text{Cm}$.

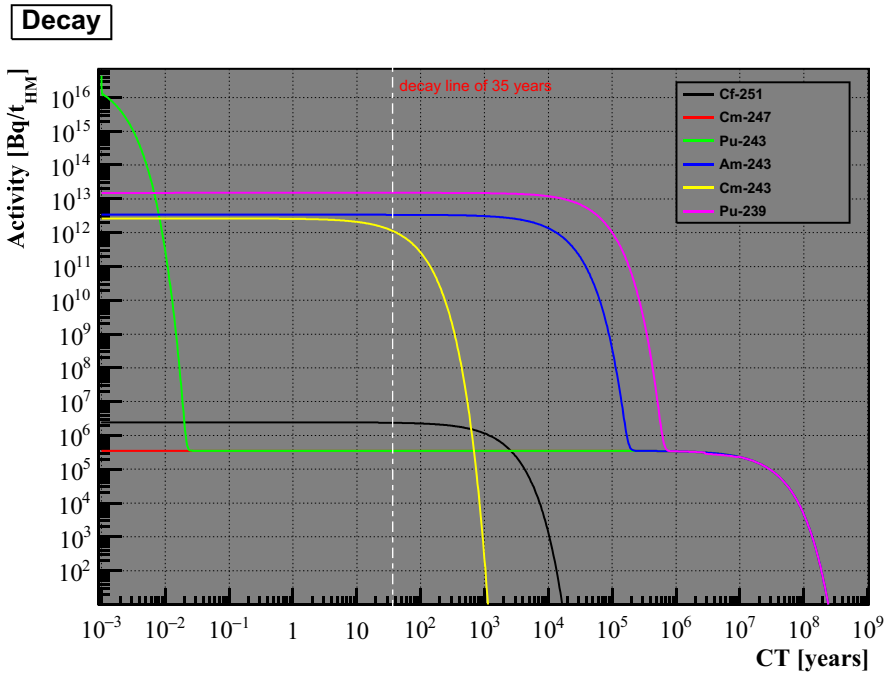


Figure 6.46: Decay chain of ${}^{247}\text{Cm}$.

²⁵¹Cf

During irradiation time ²⁵¹Cf is built-up by activation processes. There are no measurements in SFCOMPO for this radionuclide. This RN shows no strong dependence on any SRPs (cf. Figure 6.47). The theoretical bandwidth is in a good agreement with the calculated international data.

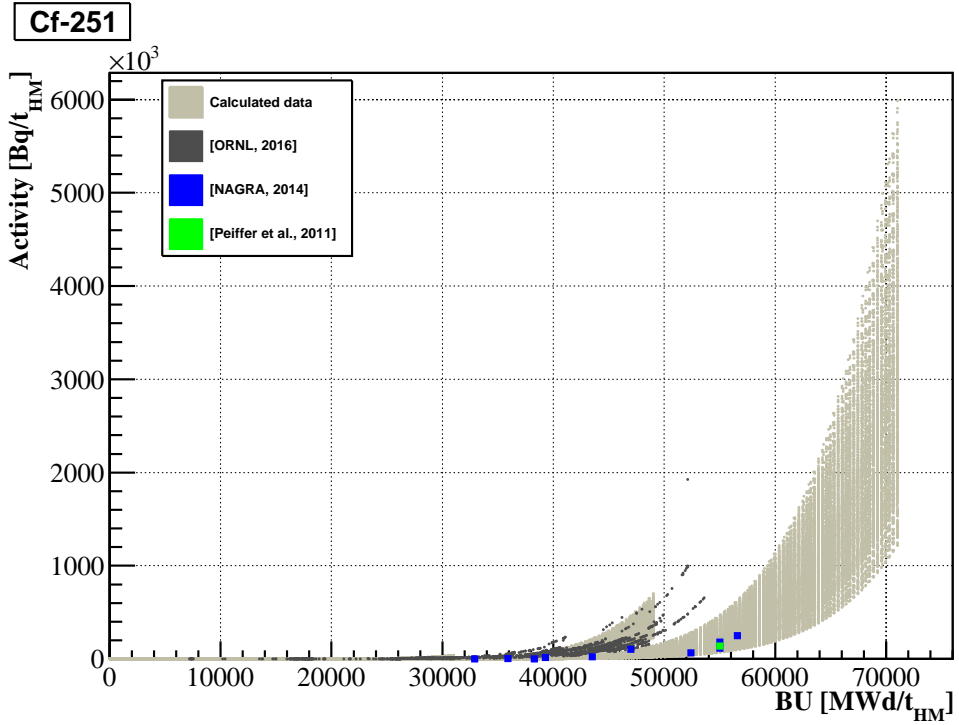


Figure 6.47: Realistic bandwidth of ²⁵¹Cf.

^{247}Cm (^{243}Pu)

During irradiation time ^{247}Cm is built-up by activation and decay processes. This RN depends on IE, which makes the most significant contribution to the bandwidth (cf. Figure 6.48). The theoretical bandwidth is in a good agreement with the experimental and calculated international data.

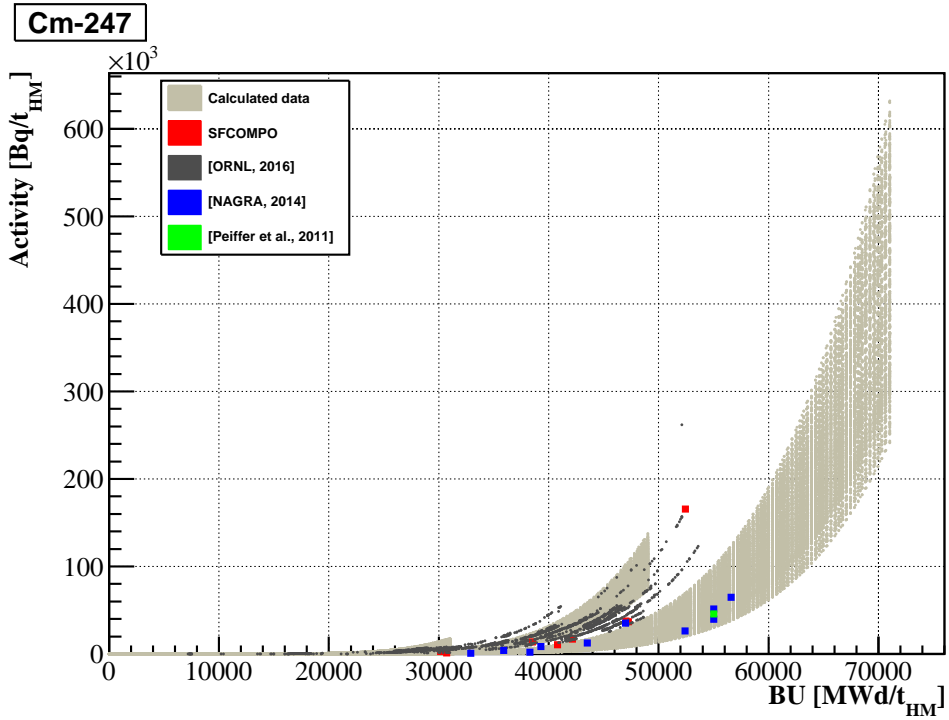


Figure 6.48: Realistic bandwidth of ^{247}Cm (^{243}Pu).

²⁴³Am

During irradiation time ²⁴³Am is built-up by activation and decay processes. This RN depends on IE, which makes the most significant contribution to the bandwidth (cf. Figure 6.49). The theoretical bandwidth is in a good agreement with the experimental and calculated international data.

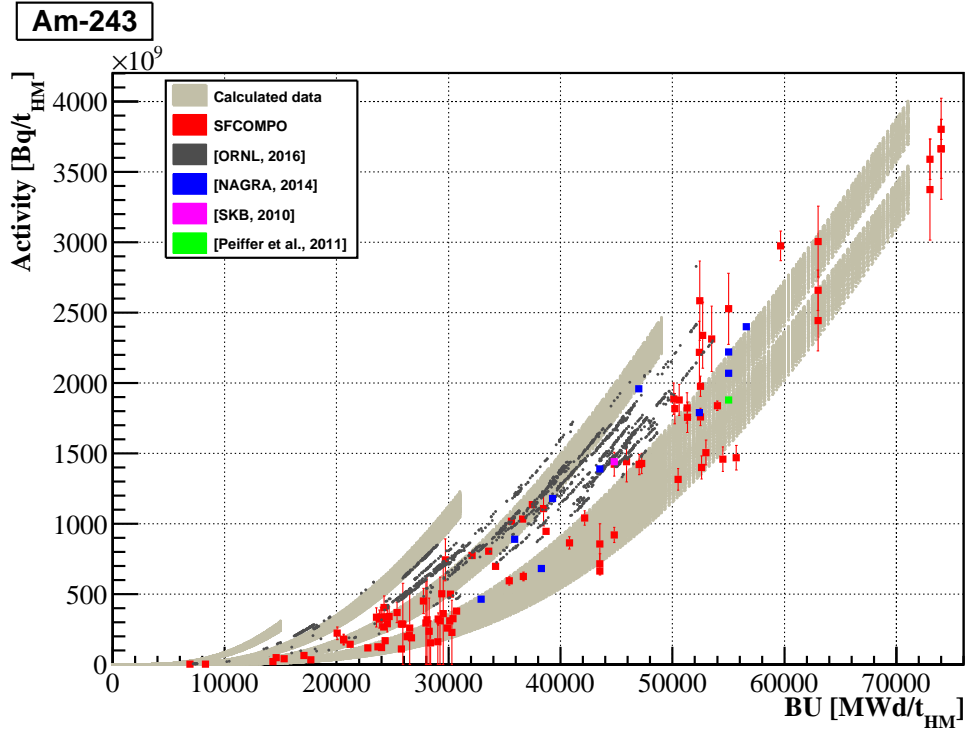


Figure 6.49: Realistic bandwidth of ²⁴³Am.

²⁴³Cm

During irradiation time ²⁴³Cm is built-up by activation processes. This RN depends on DT, which makes the most significant contribution to the bandwidth (cf. Figure 6.50). Particularly the concentration of ²⁴³Cm increases with the downtime and decreases with the cooling time (cf. Table 6.4). The theoretical bandwidth in Figure 6.50 corresponds to the DT corrected bandwidth considering the average DT of 400 days. Several calculated US data points correspond to assemblies, which experienced a cycle maximum DT of up to 5-6 years, i.e. the DT correction factor should be approximately 5-6 times higher than that in the Table 4.7. This effect is seen in the Figure 6.50. The additional calculations assuming the DT of up to 5-6 years show that all calculated US data fall within the theoretical bandwidth. Thus, the theoretical bandwidth is in a good agreement with the experimental and calculated international data.

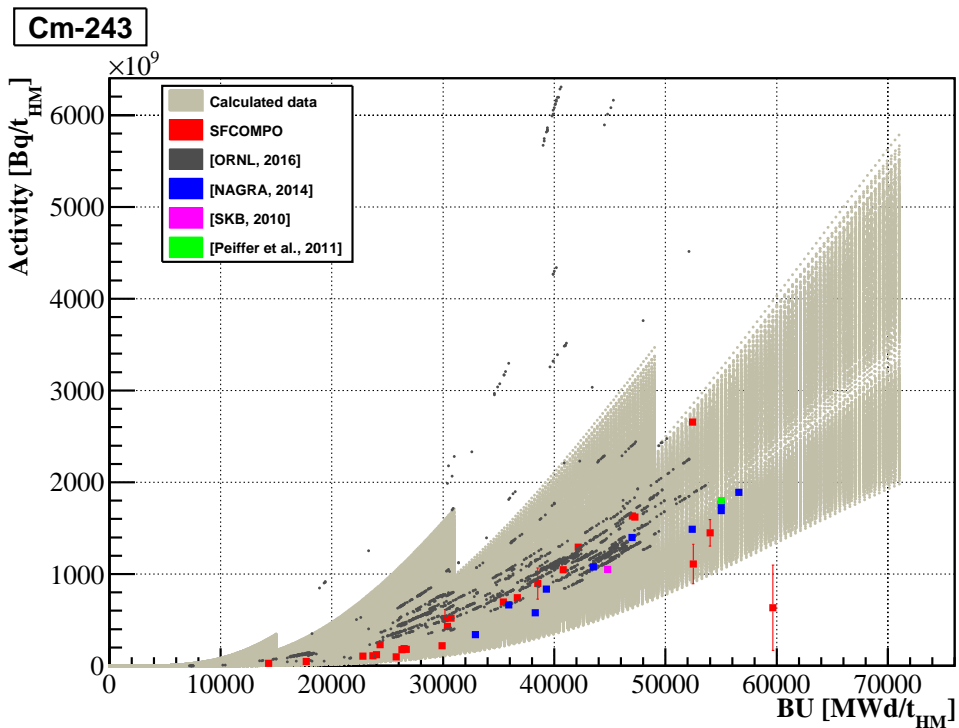


Figure 6.50: Realistic bandwidth of ²⁴³Cm.

²³⁹Pu

During irradiation time ²³⁹Pu is built-up by activation and decay processes. This RN depends on all considered SRPs, while the variation in IE makes the most significant contribution to the bandwidth (cf. Figure 6.51). The theoretical bandwidth is in a good agreement with the experimental and calculated international data.

For ²³⁹Pu all activity values of calculated US data points are slightly higher, because of control rod effects (the US modelling considers the burnable absorber exposure). Due to the effect of the thermal neutron consumption the neutron capture by ²³⁸U is increased, what leads to an increase in Pu production. The increased ²³⁹Pu generation is consistent with the higher rate of depletion in ²³⁸U (cf. Figure 6.41).

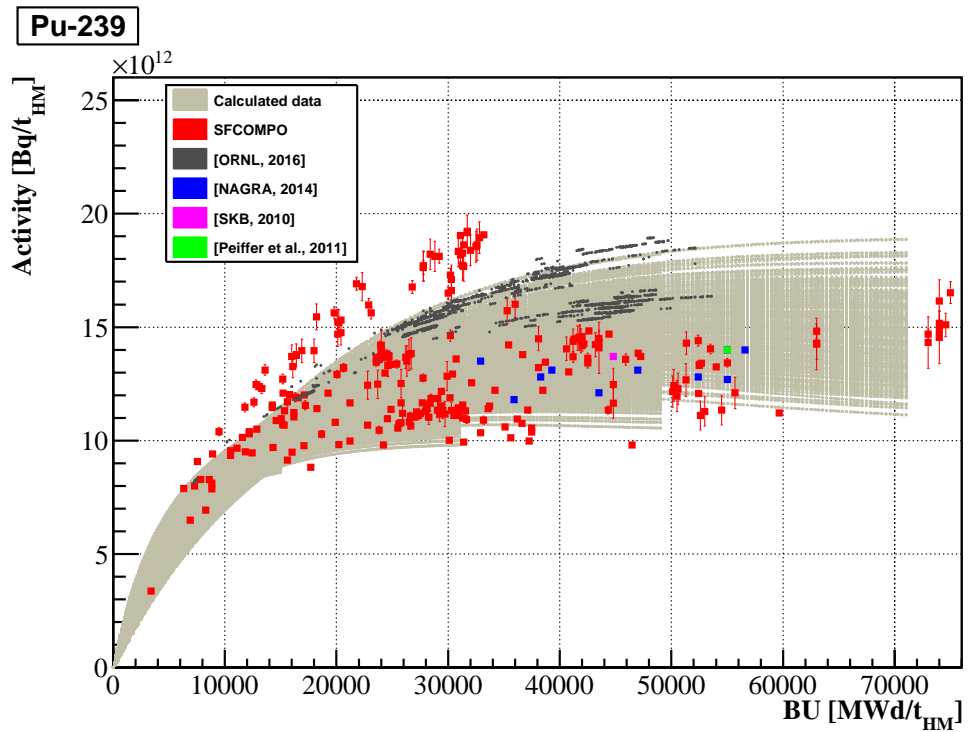


Figure 6.51: Realistic bandwidth of ²³⁹Pu.

The decay chain: $^{235}\text{U} \xrightarrow{\alpha} ^{231}\text{Pa} \xrightarrow{\alpha} ^{227}\text{Ac}$

Figure 6.52 shows that the decay of ^{239}Pu does not have a significant impact on ^{235}U for the CT of up to 35 years. The consideration of the decay of ^{239}Pu becomes important for the CT above 10 thousand years.

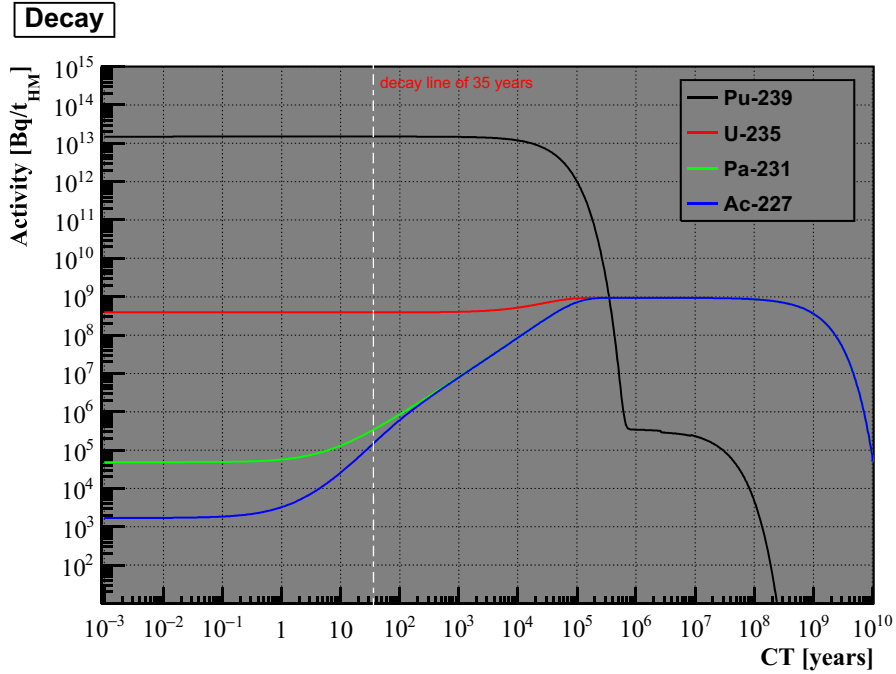


Figure 6.52: Decay chain of ^{235}U .

²³⁵U

During irradiation time ²³⁵U is depleted due to the fission. This RN depends on IE, which makes the most significant contribution to the bandwidth (cf. Figure 6.53). The theoretical bandwidth is in a good agreement with the experimental and calculated international data.

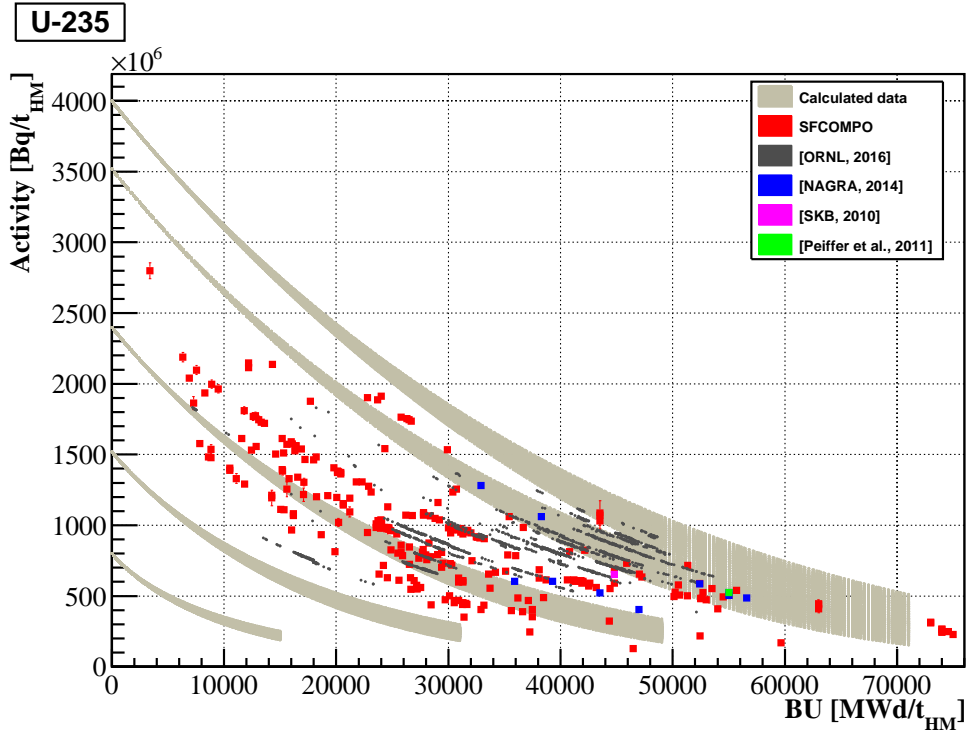


Figure 6.53: Realistic bandwidth of ²³⁵U.

²³¹Pa

During irradiation time ²³¹Pa is built-up by activation and decay processes. There are no measurements in SFCOMPO for this radionuclide. This RN depends strongly on DT, IE and SP, while DT makes the most significant contribution to the bandwidth (cf. Figure 6.54). The theoretical bandwidth corresponds to the DT corrected bandwidth considering the average DT of 400 days. However, the DT correction factor of 2.2 (cf. Table 4.7) is too small to explain the observed discrepancies with the all calculated international data. The preliminary conclusion is that there are other effects (not included within the investigated SRPs) that influence the content of ²³¹Pa. These discrepancies can be also attributed to problems in the SCALE version 6.1.0. Further analysis on this RN is needed.

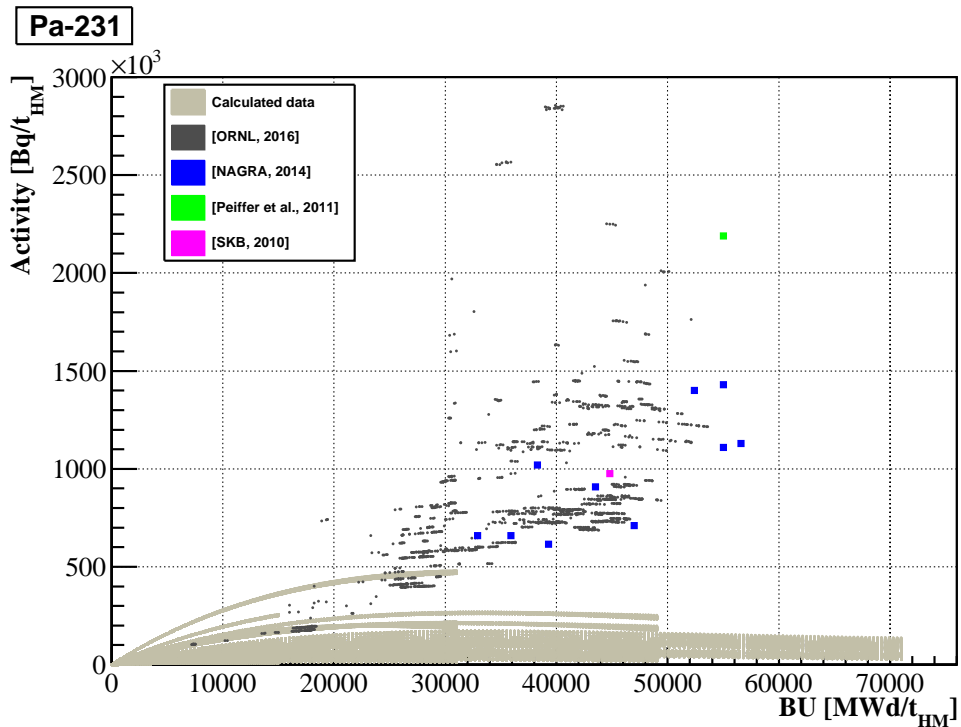


Figure 6.54: Realistic bandwidth of ²³¹Pa.

²²⁷Ac

During irradiation time ²²⁷Ac is built-up by activation and decay processes. There are no measurements in SFCOMPO for this radionuclide. This RN depends strongly on DT, IE and SP, while DT makes the most significant contribution to the bandwidth (cf. Figure 6.55). The theoretical bandwidth corresponds to the DT corrected bandwidth considering the average DT of 400 days. The theoretical bandwidth is in a good agreement with calculated international data.

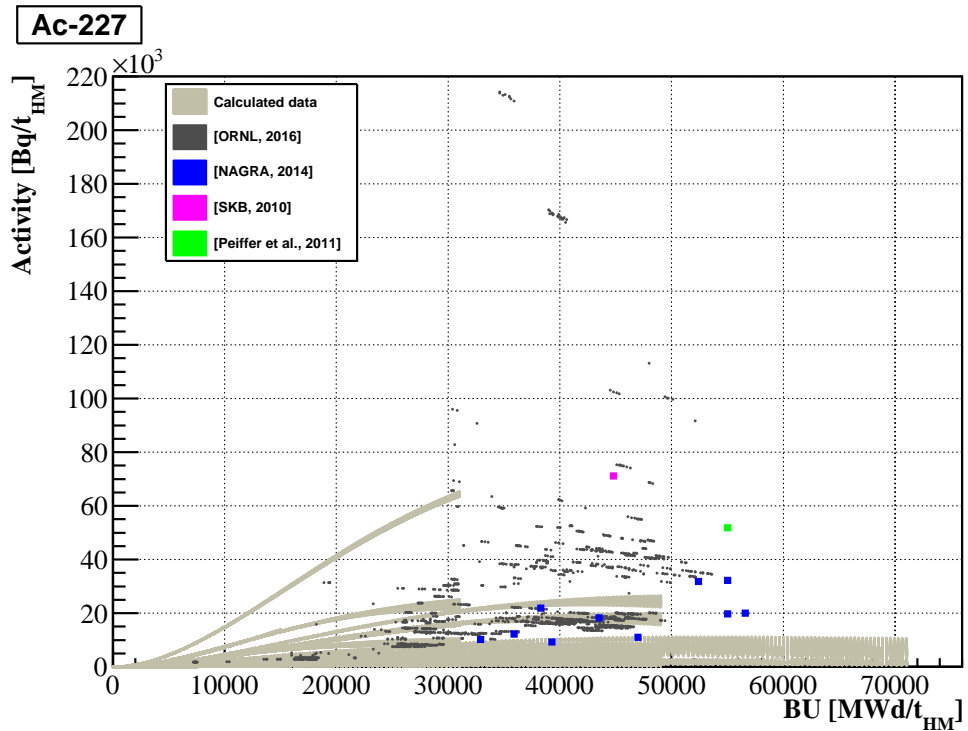


Figure 6.55: Realistic bandwidth of ²²⁷Ac.

The decay chain: $^{249}\text{Bk} \xrightarrow{\beta^-} ^{249}\text{Cf} \xrightarrow{\alpha} ^{245}\text{Cm} \xrightarrow{\alpha} ^{241}\text{Pu} \xrightarrow{\beta^-} ^{241}\text{Am}$

Figure 6.56 shows decay chain of ^{245}Cm . All radionuclides from this chain except ^{249}Bk are in the list of final disposal relevant radionuclides (cf. Table 1.1). However, ^{249}Bk is very important for the cooling time correction of ^{249}Cf concentration (cf. Figure 6.56). For example, the ORNL data cannot be correctly projected to the discharge date if the data of ^{249}Bk are missing (cf. Figure 6.58). The other precursor radionuclides of ^{249}Bk (i.e. ^{253}Es , ^{253}Cf and ^{257}Fm) do not have a significant impact on ^{249}Bk and do not need to be considered for the cooling time correction (cf. Figure 6.57).

Furthermore, ^{241}Pu has a significant impact on ^{241}Am and should be also considered for the cooling time correction for this RN.

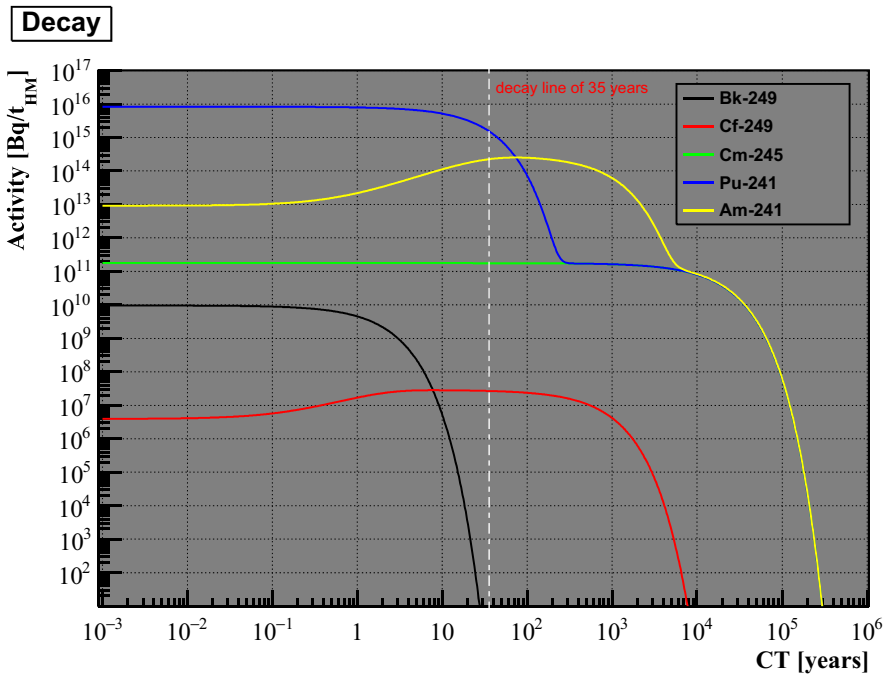
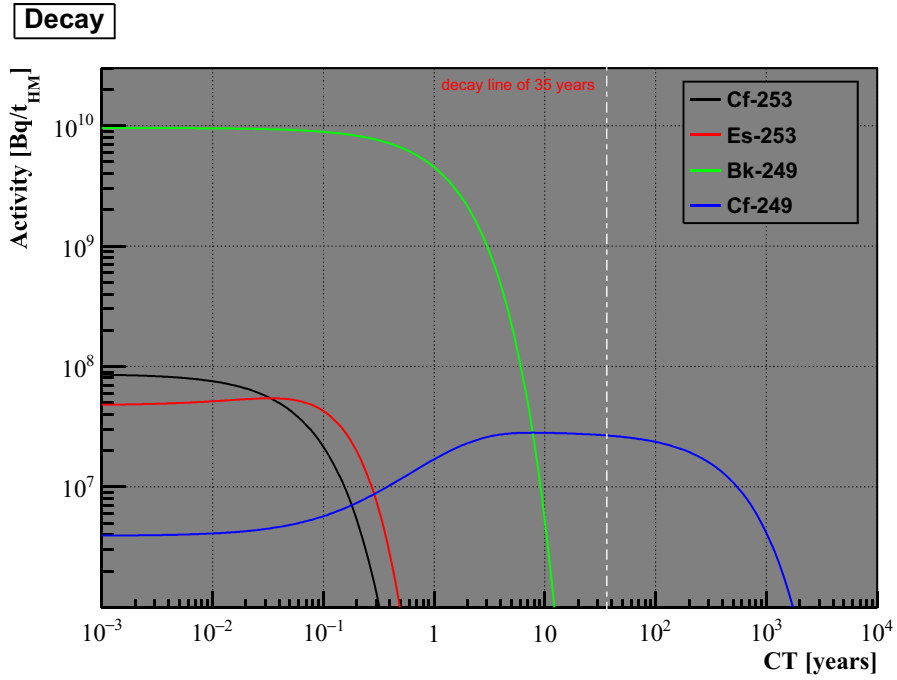


Figure 6.56: Decay chain of ^{245}Cm .

Figure 6.57: Decay chain of ²⁴⁹Cf.

²⁴⁹Cf

During irradiation time ²⁴⁹Cf is built-up by activation and decay processes. There are no measurements in SFCOMPO for this radionuclide. This RN depends on IE, which makes the most significant contribution to the bandwidth (cf. Figure 6.58).

After the discharge the concentration of this radionuclide increases rapidly up to a factor of 10 due to the decay of the precursor radionuclide ²⁴⁹Bk (cf. Figures 6.57 and 6.58). However, ²⁴⁹Bk is not included in the list of relevant radionuclides (cf. Table 1.1) and thus, the concentrations of this RN was not provided by ORNL. Therefore, the correction of the ORNL data to cooling time zero was performed without considering the decay of ²⁴⁹Bk. Consequently, the ORNL data plotted in Figure 6.58 are overestimated. On the other hand, the data provided by NAGRA and GRS included the necessary data for ²⁴⁹Bk, and thus these data could be correctly recalculated to zero cooling time. Figure 6.58 shows a very good agreement of the theoretical bandwidth with these datasets. Thus, the information on ²⁴⁹Bk should be always requested in cases the ²⁴⁹Cf is to be declared.

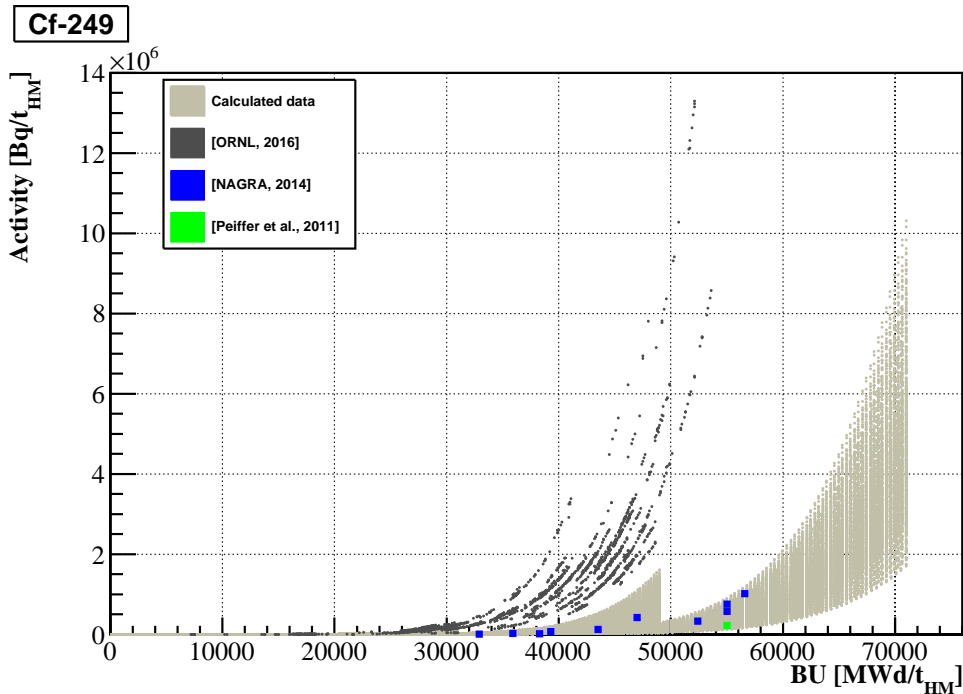


Figure 6.58: Realistic bandwidth of ²⁴⁹Cf.

²⁴⁵Cm

During irradiation time ²⁴⁵Cm is built-up by activation processes. This RN depends on all SRPs, while variation in IE makes the most significant contribution to the bandwidth (cf. Figure 6.59). The theoretical bandwidth is in a good agreement with the experimental and calculated international data.

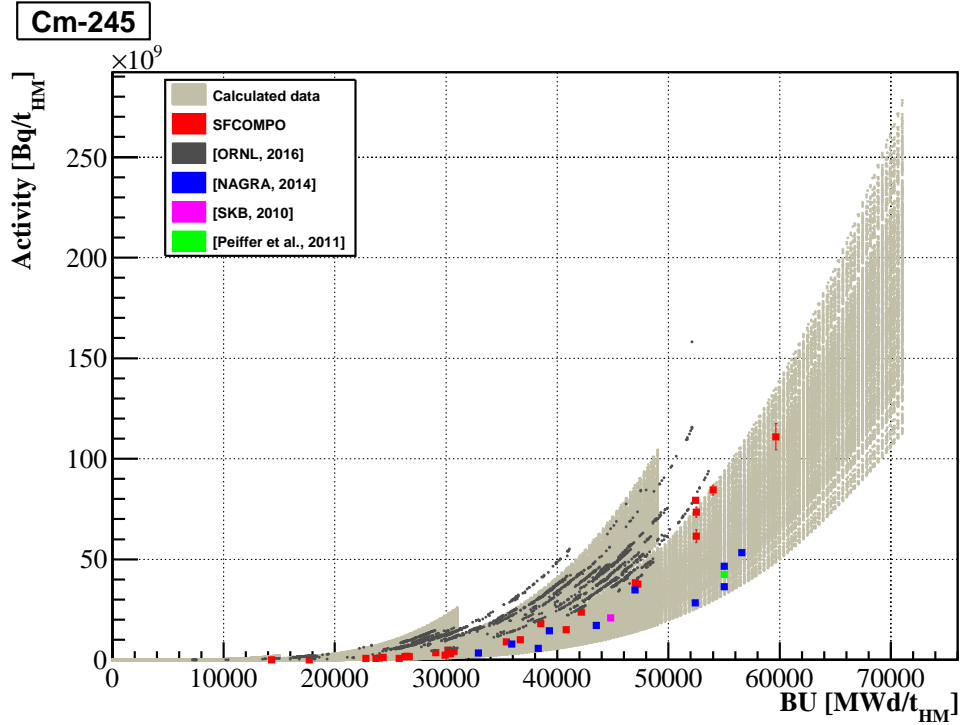


Figure 6.59: Realistic bandwidth of ²⁴⁵Cm.

^{241}Pu

During irradiation time ^{241}Pu is built-up by activation and decay processes. This RN depends on all nine considered SRPs, while the IE makes the most significant contribution to the bandwidth (cf. Figure 6.60). The theoretical bandwidth is in a good agreement with the experimental and calculated international data.

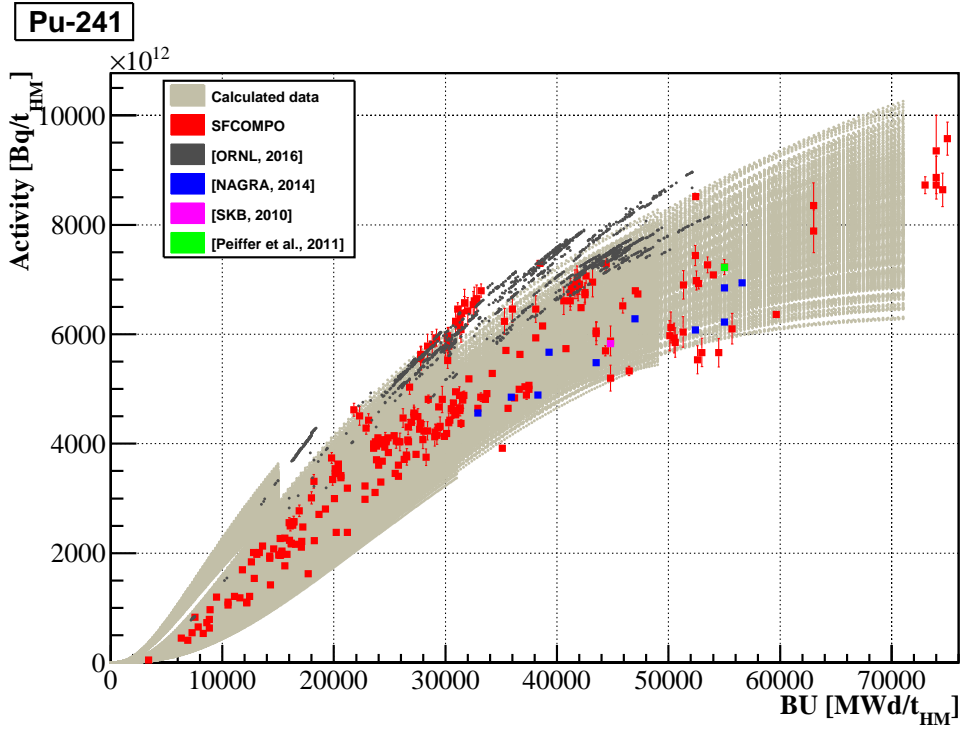


Figure 6.60: Realistic bandwidth of ^{241}Pu .

²⁴¹Am

During irradiation time ²⁴¹Am is built-up by activation and decay processes. This RN depends on all nine considered SRPs, while the IE makes the most significant contribution to the bandwidth (cf. Figure 6.61). The theoretical bandwidth is in a good agreement with the experimental and calculated international data.

This radionuclide is very sensitive to cooling time (CT), because its content increases after the discharge date due the decay of precursor radionuclide ²⁴¹Pu. In the case of the calculated data the zero time correction can be easily performed considering the decay of ²⁴¹Pu. Therefore, the calculated international data are in a very good agreement with theoretical bandwidth (cf. Figure 6.61). However, in the case of the experimental data an additional information on Pu/Am separation date is required, because it has a significant impact on the content of ²⁴¹Am. However, this information is not always available in the original reports on experimental assay data. A disregard of this effect can lead to discrepancies between the calculated and measured data as, for example, is shown in Figure 6.61.

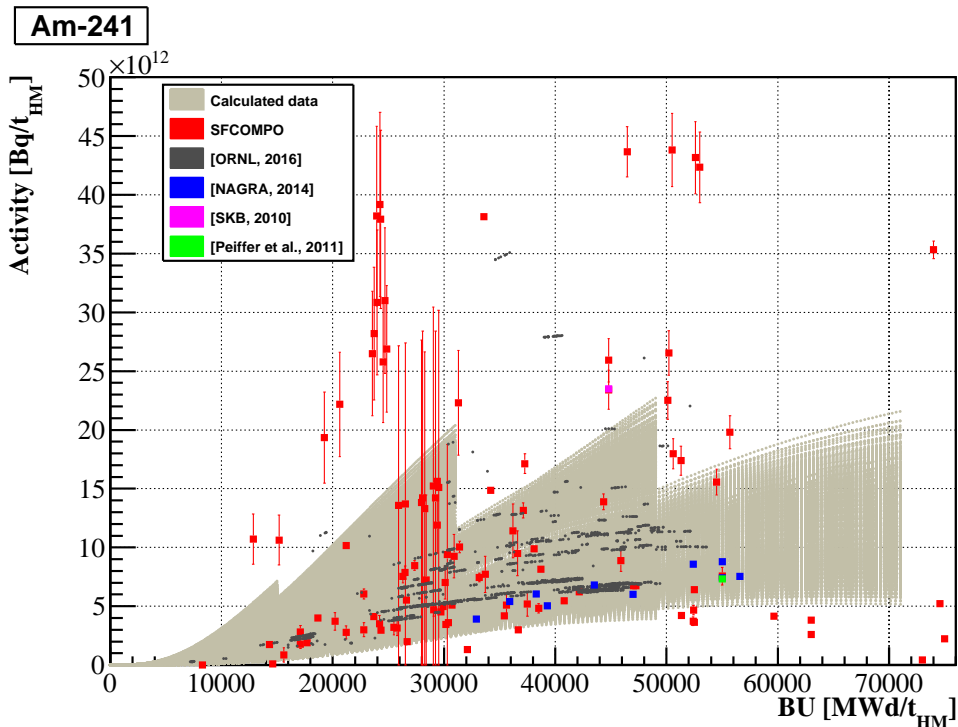


Figure 6.61: Realistic bandwidth of ²⁴¹Am.

The decay chain: $^{237}\text{Np} \xrightarrow{\alpha} ^{233}\text{U} \xrightarrow{\alpha} ^{229}\text{Th}$

Figure 6.62 shows that the decay of ^{241}Am does not have a significant impact on ^{237}Np for the CT of up to 35 years.

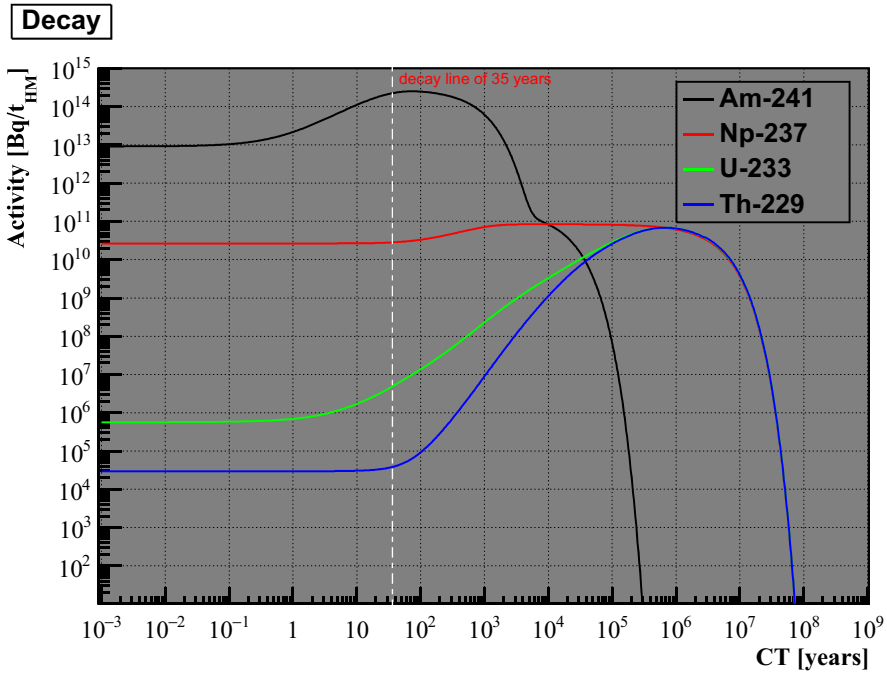


Figure 6.62: Decay chain of ^{237}Np .

^{237}Np

During irradiation time ^{237}Np is built-up by activation and decay processes. This RN does not show strong dependencies on any of the nine considered SRPs (cf. Figure 6.63). The theoretical bandwidth is in a good agreement with the experimental and calculated international data.

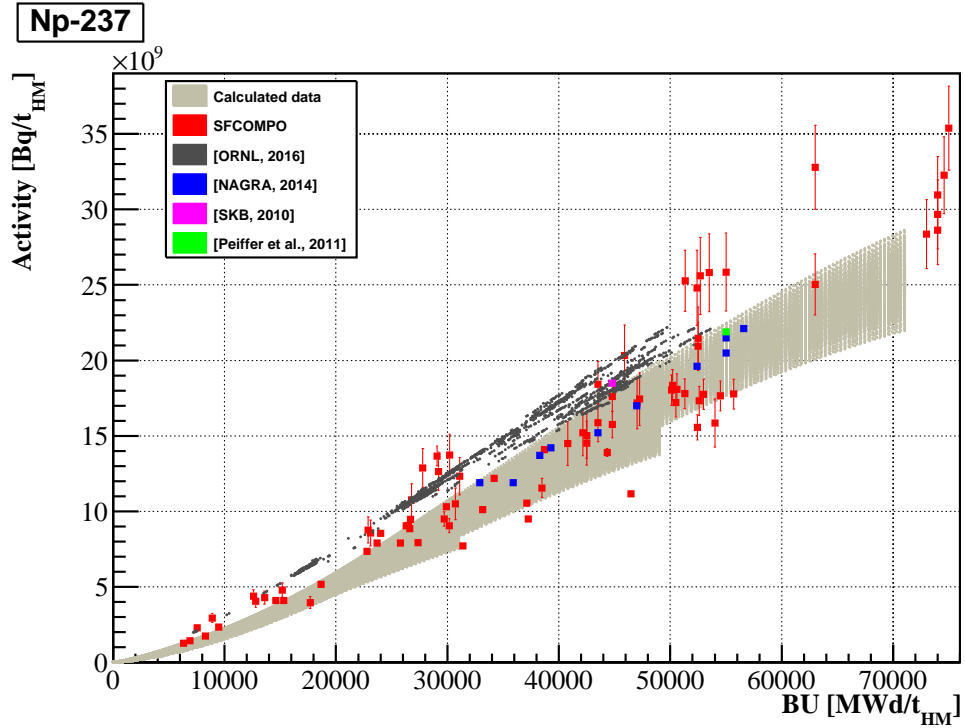


Figure 6.63: Realistic bandwidth of ^{237}Np .

²³³U

During irradiation time ²³³U is built-up by activation and decay processes. This RN depends on all nine considered SRPs, while IE and DT make the most significant contributions to the bandwidth (cf. Figure 6.64). The theoretical bandwidth corresponds to the DT corrected bandwidth considering the average DT of 400 days.

The content of this radionuclide increases after a discharge date because of the decay of the precursor radionuclide ²³⁷Np, therefore, the concentration of ²³⁷Np must be considered for the cooling time correction of ²³³U.

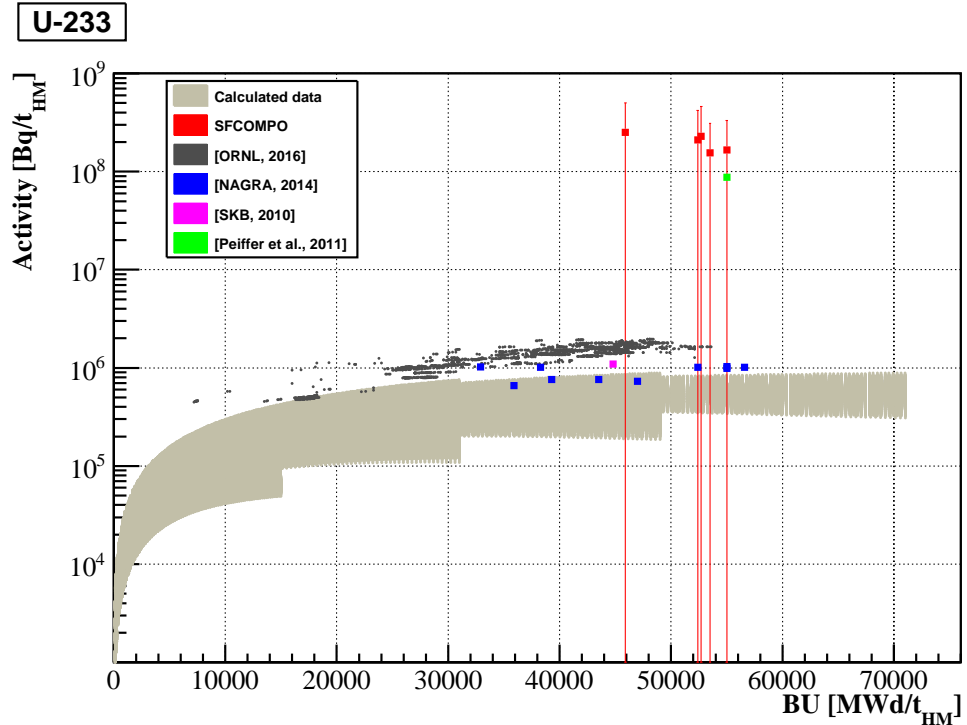


Figure 6.64: Realistic bandwidth of ²³³U effect of fuel impurities in Th.

However, Th impurities in the initial fuel are by far more important for the determination of the realistic bandwidth. In these impurities Th is represented by ²³²Th. The neutron capture by ²³²Th leads to the build-up of ²³³U. This effect can change the activity of ²³³U by a factor of 1000, what can be seen in the Figure 6.64. For example, the GRS data under assumption of 5 ppm of Th in the initial fuel provide a value, which exceeds the theoretical bandwidth and all other calculated international data by about 3 orders of magnitude. The measured data from SFCOMPO do not provide direct information on Th impurities, however, the given activity values are closer to the

GRS value. The agreement between these data suggests that the fuel assemblies used in the measurements contained about the same level of Th impurities. Therefore, the information on Th impurities in the initial fuel, especially for the reprocessed fuel, is very important for the determination of the realistic bandwidth. This information is not often available, however.

The slightly higher values of the calculated ORNL, NAGRA and SKB data (cf. Figure 6.64) in comparison to the theoretical bandwidth could be caused by problems in the SCALE version 6.1.0.

Thus, the most important SRP for ²³³U is the fuel impurity (Th). This conclusion will be also important in the case of ²³²Th (cf. Figure 6.73).

²²⁹Th

During irradiation time ²²⁹Th is built-up by activation and decay processes. There are no measurements in SFCOMPO for this radionuclide. This RN depends on all considered SRPs, while DT and IE make the most significant contributions to the bandwidth (cf. Figure 6.65). The theoretical bandwidth corresponds to the DT corrected bandwidth considering the average DT of 400 days. This bandwidth is in a good agreement with the calculated international data. Some calculated data from ORNL that fall above of theoretical bandwidth in Figure 6.65 correspond to the assemblies with DT of more than 1000 days.

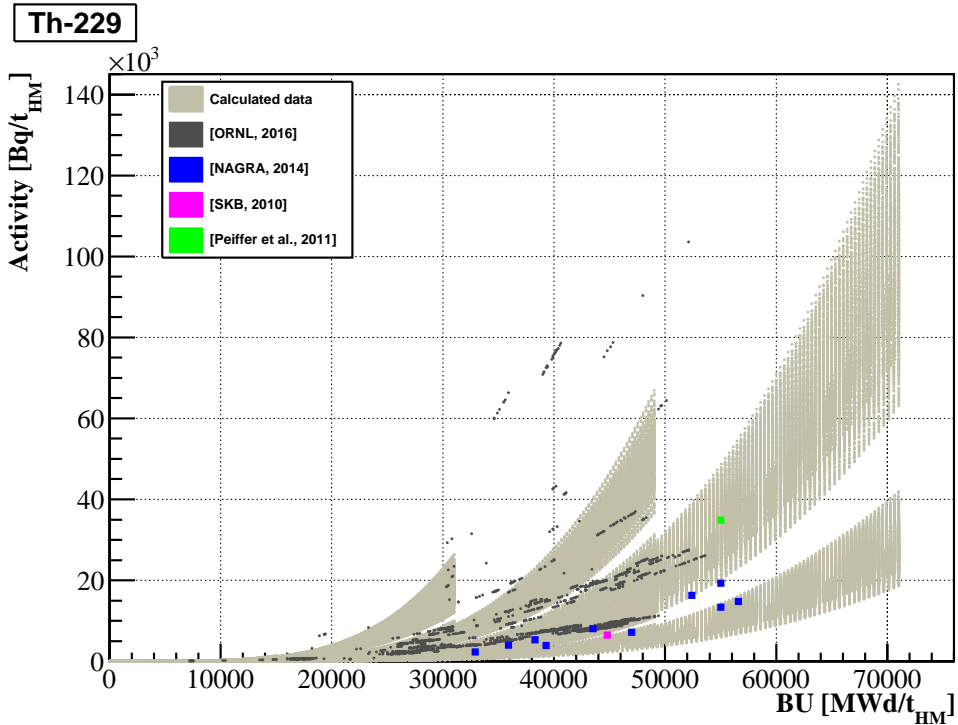
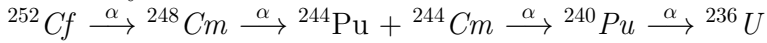


Figure 6.65: Realistic bandwidth of ²²⁹Th.

The decay chain:



All radionuclides of this chain are in the list of final disposal relevant radionuclides. However, the present burn-up calculations provided zero concentration for ²⁵²Cf. This result could be attributed to the problems in the SCALE version 6.1.0. Thus, the theoretical bandwidth of ²⁵²Cf has not been determined. However, the calculated NAGRA and GRS data include non-zero values of ²⁵²Cf. This implies that a further analysis of this inconsistency is needed.

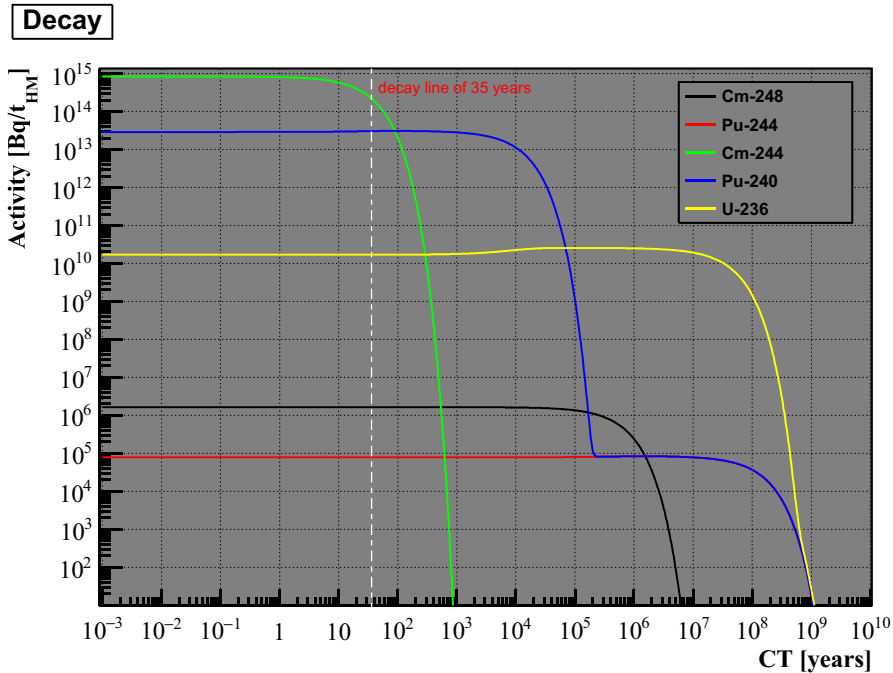


Figure 6.66: Decay chain of ²⁴⁴Pu.

^{248}Cm

During irradiation time ^{248}Cm is built-up by activation and decay processes. There are no measurements in SFCOMPO for this radionuclide. This RN depends on IE, which makes the most significant contribution to the bandwidth (cf. Figure 6.67). The theoretical bandwidth is in a good agreement with the calculated international data.

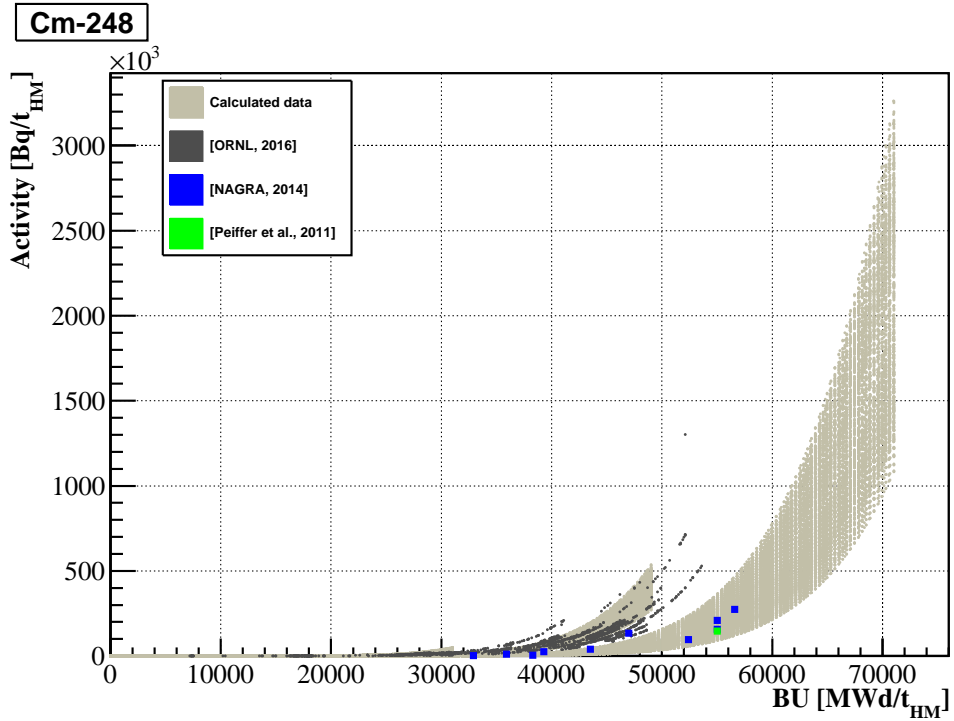


Figure 6.67: Realistic bandwidth of ^{248}Cm .

²⁴⁴Pu

During irradiation time ²⁴⁴Pu is built-up by activation and decay processes. This RN depends on IE, which makes the most significant contribution to the bandwidth (cf. Figure 6.68). The slightly higher values of the calculated ORNL data correspond to effect of burnable absorber exposure. The theoretical bandwidth is in a good agreement with the experimental and calculated international data.

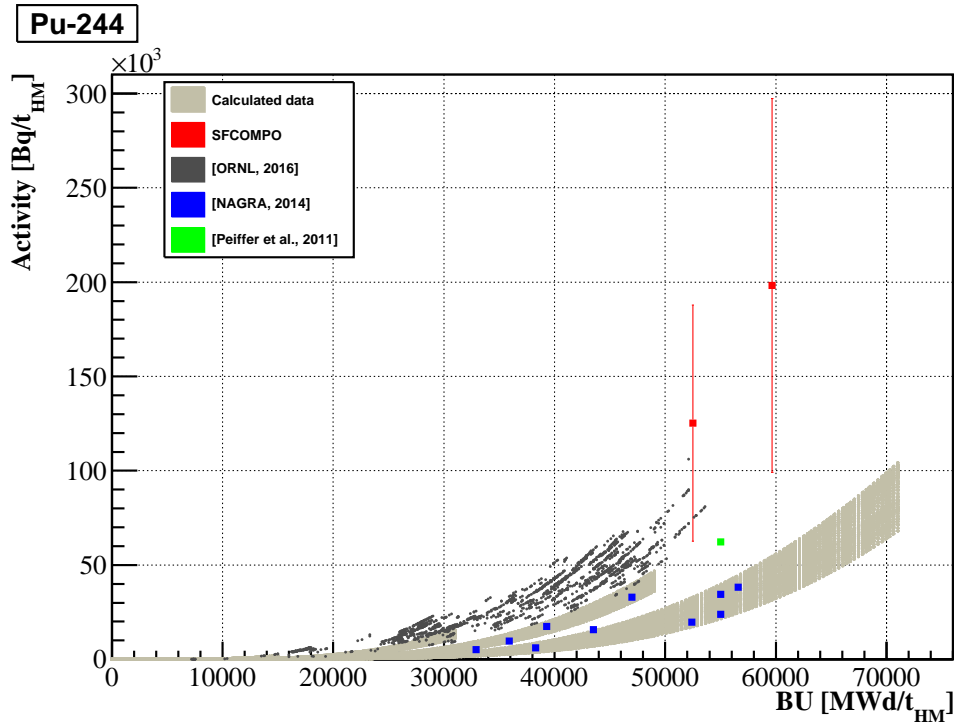


Figure 6.68: Realistic bandwidth of ²⁴⁴Pu.

²⁴⁴Cm

During irradiation time ²⁴⁴Cm is built-up by activation and decay processes. This RN depends on IE, which makes the most significant contribution to the bandwidth (cf. Figure 6.69). The theoretical bandwidth is in a good agreement with the experimental and calculated international data.

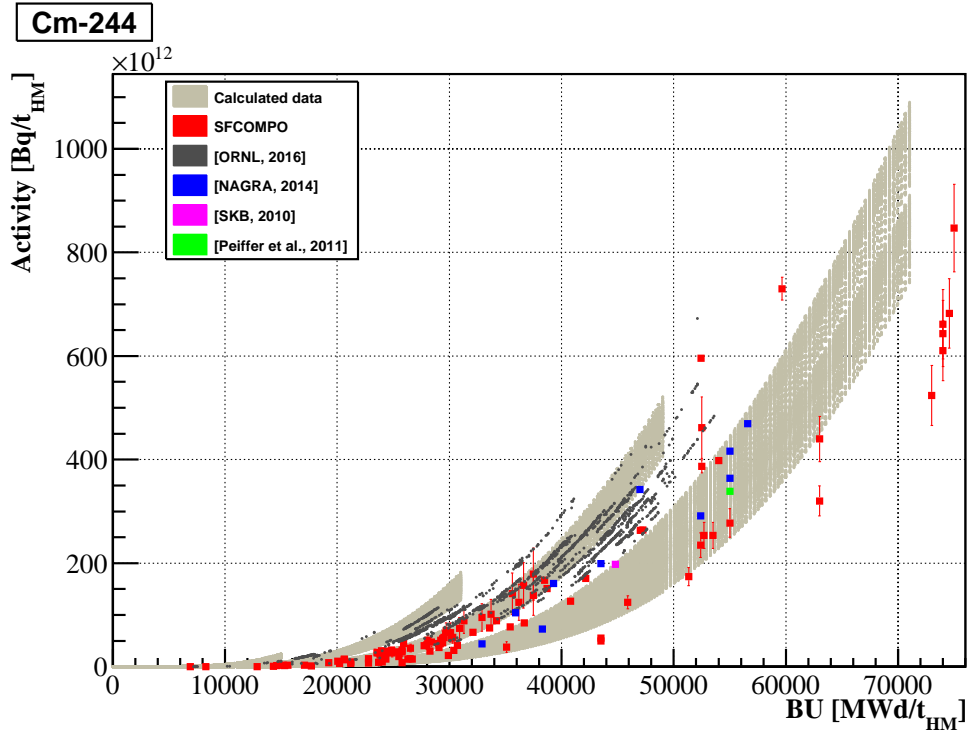


Figure 6.69: Realistic bandwidth of ²⁴⁴Cm.

²⁴⁰Pu

During irradiation time ²⁴⁰Pu is built-up by activation and decay processes. This RN depends on IE, which makes the most significant contribution to the bandwidth (cf. Figure 6.70). The theoretical bandwidth is in a good agreement with the experimental and calculated international data.

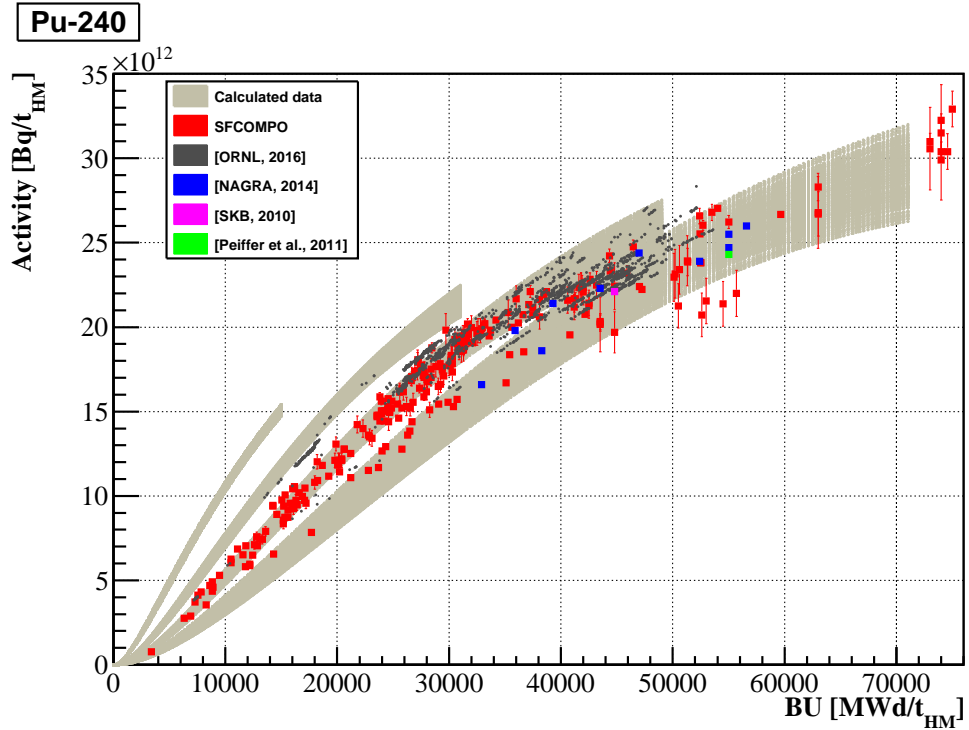


Figure 6.70: Realistic bandwidth of ²⁴⁰Pu.

²³⁶U

During irradiation time ²³⁶U is built-up by activation and decay processes. This RN depends on IE, which makes the most significant contribution to the bandwidth (cf. Figure 6.71). The theoretical bandwidth is in a good agreement with the experimental and calculated international data.

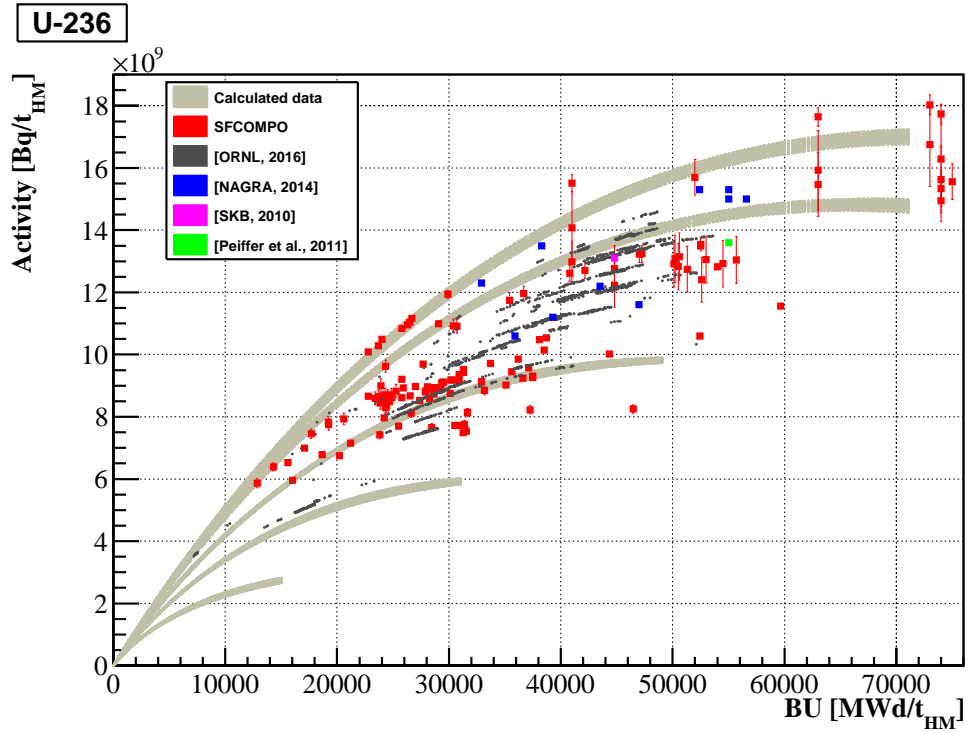


Figure 6.71: Realistic bandwidth of ²³⁶U.

The decay chain: $^{232}\text{Th} \xrightarrow{\alpha} ^{228}\text{Th} \xleftarrow{\alpha} ^{232}\text{U} \xleftarrow{\alpha} ^{236}\text{Pu} \xleftarrow{\beta^-} ^{236}\text{Np}$

This is the most interesting and challenging decay chain. Here, only two radionuclides are in the list of relevant RNs, namely ^{232}Th and ^{232}U (cf. Table 1.1). For the cooling time correction of ^{232}U , the information on its precursor radionuclide ^{236}Pu is required, because ^{232}U increases after discharge due to the decay of ^{236}Pu (cf. Figure 6.72). However, when the cooling time significantly exceeds 35 years the additional information on ^{228}Th and ^{236}Np is also required.

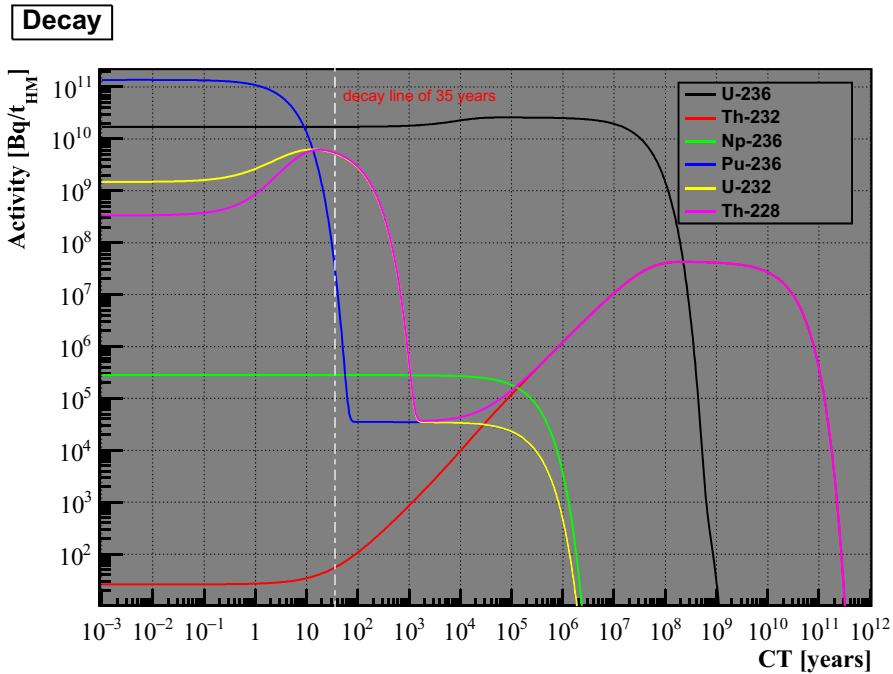


Figure 6.72: Decay chain of ^{232}Th .

²³²Th

During irradiation time ²³²Th is built-up by activation and decay processes. There are no measurements in SFCOMPO for this radionuclide. This RN depends on all considered SRPs, while IE and DT make the most significant contributions to the bandwidth (cf. Figure 6.73). The theoretical bandwidth corresponds to the DT corrected bandwidth considering the average DT of 400 days.

After discharge date the content of this radionuclide increases, because of the decay of the precursor radionuclide ²³⁶U. But Th impurities in initial fuel are by far more important. This effect of these impurities can increase the ²³²Th concentration of the factor of 10000 as is seen in the Figure 6.73. Here, the GRS data, which assume 5 ppm of Th in initial fuel, provide much higher values than the theoretical bandwidth and all other calculated international data. Therefore, the information on Th impurities in the initial fuel, especially for the reprocessed fuel, is very important for the determination of the realistic bandwidth. This information is not always available, however.

Thus, the most important SRP for ²³²Th is the fuel impurity. The same conclusion has also been achieved for ²³³U (cf. Figure 6.64).

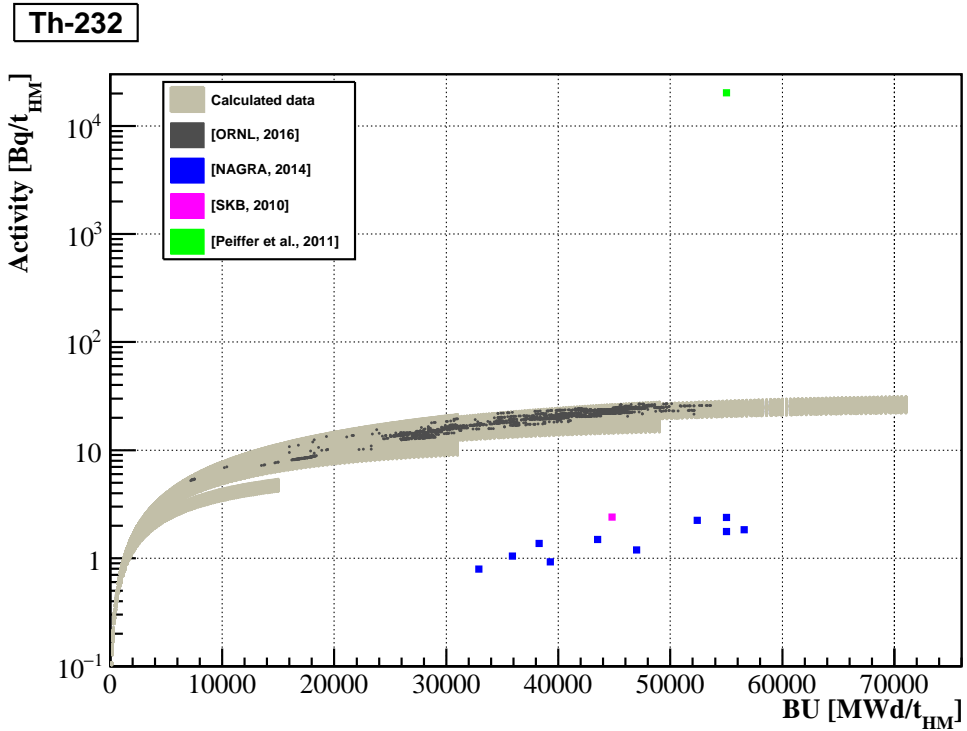


Figure 6.73: Realistic bandwidth of ²³²Th and effect of fuel impurities.

²³²U

During irradiation time ²³²U is built-up by activation and decay processes. This RN depends on all considered SRPs, while IE and DT make the most significant contributions to the bandwidth (cf. Figure 6.74).

In analogy with ²⁴⁹Cf (cf. Figure 6.58), the concentration of this radionuclide increases rapidly after the discharge up to the factor of 10 due to the decay of precursor radionuclide ²³⁶Pu (cf. Figures 6.72 and 6.74). However, ²³⁶Pu is not in the list of relevant radionuclides (cf. Table 1.1) and is not provided in the ORNL data. Thus, the disagreement between the theoretical bandwidth and the ORNL data and some measurements from SFCOMPO occurs because the decay of ²³⁶Pu is not taken into account in the cooling time correction (cf. Figure 6.74). On the contrary, NAGRA, GRS and some experimental data from SFCOMPO include the information on ²³⁶Pu. Consequently, a good agreement between these data and the theoretical bandwidth is obtained.

Thus, the information on ²³⁶Pu should be always requested in cases the ²³²U is to be declared.

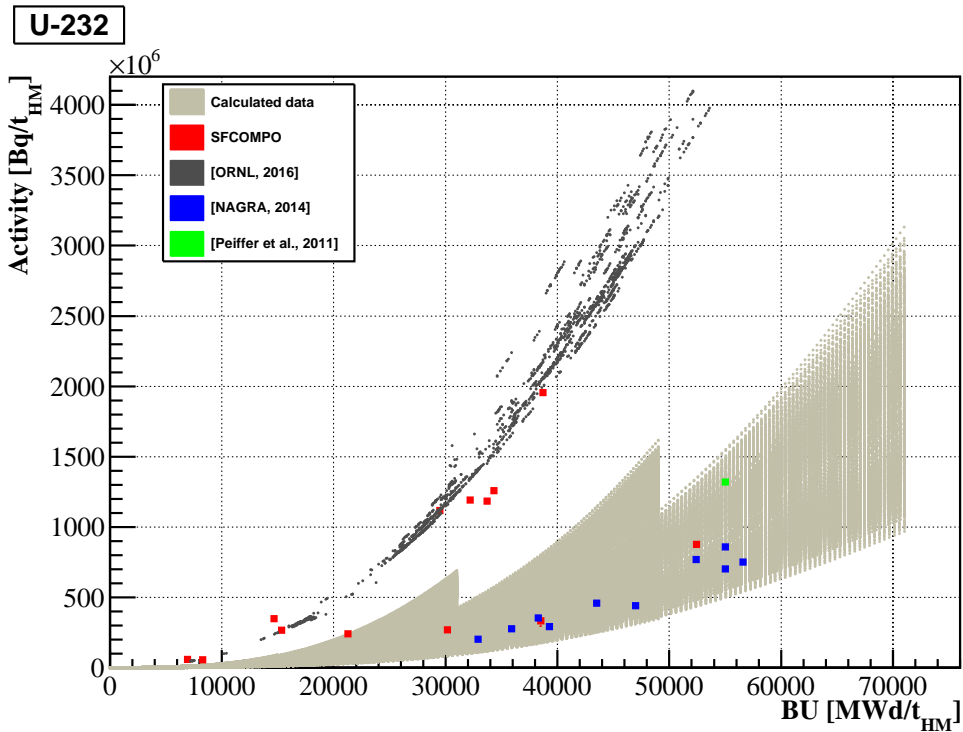


Figure 6.74: Realistic bandwidth of ²³²U.

7 Conclusion

The present work highlights the importance of the estimation of uncertainties in radionuclide inventories of spent nuclear fuel, which relate to the lack of detailed information on fuel impurities, initial composition, design and operating data. This estimation is made considering all available experimental and calculated international reference data on real spent fuel assemblies.

The developed method provides a possibility to estimate the realistic composition of PWR-UO₂ SNF inventory (i.e. the realistic bandwidths for each relevant radionuclide) using the information on burn-up and cooling time only (i.e. the Primary Reactor Parameter data). This method is based on the sensitivity analysis of nine reactor design and operating parameters, the so called Secondary Reactor Parameters (SRP), which include initial enrichment (IE), fuel density (FD), specific power (SP), downtime (DT), irradiation time (IT), fuel temperature (FT), moderator density (MD), moderator temperature (MT) and boric acid concentration (BA). The most important SRPs are the IE, SP and DT.

The theoretical (or calculated) bandwidths of radionuclides, which are relevant for the final disposal, are determined for the burn-up range of 0 – 71 GWd/t_{HM} using the burn-up code SCALE 6.1 and the nuclear data library ENDF/B-VII.0. The theoretical bandwidths are validated with the aid of radiochemical assay data (RCA) that are taken from the Spent Fuel Isotopic Composition Database (SFCOMPO), the database maintained by the OECD Nuclear Energy Agency (NEA). This database comprises measurements for more than 300 PWR-UO₂ fuel samples with the associated burn-up range between 3 and 75 GWd/t_{HM}.

Moreover, a comprehensive verification of the method is performed by comparing the theoretical bandwidths with calculated reference inventory data, which have been compiled by several countries for long-term safety assessments, spent fuel transportation, storage, and other applications. In this work the theoretical radionuclide bandwidths are compared to:

- calculated inventories of approximately 2000 US PWR-UO₂ spent fuel assemblies with a burn-up range between 7 and 53 GWd/t_{HM};
- calculated inventories of fuel assembly families that represent average data for approximately 3300 Swiss PWR-UO₂ SNF;
- calculated average inventory of the Swedish PWR-UO₂ SNF;
- calculated average inventory of the German PWR-UO₂ SNF.

The theoretical bandwidths based on the sensitivity analysis of nine SRPs yield good agreement with the experimental and calculated international PWR-UO₂ SNF data for most radionuclides, except for the six RNs (light RNs and fission products) and the six

actinides (cf. Table 7.1). For these 12 RNs the deviations between the theoretical bandwidths (those predicted here) and the variability range of the calculated international inventory or experimental data may even exceed 4 order of a magnitude. It is shown that all these large deviations can be eliminated by the correct choice of initial composition (IC), fuel impurities (FI) and nuclear data library (Lib).

Table 7.1: RNs with major impact of FI, Lib and IC

Name of SRP	RN	Deviation factor ¹
Fuel impurities (FI)	^{108m} Ag	100
	⁹³ Mo	1000
	⁹⁴ Nb	5
	¹²⁶ Sn	2
	²³² Th	10000
	²³³ U	1000
Fuel impurities (FI) and Modelling properties (Lib)	¹⁴ C	1000
	³ H	1000
Modelling properties (Lib)	²³¹ Pa	6
Initial composition (IC)	²³⁴ U	10
	²³⁰ Th	100
	²²⁶ Ra	100

¹ Deviation factor is an approximate maximum ratio of the largest and lowest activities for a given RN, which are determined by available calculated international or experimental data, or, by the theoretical bandwidths. For example, when the available data fall off the theoretical bandwidths, one of limiting values is taken equal to the lowest (or the largest) value along the theoretical bandwidth (cf. Figure 6.64).

The experimental data that are available at the scope of this work for 41 radionuclides are important for validation of the theoretical bandwidths. The comparison of theoretical bandwidths with the calculated international radionuclide data highlights the potential issues related to the unknown information on the fuel impurities, initial composition, cooling time, modelling properties, etc. and provides useful indication to the insufficiency of the available experimental data.

This work provides a possibility to classify radionuclides in terms of their sensitivity to specific reactor design and operating parameters. This classification is particularly important within the scope of interest for nuclear waste management.

The developed method of predicting the realistic RN bandwidths is widely applicable for the tasks of product quality control as well as for long-term safety analyses of final repositories and for safeguard applications. An analogue method can be applied not only for the PWR-UO₂ type spent fuel but also for other types of nuclear waste.

The main challenge of this work was in obtaining and combining information on principles of reactor physics and on radiochemical assay methods, which was essentially owned by different expert communities. Personal contacts with members of these communities and the participation in several international conferences bore the success of this work.

Bibliography

- Aksyutina, Y., I. Fast, H. Tietze-Jaensch, F. Guillaumin, and P. Pinson: 2015, 'The German Product Quality Control of the Compacted Metallic Nuclear Waste'. Phoenix, Arizona, USA, WM2015 Conference. 15311.
- Bannella, R., P. Barbero, G. Bidoglio, J. Biteau, G. Buscaglia, M. Breseli, R. Chevalier, G. Cottone, A. Cricchio, D. D'Adamo, R. Dirckx, A. Drago, S. Facchetti, A. Federici, A. Frigo, E. Ghezzi, G. Guzzi, R. Klersy, L. Lezzoli, L. Koch, F. Mannone, A. Marell, M. Paoletti-Gualandi, P. P. K. Schrader, A. Schurenkaemper, P. Trincherini, and R. Wellum: 1977, 'Post irradiation examination of the fuel discharged from the Trino Vercellese reactor after the 2nd irradiation cycle'. Technical report, Commission of the European Communities, Joint Research Centre. Nuclear Science and Technology, EUR 5605 e.
- Barbero, P., G. Bidoglio, A. Caldiroli, F. Daniele, R. D. Meester, R. Ernstberger, S. Facchetti, A. Frigo, S. Guardini, G. Guzzi, P. Hansen, L. Lezzoli, L. Koch, W. Konrad, L. Mammarella, F. Mannone, A. Marell, A. Schurenkaemper, P. Trincherini, and R. Wellum: 1980, 'Post Irradiation Analysis of the Obrigheim PWR Spent Fuel'. Technical report, Commission of the European Communities, Joint Research Centre, Ispra Establishment, Italy. European Appl. Res. Rept. – Nucl. Sci. Technol., Vol. 2, No. 1, pp. 129 – 177.
- Barner, J.: 1985, 'Characterization of LWR Spent Fuel MCC-Approved Testing Material-ATM-101'. Technical report, Pacific Northwest Laboratory operated by Battelle Memorial Institute for the United States Department Of Energy. PLN-5109 Rev. 1, UC-70.
- Barreau, A.: 2006, 'PWR-UO₂ Assembly Study of Control Rod Effects on Spent Fuel Composition'. Phase II-D 6227, Organisation for Economic Co-operation and Development (OECD), Nuclear Energy Agency (NEA). ISBN 92-64-02316-X.
- Bowman, S. M.: 2011, 'SCALE 6: Comprehensive Nuclear Safety Analysis Code System'. *Nuclear Technology* **174**(2), 126 – 148. Oak Ridge National Laboratory (ORNL).
- Brennecke, P.: 2011, 'Anforderungen an endzulagernde radioaktive Abfälle (Endlagerungsbedingungen, Stand: Oktober 2010) - Endlager Konrad -'. Technical report, Bundesamt für Strahlenschutz (Bfs). SE-IB-29/08-REV-1.
- Cerne, S. P., O. W. Hermann, and R. M. Westfall: 1987, 'Reactivity and Isotopic Composition of Spent PWR Fuel as a Function of Initial Enrichment, Burnup and Cooling Time'. Technical report, Oak Ridge National Laboratory (ORNL). ORNL/CSD/TM-244, Dist. Category UC-46.

- Chadwick, M. B., P. Oblozinsky, M. Herman, N. M. Greene, R. D. McKnight, D. L. Smith, P. G. Young, R. E. MacFarlane, G. M. Hale, R. C. Haight, S. Frankle, A. C. Kahler, T. Kawano, R. C. Little, D. G. Madland, P. Moller, R. Mosteller, P. Page, P. Talou, H. Trellue, M. White, W. B. Wilson, R. Arcilla, C. L. Dunford, S. F. Mughabghab, B. Pritychenko, D. Rochman, A. A. Sonzogni, C. Lubitz, T. H. Trumbull, J. Weinman, D. Brown, D. E. Cullen, D. Heinrichs, D. McNabb, H. Derrien, M. Dunn, N. M. Larson, L. C. Leal, A. D. Carlson, R. C. Block, B. Briggs, E. Cheng, H. Huria, K. Kozier, A. Courcelle, V. Pronyaev, and S. C. van der Marck: 2006, 'ENDF/B-VII.0: Next Generation Evaluated Nuclear Data Library for Nuclear Science and Technology'. Technical report. Nuclear Data Sheets, UCRL-JRNL-225066.
- DAEF: 2015, 'Endlagerung warmentwickelnder radioaktiver Abfalle und ausgedienter Brennelemente in bis zu 5000 m tiefen vertikalen Bohrlochern von über Tage'. Deutsche Arbeitsgemeinschaft Endlagerforschung (DAEF).
- Dahmen, W. and A. Reusken: 2006, Numerik für Ingenieure und Naturwissenschaftler. Springer-Verlag. ISBN-10 3-540-25544-3, ISBN-13 978-3-540-25544-4.
- DeHart, M. D.: 1996, 'Sensitivity and Parametric Evaluations of Significant Aspects of Burnup Credit for PWR Spent Fuel Packages'. Technical report, Oak Ridge National Laboratory (ORNL). ORNL/TM-12973.
- DeHart, M. D. and O. W. Hermann: 1996, 'An Extension of the Validation of SCALE (SAS2H) Isotopic Predictions for PWR Spent Fuel'. Technical report, Oak Ridge National Laboratory, Computational Physics and Engineering Division. ORNL/TM-13317.
- Delette, G., P. Sornay, and J. Blancher: 2004, 'Finite element modeling of the pressing of nuclear oxide powders to predict the shape of LWR fuel pellets after die compaction and sintering'. In: Advanced fuel pellet materials and designs for water cooled reactors, Vol. 329. pp. 21 – 30. IAEA-TECDOC-1416.
- Gauld, I., G. Ilas, B. Murphy, and C. Weber: 2010, 'Validation of SCALE 5 Decay Heat Predictions for LWR Spent Nuclear Fuel'. Technical report, Oak Ridge National Laboratory (ORNL). NUREG/CR-6972, ORNL/TM-2008/015.
- Gauld, I., G. Ilas, and G. Radulescu: 2011, 'Uncertainties in Predicted Isotopic Compositions for High Burnup PWR Spent Nuclear Fuel'. Technical report, Oak Ridge National Laboratory (ORNL). NUREG/CR-7012, ORNLITM-2010/41.
- Gauld, I., M. Pigni, and G. Ilas: 2014, 'Validation and Testing of ENDF/B-VII Decay Data'. Nuclear Data Sheets **120**, 33 – 36. Oak Ridge National Laboratory (ORNL).
- Gauld, I. C.: 2003, 'Strategies for Application of Isotopic Uncertainties in Burnup Credit'. Technical report, Oak Ridge National Laboratory (ORNL).

- Guardini, S. and G. Guzzi: 1982, 'Benchmark – Reference Data on Post Irradiation Analysis of Light Water Reactor Fuel Samples'. Technical report, Commission of the European Communities, Joint Research Centre Ispra Establishment. EUR-7879-EN.
- Guenther, R. J., D. E. Blahnik, T. K. Campbell, U. P. Jenquin, J. E. Mendel, and C. K. Thornhill: 1988a, 'Characterization of Spent Fuel Approved Testing Material – ATM-103'. Technical report, Pacific Northwest Laboratory operated by Battelle Memorial Institute for the United States Department Of Energy. PNL-5109-103, UC-70.
- Guenther, R. J., D. E. Blahnik, T. K. Campbell, U. P. Jenquin, J. E. Mendel, and C. K. Thornhill: 1988b, 'Characterization of Spent Fuel Approved Testing Material – ATM-106'. Technical report, Pacific Northwest Laboratory operated by Battelle Memorial Institute for the United States Department Of Energy. PNL-5109-106, UC-70.
- Guenther, R. J., D. E. Blahnik, T. K. Campbell, U. P. Jenquin, J. E. Mendel, and C. K. Thornhill: 1991, 'Characterization of Spent Fuel Approved Testing Material – ATM-104'. Technical report, Pacific Northwest Laboratory operated by Battelle Memorial Institute for the United States Department Of Energy. PNL-5109-104, DE92 006636.
- Henkel, C.: 2008, 'CSNF Loading Curve Sensitivity Analysis'. Technical report, Sandia National Laboratories. ANL-EBS-NU-000010 REV 00, Las Vegas, Nevada.
- Hermann, O. W., S. M. Bowman, M. C. Brady, and C. V. Parks: 1995, 'Validation of the SCALE System for PWR Spent Fuel Isotopic Composition Analyses'. Technical report, Oak Ridge National Laboratory (ORNL). ORNL/TM-12667.
- Hermann, O. W., M. D. DeHart, and B. D. Murphy: 1998, 'Evaluation of Measured LWR Spent Fuel Composition Data for Use in Code Validation End-User Manual'. Technical report, Oak Ridge National Laboratory (ORNL). ORNL/M-6121.
- Lamarsh, J. R. and A. J. Baratta: 2001, Introduction to Nuclear Engineering. Prentice-Hall, third edition. ISBN 0-201-82498-1.
- Murphy, B. and I. Gauld: 2010, 'Spent Fuel Decay Heat Measurements Performed at the Swedish Central Interim Storage Facility'. Technical report, Oak Ridge National Laboratory, Managed by UT-Battelle, LLC. NUREG/CR-6971, ORNL/TM-2008/016.
- NAGRA: 2014, 'Modellhaftes Inventar für radioaktive Materialien MIRAM 14'. Technical report, Nationale Genossenschaft für die Lagerung radioaktiver Abfälle (NAGRA). NTB 14-04.
- Nakahara, Y., K. Suyama, and T. Suzaki: 2002, 'Technical Development on Burn-up Credit for Spent LWR Fuels'. Technical report, Department of Environmental Sciences, Tokai Research Establishment, Japan Atomic Energy Research Institute. JAERI-Tech 2000-071 (ORNL/TR-2001/01), Translation coordination by I. C. Gauld Oak Ridge National Laboratory.

- NEA: 2014, 'JEFF-3.2 evaluated data library'. Technical report, Nuclear Energy Agency (NEA). NEA Data Bank, also available through the JANIS database.
- NEA: 2015a, 'Java-based Nuclear Data Information System (Janis)'. <http://www.oecd-nea.org/janis/>. Nuclear Energy Agency (NEA), Organisation for Economic Co-operation and Development (OECD), JANIS 4.0, visited on 2015.
- NEA: 2015b, 'Spent Fuel Isotopic Composition Database (SFCOMPO)'. <https://www.oecd-nea.org/science/wpncs/ADSNF/>. Nuclear Energy Agency (NEA), Organisation for Economic Co-operation and Development (OECD), Expert Group on Assay Data of Spent Nuclear Fuel (ADSNF), visited on 2015.
- NEI: 2004, 'Fuel design data'. Nuclear Engineering International pp. 26–35. Nuclear Engineering International.
- ORNL: 2003, 'ARIANE International Programme Final Report'. Technical report, Oak Ridge National Laboratory (ORNL), UT-BATTELLE, LLC. Fissile Materials Disposition Program, ORNL/SUB/97-XSV750-1.
- ORNL: 2011, 'Scale: A Comprehensive Modeling and Simulation Suite for Nuclear Safety Analysis and Design'. Oak Ridge National Laboratory (ORNL). ORNL/TM-2005/39, Version 6.1.
- ORNL: 2016. Personal communication, Oak Ridge National Laboratory.
- Parks, C. V., M. D. DeHart, and J. C. Wagner: 2001, 'Phenomena and Parameters Important to Burnup Credit'. In: Implementation of burnup credit in spent fuel management systems, Vol. 350. pp. 233–247, Nuclear Fuel Cycle and Materials Section, International Atomic Energy Agency (IAEA). Oak Ridge National Laboratory (ORNL), IAEA-TECDOC-1241.
- Peiffer, F., B. M. (GRS), D. G. (ISTec), F. E. (ISTec), B. T. (nse), A. H. (nse), and J. K. (nse): 2011, 'Abfallspezifikation und Mengengerüst'. Technical report, Gesellschaft für Anlagen- und Reaktorsicherheit (GRS) mbH. GRS - 278, Basis Ausstieg aus der Kernenergienutzung, Bericht zum Arbeitspaket 3, Vorläufige Sicherheitsanalyse für den Standort Gorleben.
- Posiva: 2013, 'Nuclear Waste Management at Olkiluoto and Loviisa Power Plants: Review of Current Status and Future Plans for 2013-2015'. Technical report, Posiva Oy.
- Radulescu, G.: 2010, 'Propagation of Isotopic Bias and Uncertainty to Criticality Safety Analyses of PWR Waste Packages'. Technical report, Oak Ridge National Laboratory (ORNL). ORNL/TM-2010/116.
- Radulescu, G., I. Gauld, G. Ilas, and J. C. Wagner: 2012, 'An Approach for Validating Actinide and Fission Product Burnup Credit Criticality Safety Analyses – Isotopic

-
- Composition Predictions'. Technical report, Oak Ridge National Laboratory (ORNL). NUREG/CR-7108, ORNLITM-2011/509.
- Radulescu, G., I. C. Gauld, and G. Ilas: 2010, 'SCALE 5.1 Predictions of PWR Spent Nuclear Fuel Isotopic Compositions'. Technical report, Oak Ridge National Laboratory (ORNL). ORNL/TM-2010/44.
- Schneider, S.: 2014, 'Numerische Simulationen von Abfallgebinden aus der Wiederaufarbeitung von Kernbrennstoffen'. Ph.D. thesis, Rheinisch-Westfälischen Technischen Hochschule Aachen (RWTH). Forschungszentrum Jülich GmbH.
- SKB: 2010, 'Spent nuclear fuel for disposal in the KBS-3 repository'. Technical report, Swedish Nuclear Fuel and Waste Management Co (SKB), Svensk Kärnbränslehantering AB. TR-10-13.
- Wagner, J. C. and C. V. Parks: 2002, 'Parametric Study of the Effect of Burnable Poison Rods for PWR Burnup Credit'. Technical report, Oak Ridge National Laboratory (ORNL). NUREG/CR-6761, ORNL/TM-2000/373.

Acknowledgement

The present work has been created at the Institute of Energy and Climate Research (IEK-6) of the Forschungszentrum Jülich GmbH.

I want to thank my supervisor Prof. Dr. Dirk Bosbach for the opportunity for this dissertation and for his support. I wish to thank Prof. Dr. Georg Roth for his reviewing as second examiner and for constructive discussions about this work.

My special thanks are sent to the employees of the IEK-6 Institute and the Product Quality Control Office. In particular, I want to thank my advisor Dr. Holger Tietze-Jaensch for his advice and discussions, motivation and immersion directed from the perspective of the nuclear waste management applications. Moreover, I thank Dr. Stephan Schneider for the irreplaceable support in SCALE, C++ and ROOT, and Dr. Yuliya Aksyutina for numerous constructive and critical discussions about this work. To Claudia Ruhnau I send my thanks the support in organizational and administrative matters. I am very grateful to Dr. Andrey Bukaemskiy and Dr. Victor Vinograd for their constant readiness for discussion and new ideas, and to Dr. Eric Mauerhofer, Dr. Matthias Rossbach, Dr. Hildegard Curtius und Marc Weidenfeld for all the innumerable and valuable comments and suggestions.

I indebted to our external partners and colleagues. Last not least, I would like to thank Dr. Anna Braun and Dr. Sven Tittelbach from the Wissenschaftlich Technische Ingenieurberatung GmbH (WTI) in Jülich for providing the anonymized FA design and operating data. Many thanks go to Dr. Franco Michel-Sendis, NEA-OECD, for providing the access to the SFCOMPO database and to Dr. Stefano Caruso, NAGRA, for providing the calculated Swiss radionuclide inventory data.

Most heartedly, I wish to thank Ian Gauld, ORNL, for his expertise and valuable support as the best external mentor and for countless discussions and advices. My gratitude goes to ORNL for providing the calculated US radionuclide inventory data.

Finally I want to thank very personally my family and my friends, namely my parents, brothers and most particularly my wife Natalia with our little daughter Alice for they have always believed in me, endured and supported me through all stages of my work and encouraged me to carry-on and complete.

Eidesstattliche Erklärung

Hiermit versichere ich eidesstattlich, dass ich die vorliegende Dissertation selbstständig verfasst und alle in Anspruch genommenen Hilfen in der Dissertation angegeben habe.

Aachen, den January 18, 2017

Band / Volume 345

**Light Management by Intermediate Reflectors
in Silicon-based Tandem Solar Cells**

A. Hoffmann (2016), 199 pp
ISBN: 978-3-95806-186-6

Band / Volume 346

**Design eines hocheffizienten Festoxid-Brennstoffzellensystems
mit integrierter Schutzgaserzeugung**

M. Engelbracht (2016), 190 pp
ISBN: 978-3-95806-189-7

Band / Volume 347

**On model and measurement uncertainty in
predicting land surface carbon fluxes**

H. Post (2016), xviii, 135 pp
ISBN: 978-3-95806-190-3

Band / Volume 348

Bipolarplattenmaterialien für Polymer-Elektrolyt-Membran Elektrolyse

M. Langemann (2016), I-III, 189, IV-XVIII pp
ISBN: 978-3-95806-192-7

Band / Volume 349

**Modellbasierte Ansteuerung räumlich ausgedehnter Aktuator-
und Sensornetzwerke in der Strömungsregelung**

M. Dück (2016), XIII, 153 pp
ISBN: 978-3-95806-193-4

Band / Volume 350

TRENDS 2015 – Transition to Renewable Energy Devices and Systems

ed. by D. Stolten and R. Peters (2016), 200 pp
ISBN: 978-3-95806-195-8

Band / Volume 351

**Dual Phase Oxygen Transport Membrane
for Efficient Oxyfuel Combustion**

M. Ramasamy (2016), VIII, 136 pp
ISBN: 978-3-95806-196-5

Band / Volume 352

**Transport, co-transport, and retention of functionalized
multi-walled carbon nanotubes in porous media**

M. Zhang (2016), VII, 112 pp
ISBN: 978-3-95806-198-9

Band / Volume 353

Untersuchungen zur Luftqualität in Bad Homburg

C. Ehlers, D. Klemp, C. Kofahl, H. Fröhlich, M. Möllmann-Coers
und A. Wahner (2016), IV, 93 pp

ISBN: 978-3-95806-199-6

Band / Volume 354

**Herstellung thermisch gespritzter Schichten
mit optimierten Spannungseigenschaften**

M. Mutter (2016), VI, 142, VII-XXII, xxvi pp

ISBN: 978-3-95806-200-9

Band / Volume 355

Entwicklung selbstheilender Wärmedämmschichten

D. Koch (2016), X, 120 pp

ISBN: 978-3-95806-201-6

Band / Volume 356

**Betriebsstrategien für Brenngaserzeugungssysteme
zur Anwendung in HT-PEFC-Hilfsstromaggregaten**

D. Krekel (2017), IX, 265 pp

ISBN: 978-3-95806-203-0

Band / Volume 357

**Korrosion metallischer Bipolarplatten in
Hochtemperatur-Polymer-elektrolyt-Brennstoffzellen**

V. Weißbecker (2017), viii, 194 pp

ISBN: 978-3-95806-205-4

Band / Volume 358

**Realistic Bandwidth Estimation in the Theoretically
Predicted Radionuclide Inventory of PWR-UO₂ Spent
Fuel Derived from Reactor Design and Operating Data**

I. Fast (2017), XI, 129 pp

ISBN: 978-3-95806-206-1

Weitere *Schriften des Verlags im Forschungszentrum Jülich* unter
<http://www.zb1.fz-juelich.de/verlagextern1/index.asp>

**Energie & Umwelt /
Energy & Environment
Band / Volume 358
ISBN 978-3-95806-206-1**

